INVESTIGATING THE PERFORMANCE OF GEOCELL REINFORCED UNBOUND LAYER USING LIGHT WEIGHT DEFLECTOMETER

A Dissertation submitted in partial fulfilment of the requirements for the Award of the Degree of

MASTER OF ENGINEERING

IN

INFRASTRUCTURAL ENGINEERING

Submitted by

Junaid Altaf
Roll No.: 802023031

Under the Guidance of

Dr. Tanuj Chopra
Assistant Professor,
Civil Engineering Department,
TIET, Patiala

Mr. Rajesh Pathak
Associate Professor,
Civil Engineering Department,
TIET, Patiala

DEPARTMENT OF CIVIL ENGINEERING
Thapar Institute of Engineering and Technology, Patiala
(Deemed-to-be-University u/s 3 of the UGC Act, 1956)
July 2022

DECLARATION

I hereby declare that this work which is being presented in the report entitled "**INVESTIGATING THE PERFORMANCE OF GEOCELL REINFORCED UNBOUND LAYER USING LIGHT WEIGHT DEFLECTOMETER**," in partial fulfillment of the requirement for the degree of Master's of engineering in the field of **Civil Engineering** at **Thapar Institute of Engineering and Technology (Patiala)**, is an authentic record of work carried out by me under the supervision of Dr. Tanuj Chopra (Assistant professor) and Mr. Rajesh Pathak (Associate professor), Civil Engineering Department, Thapar Institute of Engineering and Technology, Patiala, Punjab.

The matter embodied in this thesis has not been submitted by me for the award of any other degree or diploma

Date: 20/07/2022

(Junaid Altaf)

(802023031)

CERTIFICATE

This is to certify that the above declaration made by the student concerned is correct according to the best of our knowledge and belief.

Dr. Tanuj Chopra
Assistant Professor,
Civil Engineering Department,
TIET, Patiala

Dr. Rajesh Pathak
Associate Professor,
Civil Engineering Department,
TIET, Patiala

ACKNOWLEDGEMENT

The research work which is presented in this dissertation, is more of a teamwork, and I would like to thank many who have contributed their time and energy to the study.

First and foremost, I am grateful to my advisor **Dr. Tanuj Chopra and Mr. Rajesh Pathak**, Department of Civil Engineering, Thapar Institute of Engineering and Technology, Patiala, who consistently kept me motivated and instilled good thoughts not only for research but for life as well. Their constant and enthusiastic support throughout is the root cause for the research work to see its end.

I would like to express my gratitude to Dr. Prem Pal Bansal, Head of the Department of Civil Engineering, Thapar Institute of Engineering and Technology, Patiala, for his kind cooperation and encouragement, which helped me in the completion of my work.

I am incredibly thankful to Mr. Amarjit Singh and Mr. Jaspreet Singh for helping me carry out the experimental work.

I also wish to express my special thanks to Terrain Infratech, Inc. Gurgaon- 122018, Haryana, India for providing Geocell material that was used in this study and extend my heartfelt thanks to all the employees of the organization for providing their unconditional support & valuable suggestions wherever required.

I would like to thank and remember my friends and classmates: Mr. Sheikh Hazim Javaid, Ms. Komaldeep and Mr. Rohan Sharma who have helped in the various stages of this research and made this period a real educative, enlightening, pleasurable and memorable one.
I would like to dedicate this thesis to my father and thank my mother and brother for their constant encouragement during the entire course of my thesis work.

Above all, I am grateful to The Almighty Allah.

ABSTRACT

Rapid road infrastructure construction has become a trend in India and around the world. Many road projects have necessitated early-stage maintenance during the last few decades. To figure out what's causing it, a structural evaluation study is needed to analyze the existing material qualities of the pavement. Many studies have evaluated flexible pavements using widely used NDT technologies such as LWD, BBD, and FWD. While LWD is gaining acceptance and popularity as an in-situ spot-testing device all over the world, only a few studies have been done and are necessary to be carried out in India in order to make the use of the LWD technique beneficial in road repair projects. The primary objective of this research is to use LWD to estimate the subbase surface and subgrade modulus of the unreinforced and reinforced sections and to provide rehabilitation options based on the LWD results. The lightweight deflectometer (LWD) is a highly advanced and sophisticated device that was developed to evaluate the deformation modulus (E_{sub} LWD) of compacted geomaterials as an alternative density test.

One of the ground improvement techniques rapidly expanding is geosynthetic soil reinforcement, primarily due to cost-effectiveness, simplicity, and ease of construction. The most recent development in the field of geosynthetics soil reinforcement is the use of geocells at the base and subbase courses of the pavement systems. Geocells improve pavement performance while also attaining sustainable goals, as shown by research, testing, field trails, and case studies. This research aimed to figure out what causes improved bearing capacity and what benefits geocells deliver. Geocell was used in this study in a variety of layouts and sizes with gradation (Grade I as per MoRTH for both Laboratory and Field Evaluations. It was also discovered that the best performance is achieved when a geocell of height 125 mm layer is installed in the unbound layer.

The performance improvement was presented in terms of Modulus Improvement Factor (MIF). This study intends to use the LWD device and present the ranges of deformation modulus for various geomaterials from several studies. For instance, in the case of soils and aggregates, deformation modulus values were found to be in the range of 35-60 MPa and 80-120 MPa, respectively. In addition, several studies have been compiled to completely comprehend the relationship between LWD and various geocell layouts. In addition to the cost savings, this would

conserve natural materials like aggregates used in pavement construction. Overall, the inclusion of geocell in the subbase layer helps improve the life, uniform distribution of load and provides an economical and sustainable solution to the present practices.

Finite Element Analyses (FEA) were used in the investigation, and the results were confirmed through laboratory tests. The objective is to understand the behavior of unpaved roads with unreinforced and geocell-reinforced subbase. Based on FEA and laboratory evaluation, the study investigated that the geocells are beneficial when construction is performed with a lower/marginal subbase and subgrade material. The geocells allow placement on top of the weak quality subgrade.

TABLE OF CONTENTS

			Page No.
		TITLE PAGE	i
		DECLARATION	ii
		ACKNOWLEDGEMENT	iii
		ABSTRACT	iv-v
		CONTENTS	vi-ix
		LIST OF TABLES	x-xi
		LIST OF FIGURES	xii-xv
1		**INTRODUCTION**	1
	1.0	General	1-2
	1.1	Concept of Technology	2
	1.2	Classification of Geosynthetics	3
	1.3	Application and Function of Geosynthetics	4-5
	1.4	Benefits of Geosynthetics in Roadways	5
	1.5	Geocell Manufacturing Plant	6
	1.5.1	Raw material Feeding	6
	1.5.2	Sheet extruding & embossing	7
	1.5.3	Strips Cutting	8
	1.5.4	Perforating	8
	1.5.5	Ultrasonic Welding	9
	1.5.6	Packing of Geocells	9
	1.6	Geocells	10
	1.6.1	Reinforcement of geosynthetics	11
	1.6.2	Geocell reinforced Granular Subbase	11-12
	1.7	Nature of the Problem	13
	1.8	Objectives and Scope	13
	1.9	Outline of Thesis	14
2		**LITERATURE REVIEW**	15
	2.0	General	15
	2.1	Construction with Geocell	16
	2.2	Geocell Applications	17-21
	2.3	Model tests	21-26

	2.4	Strength-stiffness behavior	26-31
	2.5	Gap in Literature Review	32
3		**EXPERIMENTAL METHODOLOGY**	33
	3.0	General	33-34
	3.1	Laboratory Evaluation (Prototype Section)	34
	3.2	Materials	34
	3.2.1	Characteristics of Subgrade Soil	34-35
	3.2.1.1	Sieve Analysis	35
	3.2.1.2	Atterberg's Limits	36
	3.2.1.3	Specific Gravity	36-37
	3.2.1.4	Compaction Characteristics (Automatic Compactor Testing)	37-38
	3.2.1.5	California Bearing Ratio	38-39
	3.2.2	Characteristics of Geocell	39-40
	3.2.3	Characteristics of Granular Subbase	40
	3.2.3.1	Compaction Characteristics	41
	3.2.4	Stone Dust	41
	3.2.5	Properties of Aggregates	42
	3.2.5.1	Aggregate Impact Value (AIV)	42
	3.2.5.2	Specific Gravity Test	42
	3.2.5.3	Water Absorption Test	43
	3.2.5.4	Flow Chart for the Construction of Granular Subbase	44
	3.3	Mix Design	45-50
	3.4	Light Weight Deflectometer	51
	3.4.1	LWD Working Principles	51-54
	3.4.2	Characteristics of the studied LWD	55-56
	3.5	Moisture Content Measurement Devices	56
	3.5.1	Speedy Moisture Tester (SMT)	56-57
	3.6	Test Methodology	57
	3.6.1	Preparation of test beds for different sizes of geocells	58
	3.6.1.1	Preparing of Calibration Charts	58
	3.6.1.2	Test Bed Preparations	58-59
	3.6.1.3	Subbase Course Preparation	59-61
	3.7	Performance Measures	61-62
	3.8	Field Test Evaluation	62
	3.8.1	Site Location and Material Properties	63
	3.8.2	Soil Classification	63

	3.8.2.1	Subgrade Soil Classification	63
	3.8.2.2	Subbase Material Classification	64
	3.9	Instrumentation	64
	3.9.1	Geocell Pavement Section	64-65
	3.9.2	Construction of Reinforced and Unreinforced Sections	66
	3.10	Construction of Work	66
	3.10.1	Preparation of Subgrade	66-67
	3.10.2	Unreinforced Section Instrumentation	67-68
	3.10.3	Reinforced Section	69-71
	3.10.4	Mixing of Aggregate Materials	71
	3.10.5	Spreading and Compacting	72-75
	3.11	Data Collection and Analysis	75-77
4		**RESULTS AND DISCUSSIONS**	78
	4.0	General	78
	4.1	Performance results for LWD Testing	80
	4.2	Laboratory Testing (Prototype Evaluation)	81-84
	4.2.1	Lab Test Modulus Results	84-85
	4.3	Field Test Results	85
	4.3.1	Field Test E_{mod} Results	86
	4.4	Comparison of Modulus with respect to Thickness of Unbound layer	87
	4.5	Comparison with respect to Thickness (Prototype Model	88
	4.6	Comparison of Field and Lab Test Moduli	88
	4.7	Deflection Results	89
	4.8	Deflection Comparisons of Field and Lab Test Results	90
	4.9	Field Modulus Improvement Factor (MIF)	90
	4.10	Lab Modulus Improvement Factor (MIF)	91-92
5		**ANALYSIS AND DESIGN OF FLEXIBLE PAVEMENT**	93
	5.0	General	93
	5.1	Rutting Model	93
	5.2	Fatigue Model	94-95
	5.3	Analysis of flexible pavements using IITPave Software	95-96
	5.4	Procedure of Pavement Design	97
	5.5	High Volume Roads	98
	5.5.1	Design of Unreinforced Sections	98-102
	5.5.2	Design of Reinforced Sections	102-106
	5.6	Low Volume Roads	107

	5.6.1	Design of Unreinforced Sections	107-111
	5.6.2	Design of Reinforced Sections	112-115
	5.7	Summary	116
	5.8	Comparison of Thickness	117-118
	5.9	Cost Analysis	119
	5.9.1	High Volume Roads (50 msa Traffic)	119-121
	5.9.2	Low Volume Roads (5msa Traffic)	121-123
	5.10	Summary	123-126
6		**FINITE ELEMENT MODELLING (FEM) AND ANALYSIS OF RESULTS**	127
	6.1	Parametric Study	128-130
	6.2	Influence of Subbase Modulus Values	130-132
	6.3	Influence of Geocell Layer Thickness or Geocell Height	132-133
	6.4	Finite Element Model Development	133
	6.5	Soil Models	133
	6.6	Shell Element Type for Geocell Modelling	134
	6.7	Geocell Dimensions and Properties	134
	6.8	Contact Model	135
	6.8.1	Finite Element Types and Mesh Size	135
	6.8.2	Boundary Conditions	136
	6.8.3	Loading Conditions	137-139
	6.9	Results	139
	6.10	Field Strain Values Calculated	139
	6.11	Laboratory Strain Values Calculated	140
	6.12	Flexible Pavement Model	140-144
7		**CONCLUSION**	145
	7.1	Conclusions of the study	145-146
		REFERENCES	147

TABLES

Table	Title	Page No.
1.1	Material Test Methods for Geocell	10
3.1	Gradation of GSB as per MORTH	40
3.2	Results of Aggregate Impact Value Test	42
3.3	Specific Gravity Result Value for Aggregates	43
3.4	Water Absorption Test result value	43
3.5	Gradation for GSB (Grade-I) as per MoRTH	45
3.6	Design Details of Granular Subbase Material	46
3.7	Individual Grading of 40 mm Aggregate	47
3.8	Individual Grading of 20 mm Aggregate	47
3.9	Individual Grading of 10 mm Aggregate	48
3.10	Individual Grading of fine aggregate (Stone Dust)	49
3.11	Blending for Granular Subbase material (GSB I)	50
3.12	Stress distribution factors for different soil types	54
3.13	Characteristics of the studied LWD	55
3.14	Dynatest 3031 (LWD) Specifications	55
3.15	Factors Investigated in the experiment methodology	57
4.1	Experimental Program Stages	79
4.2	Modulus Results of Field Testing	90
4.3	Modified Modulus values using AASHTO	91
4.4	Modulus Results of Lab Testing	91
5.1	Standard conditions of pavement analysis using IITPAVE (Source: IRC: 37-2018)	96
5.2	Calculated Strain Values for High Volume Roads	106
5.3	Calculated Strain Values for Low Volume Roads	116
5.4	Design of Unreinforced Section 1	119
5.5	Design of Unreinforced Section 2	119
5.6	Design of Unreinforced Section 3	120
5.7	Design of Reinforced Section 4	120
5.8	Design of Reinforced Section 5	120
5.9	Design of Reinforced Section 6	121
5.10	Design of Unreinforced Section 7	121

5.11	Design of Unreinforced Section 8	121
5.12	Design of Unreinforced Section 9	122
5.13	Design of Reinforced Section 10	122
5.14	Design of Reinforced Section 11	122
5.15	Design of Reinforced Section 12	123
5.16	Cost Analysis of High Volume Roads	123
5.17	Cost Analysis of Low Volume Roads	124
5.18	Cost Saving Using Geocell (High Volume Roads)	124
5.19	Cost Saving Using Geocell (Low Volume Roads)	124
6.1	Dimension and Properties of Geocell-Reinforced Pavement FE Model	128
6.2	Geocell Dimension and Properties	134
6.3	Strain values calculated for field evaluation using software's	139
6.4	Strain values calculated for laboratory evaluation using software's	140
6.5	Comparison of strain values calculated using software's	144

FIGURES

Figure	Title	Page No.
1.1	Classification of geosynthetics used in pavements	3
1.2	Geocell manufacturing plant Equipment's	6
1.3	Raw material (HDPE) used in manufacturing geocells	6
1.4	Extruding and embossing of geocell sheets	7
1.5	Strip Cutting of Geocell Sheets	8
1.6	Perforation process of geocells	8
1.7	Ultrasonic welding machine	9
1.8	Packing of Geocells	9
1.9	Loading mechanism of geocell reinforced bases (Biabani et al.)	12
1.10	Load transfer mechanism of geocell mattress	12
2.1	Geocell bought from the manufacturer	15
2.2	Various Stages of laying Geocell	16
3.1	Sieve Shaker	35
3.2	Sieve Analysis of the Subgrade Soil	35
3.3(a)	Equipment used in Atterberg's Limit testing	36
3.3(b)	Flow Curve of Clayey Soil	36
3.4	Specific Gravity test by density bottle method	37
3.5	Equipment used in the Automatic Compaction Test	37
3.6	Relationship between unit weight and moisture content	38
3.7	California Bearing Ratio	39
3.8	Geocell used in the Project.	40
3.9	Relationship between unit weight and moisture content.	41
3.10	Flow Chart for the construction of Granular sub base.	44
3.11	Design Gradation for GSB (Grade-I) mix as per MoRTH guidelines	45
3.12	GSB (Grade-I) Sieve Analysis	46
3.13	Diagram of LWD and its parts	52
3.14	Schematic of the LWD-ground movement 2 DOF system	52

3.15	An example of load and deflection time history (from LWDmod software-Dynatest)	53
3.16	An example of load versus deflection hysteresis (from LWDmod software- Dynatest)	53
3.17	LWD testing on one layer and two layer systems	54
3.18	Dynatest LWD 3031	56
3.19	Rapid Moisture meter	57
3.20	Calibration curve for subgrade	58
3.21	Sequence of soil in-filling	59
3.22	Staged Preparation of Test Bed	60
3.23	LWD Testing on GSB	61
3.24	Location of the site for field testing	63
3.25	Test Section, Pavement Section of Geocell-Reinforced at Testing Site.	65
3.26	Cross section Pavement cross-section at Testing Site	65
3.27	Instrumentation of the stretch at Testing Site	65
3.28	Subgrade Preparation on site	66
3.29	LWD Testing on prepared Subgrade	67
3.30	Unreinforced Section Instrumentation	68
3.31	Reinforced Section Preparation and Instrumentation	69-71
3.32	Filling and Mixing of Materials	71
3.33	Filling of Geocells	72
3.34	Spreading of aggregate materials	73
3.35	Spreading and preparing reinforced sections	73
3.36	Rolling and Compacting of prepared GSB layer	74
3.37	Marked locations of Different Sections	74
3.38	Aerial View of the Site	74
3.39	Shows a typical reading on the JUNO to a drop.	76
3.40	Input Data in LWDmod software	76
4.1	Graphical representation of experimental program	80
4.2	URSB100 section used in the study	81
4.3	URSB125 section used in the study	81
4.4	URSB200 section used in the study	82
4.5	RGC100 section used in the study	82
4.6	RGC125 section used in the study	82
4.7	RGC200 section used in the study	83

4.8	Deformation profile of Unreinforced and Reinforced Sections (Lab)	83
4.9	Elastic Modulus calculated at different locations of the test box for 100 mm GSB layer	84
4.10	Elastic Modulus calculated at different locations of the test box for 125 mm GSB layer	84
4.11	Elastic Modulus calculated at different locations of the test box for 200 mm GSB layer	85
4.12	Deformation profile of Unreinforced and Reinforced Sections (Field Data)	85
4.13	Elastic Modulus calculated at different locations of the stretch on site for 100 mm GSB layer	86
4.14	Elastic Modulus calculated at different locations of the stretch on site for 125 mm GSB layer	86
4.15	Elastic Modulus calculated at different locations of the stretch on site for 200 mm GSB layer	87
4.16	Comparison of Field Modulus with respect to thickness of unbound subbase layer	87
4.17	Comparison of Laboratory Modulus with respect to thickness of unbound subbase layer	88
4.18	Comparison of Field and Lab test Moduli	88
4.19	Deflection calculated using LWD (Field Testing)	89
4.20	Deflection calculated using LWD (Lab Testing)	89
4.21	Comparison of Field and Lab Deflections	90
4.22	Modulus Improvement Factor	92
5.1	Cross Section of Reinforced Section	93
5.2	Typical cross-section of pavement	95
5.3	Outline of design for unreinforced section	97
5.4	Design Catalogue (Plate-2) Effective CBR 6%	98
5.5	Comparison of Sections	116
5.6	Thickness of pavements for unreinforced and reinforced Sections (High Vol. Road)	117
5.7	Thickness of individual layers (High Vol. Road)	117
5.8	Thickness of pavements for unreinforced and reinforced Sections (LOW Vol. Road)	118
5.9	Thickness of individual layers (High Vol. Road	118
5.10	Cost Analysis of High Vol. Conventional Pavement	125
5.11	Cost Analysis of High Vol. Geocell Reinforced Section	125
5.12	Cost Analysis of Low Vol. Conventional Pavement	126
5.13	Cost Analysis of Low Vol. Geocell Reinforced Section	126
6.1	Model used in the parametric study	129

6.2	Location of output evaluated from FEA	130
6.3	Field Strain Distribution (Geocell vs. No Geocell) along the Subgrade	131
6.4	Laboratory Strain Distribution (Geocell vs. No Geocell) along the Subgrade	132
6.5	Geocell and infill material	133
6.6	Mesh for all layers	135
6.7	Reinforced model used in the study	136
6.8	Boundary Conditions	137
6.9	Position of Wheel/loading	138
6.10	Location of output evaluated from FEA	138
6.11	Deformation due to loading conditions	139
6.12	Cross section of Unreinforced Section	141
6.13	Boundary Conditions	141
6.14	Effect due to loading on the surface layer	142
6.15	Screenshot of output strain values from IITPave	142
6.16	Cross section of geocell reinforced section	143
6.17	Deformation sketch of the section model	143
6.18	Effect of cyclic loading on the entire pavement section	144
6.19	Calculated strain values using software's	144

CHAPTER 1
INTRODUCTION

1.0 GENERAL

Road construction has a long history, as roadways serve as the foundation for all human settlements and subsequent growth. Road and transportation networks account for a significant portion of modern society's investment. Although it has always been a goal to build a road that will last forever, even building a road that will last for the design period has proven difficult. The pavement structure must be sturdy enough to sustain rising traffic demand while minimizing construction costs and materials used. Rapid industrialization and urbanization have emanated in a scarcity of suitable construction land. As a result, lands that were previously unsuitable for construction must be transformed using some form of ground modification. Building on soft soils was complex because of their limited bearing capacity, extreme compressibility, and differential settlement. Before the structure can be built, the engineering qualities of these soils must be changed. Mechanical alteration, chemical treatment, rapid consolidation, and soil reinforcement were among the methods used. Soil reinforcement is popular because of its versatility and efficiency. As a result, substantial efforts have been made to develop a strategy that balances pavement structure and construction costs to ensure that the available resources are used wisely. These approaches are designed to determine pavement structure in order to offer enough support for a specific quantity of traffic loading over a specified time period.

Constant increase in the traffic frequency and axle loads place great demand on the existing road networks. The stress induced between layer soon result in crack formation, and any local differential settlement may lead to subsequent settlement of upper layers. These stresses cause surface layer cracking, or fatigue, as well as rutting from local differential settlement. The kind of soil found all throughout the world is diverse, ranging from stiff to weak, and from very loose to dense. When avoiding of such sites is not possible, there is a need to improve them because the supply of suitable construction sites is limited, regardless of how weak the soil will be at the site.

Geosynthetics are gaining advantages over other advance methods for past few decades, particularly in the pavement industry. Geocells have recently been used in pavement layers to

increase performance, as they provide additional lateral confinement to the infill material in addition to the reinforcement's functions offered by conventional geosynthetics. Geosynthetics are the planar products made from polymeric substances that are integrated with rock, soil, earth, or other natural material as an integral part of a civil engineering project or system.

Several studies have proven that when the granular infill is employed over a weak subgrade under loading conditions, geocell reinforcement is effective. Hence it is important to know the behaviour of geocell reinforced granular aggregates sub-bases and bases over weak subgrades when subjected to traffic loads. Geocell has been found in studies to be effective in soil confinement and providing additional stiffness and strength to the subbase course. Figure 1.1 depicts the various types of geosynthetics that can be used in pavements.

1.1 CONCEPT OF TECHNOLOGY

The polymeric nature of products makes them ideal for application in the ground where long-term durability is required. They can, however, be employed in exposed applications if properly prepared. Geosynthetics come in variety of shapes and materials, each suited to a certain application. These materials are utilized in a variety of civil, geotechnical, transportation, hydraulic, and private development applications. The geosynthetic is used as a reinforcing element within a soil mass or in combination with the soil to create a composite with improved strength and deformation qualities than unreinforced soil. Environmental considerations, subgrade conditions, traffic loading, utility, and ageing are the main detrimental elements that shorten the service life of pavements. The expense of maintenance is greatly raised by the quick propagation of cracks up through the pavement layers, which is caused by pavement distresses, including surface cracks, joints, and subgrade failures. As a result, protecting the pavement during initial construction is the best method for long-term road pavement performance. Numerous practices have been implemented to improve the performance of pavements, including protecting the subgrade from moisture intrusion and associated weakening, strengthening the granular base and sub-base through efficient drainage of infiltrated water, and improving moisture proofing capabilities and stress absorption.

1.2 CLASSIFICATION OF GEOSYNTHETICS

Geosynthetics are categorized in a variety of ways depending on the process of manufacturing, the materials utilized, and the function.

The classification system is based on the geosynthetic material's spatial characteristics.

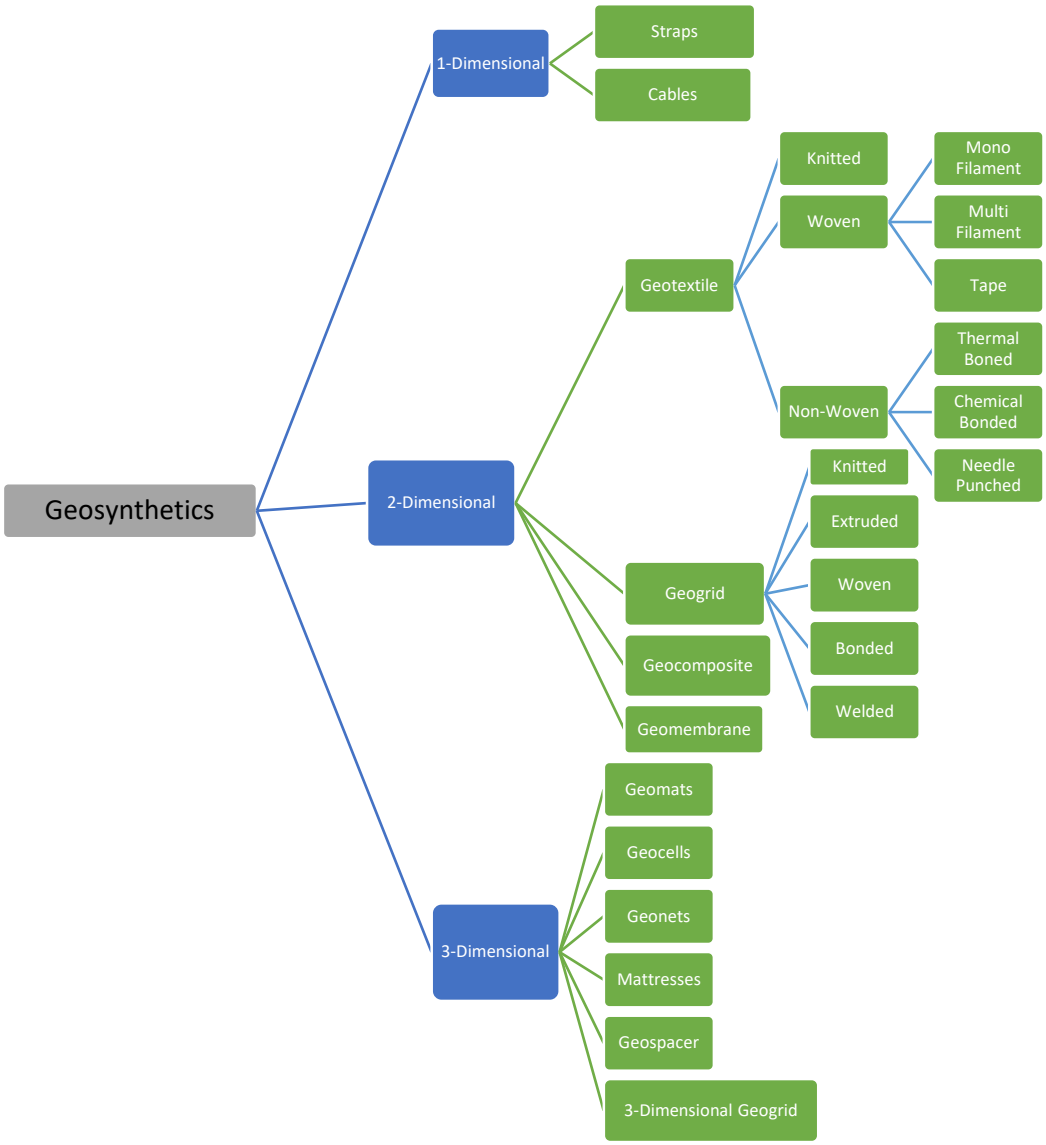

Figure1.1 Classification of geosynthetics used in pavements.

1.3 APPLICATION AND FUNCTION OF GEOSYNTHETICS

A geosynthetic can fulfill one or more roles in a given application in improving the mechanical and/or hydraulic behaviour of the structure into which it is included. A geosynthetic performs the following basic functions:

1. Separation
2. Filtration
3. Drainage
4. Reinforcement
5. Protection

Geosynthetics are materials that are durable, long-lasting, and flexible. They are better than concrete and metallic materials as they do not break or separate from the earth as the soil settles. Geosynthetics are quite versatile and can perform a variety of functions, and certain materials can perform different functions at the same time. The following are some of the applications of geosynthetics:

1) SEPARATION

When porous geosynthetics are placed between two soil types with significantly different particle sizes, they keep the particles apart and avoid particle mixing. When road pavements are built, for example, a gravel-sized base course material is deposited directly on the subgrade soil. If the subgrade is soft clay, the gravel will tend to seep into the subgrade soil, resulting in a mixed soil. Due to mixing, the performance of the base course degrades over time. Geosynthetics can be used at the interface between the subgrade and the base course to prevent this. It reduces mixing and improves the performance of the pavement.

2) FILTRATION

When placed between two soil layers, one fine-grained and the other coarse-grained, porous geosynthetics serve as a transition filter for water passing through them. They let water pass through without allowing fine soil particles to pass through as well. If adequate

soil is not available near the construction site, geosynthetics might be utilized in place of transition filters of soil.

3) **DRAINAGE**

Performs the functions of drains when porous geosynthetics with high in-plane permeability are put within a soil mass to intercept seeping water and transfer it quickly along the in-plane direction without fine particle migration.

4) **REINFORCEMENT**

When geosynthetics with high tensile strength are applied in single or multiple layers, they improve the engineering behaviour of the soil mass and serve as reinforcement within the layer. Soil performs well under compression but poorly in tension, and the performance of the soil is enhanced by the tension carrying capacity of geosynthetics. This improves soft soils bearing capacity, steep slope stability is improved, and earth pressure behind retaining structures is reduced.

5) **PROTECTION**

Geosynthetics are used to protect an underlying layer from damage caused by angular material such as gravel and stones that may be present above the layer.

1.4 BENEFITS OF GEOSYNTHETICS IN ROADWAYS

Subgrade stabilization, separation, subbase or base reinforcement, and the overlay stabilization are four main uses for geosynthetics in roadways. Subgrade stabilization and subbase or base reinforcements entails injecting a suitable geosynthetic material into the road construction as it is being built.

In a summary, the following are geosynthetics' applications in highways and pavements:

• Separation and stabilization of the subgrade

• Strengthening of the base or subbase

• Overlay stress absorption and reinforcement

1.5 GEOCELL MANUFACTURING PLANT

Figure 1.2 Geocell manufacturing plant Equipment's

1.5.1 RAW MATERIAL FEEDING

The Geocell material strictly in accordance with the product quality standard are utilized; recycled HDPE resin is used to create GB-grade Geocell, and virgin HDPE resin is used to create ASTM-standard Geocell.

Figure 1.3 Raw material (HDPE) used in manufacturing geocells

1.5.2 SHEET EXTRUDING & EMBOSSING

Figure 1.4 Extruding and embossing of geocell sheets

1.5.3 STRIPS CUTTING

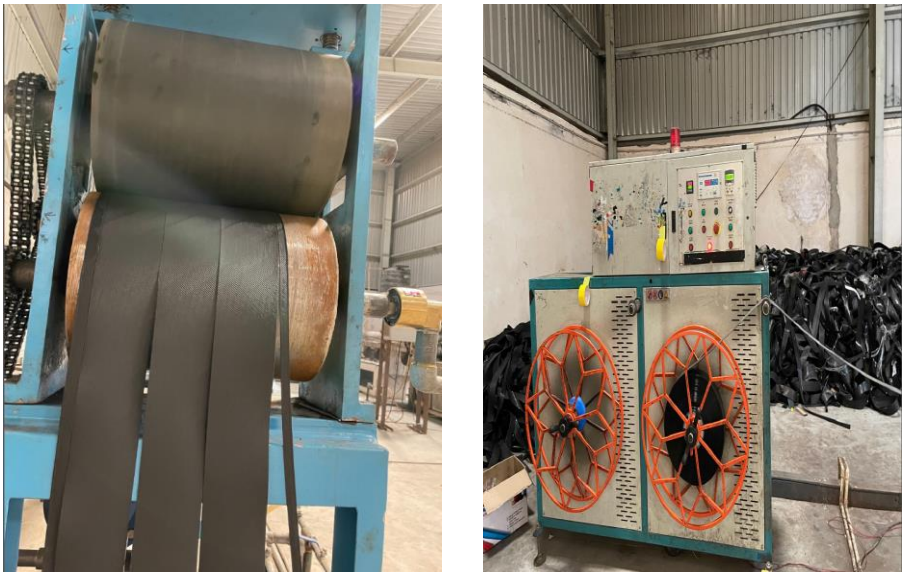

Figure 1.5 Strip Cutting of Geocell Sheets

1.5.4 PERFORATING: This procedure creates drainage holes; most clients want perforated Geocells, which are effective in facilitating drainage. Another option is a kind without perforations.

Figure 1.6 Perforation process of geocells

1.5.5 ULTRASONIC WELDING: Weld the Geocell sheets using an ultrasonic welding equipment.

Figure 1.7 Ultrasonic welding machine

1.5.6 PACKING: The finished products are well packed, neat & stable, easy to transport & avoid any damage.

Figure 1.8 Packing of Geocells

1.6 GEOCELLS

The concept of cellular structures providing lateral confinement dates back to the 1970s. The idea for lateral confinement was created by the US Army Corps of Engineers to improve the bearing capacity of poorly graded sand. Sand grids constructed of paper saturated in phenolic water-resistant glue were the earliest kind of geocells. Later, because of the strength requirements, metallic geocells, particularly those constructed of aluminium, were chosen, but these proved problematic due to the difficulties of handling and high cost. Geogrid sheets joined by bodkin bars have also been used to create geocells. Nowadays, the most common polymer used to produce geocells is high-density polyethylene (HDPE), which is made by welding extruded HDPE strips together to form honeycombs.

Geocell is a three-dimensional structure element formed of interconnecting cells stabilized with carbon black and made of polyester, polypropylene, and high-density polyethylene. Geocells primary function is to provide lateral confinement and thus stability. Physical, mechanical, and chemical properties are among its many characteristics. The attributes and test methods for the Geocell are represented in Table 1.1.

Table 1.1 Material Test Methods for Geocells

Test Properties	Test Method
Wall Thickness Nominal.	ASTM D5199
Seam Efficiency, (min. avg.)	GRI-GSI3
Density, (min. avg.)	ASTM D1505/D792
Tensile Properties, (min. avg.) (1)Yield Strength break strength yield elongation break elongation	ASTM D6693
Tear Resistance, (min. avg.)	ASTM D1004
Puncture Resistance, (min. avg.)	ASTM D4833
Carbon Black Content, (range) (2)	ASTM D4218
Carbon Black Dispersion, (3)	ASTM D5596
Direct Shear Friction Angle, (4)	ASTM D5321

1.6.1 Reinforcement of geosynthetics in base or subbase is done to achieve the following:

- Improve the strength of the pavement foundation for pavement construction over a weak subgrade to induce subgrade restraint and create a more stable construction platform.
- To add strength to the granular layers.
- To give the aggregate base layer more rigidity, allowing it to better protect the surrounding soil layers from traffic loads.
- It is believed to improve both the short-term and long-term performance of the roadway by assisting with aggregate compaction during construction.
- In order to provide structural advantages including lateral restraint, increased soil bearing capacity, and mobilisation of the tensioned membrane effect.

1.6.2 GEOCELL REINFORCED GRANULAR SUBBASES

At present, geocells are generally used in subbase and base layers to prevent material from spreading laterally owing to traffic movement. The geocell reinforcement helps in the confinement of the infill material. A typical section consists of a surface layer, base layer, a geocell-reinforced granular subbase, and a moderate subgrade. The overall behaviour of the reinforced composite section is characterized by the properties of geocell reinforced subbases and interaction of geocell with the materials contributing to horizontal and vertical confinement. It has been shown to be advantageous to use a three-dimensional geocell structure as a basal reinforcement in lateral confinement.

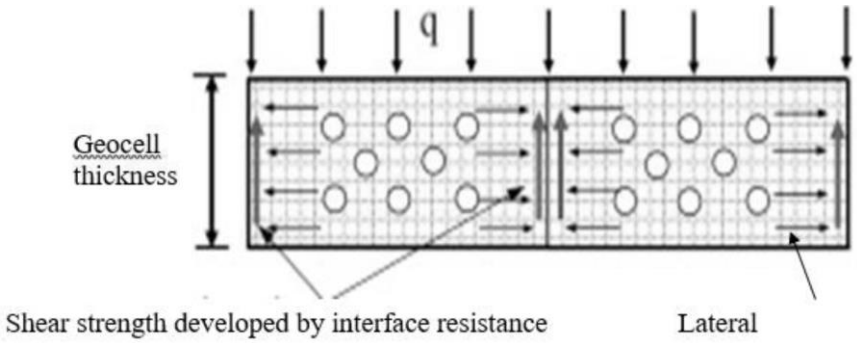

Figure 1.9 Loading mechanism of the geocell reinforced bases (Biabani et al.)

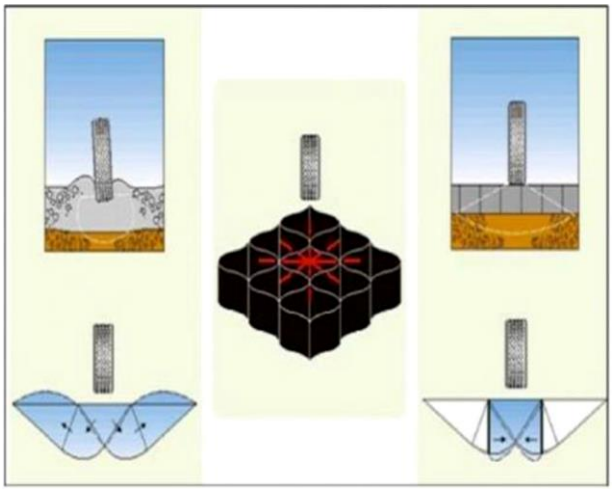

Figure 1.10 Load transfer mechanism of the geocell mattress (Kim et al.)

The following are the long-term benefits of using geocell:

1. Provides the same level of performance at considerably less cost

2. Immediate aggregate material cost savings.

3. Maintenance costs are reduced.

4. Maintaining the road base system's structural strength.

5. Pavement thickness optimization.

6. Carbon footprint reduction

1.7 NATURE OF THE PROBLEM

Since the 1970s, geosynthetics, or factory-made plastic materials, have been utilized more frequently in civil engineering projects to tackle geotechnical challenges (for example, roadway building over soft subgrade). Although geosynthetics for unpaved roads have received much attention, little research has been done on geosynthetics for unpaved roads. In order to increase the subgrade's bearing capacity, the geocell has been promoted as one of the items that reduces the traffic load's magnitude on the subgrade layer by laterally spreading traffic load through lateral confinement. Over the last decade, the product has also been promoted as a way to minimize the thickness of the subbase and base layer when a low grade or recycled subbase materials are employed. The ability of geocell to reduce the subbase layer thicknesses when poor quality subbase and subgrade materials are readily available has not been studied, so the goal of this study is to evaluate geocells ability to reduce subbase layer thicknesses when poor quality subbase and subgrade materials are readily available. A design system will be built as part of this project to implement and use geocells successfully.

1.8 OBJECTIVES AND SCOPE

- This study evaluates the elastic modulus of unbound sub-base layers with Gradation I and Geocell reinforcement states (i.e., the height of the geocells and the geocell layout). For this purpose, a full-scale test box was prepared, and both the subgrade and sub-base layers were installed for different unreinforced and geocell reinforced conditions.
- Design the strategy for better support.
- Conduct a laboratory and field evaluation and statistical analysis of the obtained data to determine parameters that substantially impact the performance of a geocell-based pavement system and compare them.
- Build an experimental design to analyze the mechanism for more significant support that geocells offer to the layers' bearing capacity, resulting in subbase layer thickness reduction.

- Create a finite element model and do a parametric analysis to simulate the laboratory experiment setup and thereby compare the calculated strain and modulus values obtained from IITPave software with the Abaqus (FEA) model results.

1.9 OUTLINE OF THESIS

This dissertation consists of the following chapters:

Chapter 1 Introduction of the thesis

Chapter 2 Literature review

Chapter 3 Explains the specifics of the various materials used and testing techniques employed in this study.

Chapter 4 Results and Discussions

Chapter 5 Design of Pavements and Cost Analysis

Chapter 6 Finite Element Modelling

Chapter 7 Conclusions drawn from the study are presented

CHAPTER 2
LITERATURE REVIEW

2.0 GENERAL

Geosynthetics are the factory-made plastic materials used in geotechnical engineering applications. Earlier straws were utilized as reinforcements in the construction of the Great Wall in ancient China around 200 B.C. Since then, geosynthetic-like materials have been used in civil engineering projects. Geosynthetic has evolved from a 2-dimensional material to cellular confinement system, which have added third dimension to geosynthetics. Geocell is a lightweight, durable, 3-dimensional manufactured system that can be expanded on-site which forms a honeycomb like structures and is a popular name for the Cellular Confinement Systems (Figure-2.1). The Geocell is filled with soil and compacted in order to increase the bearing capacity of the subgrade layer. The infill material in the geocell may be non-cohesive recycled materials as the geocell provides friction and confinement (geocells texture). In this study, geocells were investigated for the stabilization of granular subbases and weak subgrade in unpaved roads. This chapter presents a literature review of past studies and projects on geocell systems for roadway applications.

(a) Packed Geocell (b) Spread Geocell

Figure 2.1 Geocell bought from the manufacturer

2.1 CONSTRUCTION WITH GEOCELL

The construction process steps are shown in the Figure 2.2. The subgrade is levelled and compacted before the geocell is installed. The geocell was initially laid on top of the subgrade. The manual spreading and interconnection of geocells is done with ties and metal anchors or wooden stakes. A loader or comparable piece of equipment is used to fill the spread open geocell, which is then compacted with a roller compactor. An additional layer of filler material is placed on top to provide a smoother ride.

Fig 2.2 Various stages of laying Geocell

The application of geocells, model tests, and the strength-stiffness behaviour of geocells are the key topics of this report's study of the geocells literature review.

2.2 GEOCELL APPLICATIONS

Bush et al. (1990) described how a geocell foundation mattress is used to build a full-scale embankment over the soft soil deposit. Geocells were made out of polymer grid reinforcement and placed directly on top of the foundation soil, then infilled with granular materials to create a semi-rigid base around 1 meter deep. The geocell-soil mattress not only provided a working surface for the construction but also significantly increased the bearing capacity. The rough bottom of the geocell mattress restrained deformations in the foundation soil, resulting in greater system stability.

Bathurst and Crowe (1992) reported the application of geocell confinement devices in the construction of flexible gravity walls and steepened slopes. In extensive unconfined compression studies, they evaluated the stability of many layers of geocell mattresses under vertical surcharge. With a 1.4 percent vertical strain, the 1.44 m sand-geocell column, which contained eight layers of geocell, remained stable up to a maximum surcharge pressure of 155 kPa (10 m equivalent height of structure).The authors used this information to design and construct full-scale retaining walls that did not distort or collapse.

Cowland and Wong (1993) published a case study of the performance of a geocell-supported embankment on soft clay by Geogrids made of high-density polyethylene and polypropylene were used to create the geocell mattress. The geocell pockets were filled with angular formed rock fill that was 25mm deep. Pneumatic piezometers, inclinometers, hydrostatic profile gauges, settlement plates, surface settlement markers, and lateral movement blocks were all installed on the embankment. During the construction of the embankment, the performance of the geocell mattress foundation was monitored. The geocell mattress's recorded extensions were discovered to be less than 1%. The geocell mattress appears to have acted as a raft foundation for the embankment.

Gupta and Somnath (1994) employed Geocells in the construction of box culverts over marine clay deposits in the New Bombay area. The marine clay was found at a depth of more than 6 meters. The first tubular gabions were built in soft soil, with the ends resting on the firm moorum

layer beneath. The geocell mattress was then built on top of the clay surface. The gabions act as granular piles, while the geocell mattress acts as a flexible pile cover in this design. The geocell mattress's performance has been described as satisfactory.

Latha et al. (2006) looked at the benefits of using geocells on embankments. It was discovered to aid in boosting bearing capacity and reducing bank erosion. The bearing capacity and solidity of geocells with a larger adaptable modulus were higher.

Bhagaban Acharya et al. (2007) When compared to unreinforced asphalt, found that geocell enhanced regular flexible pavement and prolonged its life by around 2 to 3 times. They aid in the distribution of vertical loads over a larger area of the subgrade and reduce lateral soil particle movement, consequently boosting bearing capacity.

Hoe I Ling et al. (2009) investigated the use of geocells to strengthen soft clay subgrades. The seismic response of five large-scale geocell-facing retaining walls is summarized in this research. The backfill and foundation material were fine sand compacted to 90% standard Proctor density, and the walls were 2.8m high (relative density of 55 percent). The first two walls were identical in geometry, with a tapering facing composed of 20cm-high geocells, one filled with gravels and the other with sand. A 60cm-deep face was built in Wall 3, with polyester geogrid reinforcing the backfill sand. The backfill on Wall 4 was reinforced with many geocell layers, which was comparable to the backfill on Wall 3. In comparison to Wall 4, Wall 5 had thin geocell layers of 5cm height as reinforcements to increase performance. The walls were subjected to scaled horizontal and vertical vibrations observed during the 1995 Kobe earthquake, with maximum horizontal accelerations of 4.5m/s2 (450gal) and 9.0m/s2 (900gal) in the first and second excitations, respectively. Walls 3-5 were exposed to a third shaking with horizontal accelerations scaled to 12.0m/s2 in an attempt to produce failure and thereby explore the failure process (1,200gal). Accelerometers, strain gauges, laser displacement transducers, and force transducers were all installed on the walls. Under the simulated earthquake motions, all five walls functioned admirably. The geocells functioning as reinforcing layers increased the wall's performance. The investigations show that the geocell can be used successfully to form gravity walls as well as

reinforcement layer even when subjected to a very high seismic load beyond that of the Kobe earthquake.

Khedkar and Mandal (2009) studied the behaviour of geocell-contained sand under triaxial loading conditions. Peak deviator stress is seen to increase as the height of cellular reinforcement increases, which is due to the cellular reinforcement's generated confining effect. The reinforced samples' horizontal displacement pattern revealed multi-zoned failures. Furthermore, cellular reinforcement was observed to boost performance more than planar reinforcement.

K. Rajagopal et al. (2012) In order to improve the pavement's longevity, conducted research on geocell reinforced road pavement systems. Field plate load experiments and a series of laboratory plate load tests were used to evaluate how geocell confinement improved the strength and stiffness of the sub-base layer in a flexible pavement system. The increase in modulus of the segment confined with geocell compared to the part without geocell confinement reflects the improvement in pavement strength. The results of this study led to the conclusion that the introduction of a geocell layer in flexible pavements increases the structural stiffness of the pavement system. The use of a geocell layer has been found to lower the thickness of granular layers by up to 50%. Even with the use of an expensive geocell layer, the total cost of the pavement system per unit area was found to be cheaper. The rigidity of the pavement improves its performance and extends its service life. For maximum influence, a geocell layer should be placed as close to the surface loads as practicable. In addition, if a second layer is required, it could be installed at the subgrade level. This will also be effective in a lower carbon footprint due to the shipping of fewer resources from far-flung locations.

Tanyu, B. F. et al (2012) Over poor subgrades, a geocell-reinforced gravel subbase was evaluated in the lab. Large-scale cyclic loading studies were carried out to see how the addition of HDPE geocells impacts the rutting qualities of working platforms and the resilient capabilities of a subbase in a pavement system over soft subgrades. This study used four distinct geocells to reinforce common subbase/base course gravel. Experiments were carried out using 225 mm and 450 mm thick unreinforced and reinforced gravel, as well as crushed rock, which is commonly

used for cut-and-fill working platforms. Experiments were carried out to model loading loads during construction due to construction equipment and after construction due to traffic conditions over the asphalt pavement once the pavement structure had been built. To assess the effect of geocells, specifically with gravel material that is compacted to lower than average standards, the materials employed in this study were compacted to 90 percent relative compaction based on standard Proctor. Each section's deflections, subgrade reaction modulus, and resilience modulus were measured. In conclusion, geocells reduced the plastic deflection of working platforms by 30–50%, increased the resilient modulus of the subbase by 40–50%, and increased the modulus of subgrade reaction by more than 2 times.

Nitesh Ashok Bhange et al. (2020) studied the load-carrying ability of pavement with geocell and simple CC road using compression strength testing. The study's findings revealed that the thickness and weight of structural support parts were decreased by 50% or more. It allows subgrade material to resist more than 10 times the number of cyclic-load applications before experiencing irreversible deflection. It also reduces stress by nearly 30% when supporting aggregate beneath the pavement. According to the findings, the geocell material could be utilized as reinforcement, and the pavement could be improved by adding geocell to one-third of the base of the pavement. By dispersing the traffic load over a vast subgrade region, Geocell helps to reduce permanent displacement in the subgrade layer. When geocell reinforcement is placed, interlocking allows for around half of the base decrease. The design result showed that using geocell in pavement design can reduce thickness by roughly 20% to 40%, with more significant thickness reduction feasible with stronger subgrade material. Reduces overall cross-section by 15–25%, much more so where concrete costs are high and resources are limited. Hydrostatic pressure is relieved, and surface water is managed. It removes the need for formwork and additional reinforcement. It prevents cracking without the use of expansion joints. Allows for precise concrete depth and easier installation with less time spent on site.

Gaofeng Song et al. (2021) studied the application of geocell as soil stabilization and soil erosion countermeasures**.** Using geocell structures and wheat straws, this study presented a composite soil reinforcement approach to encourage vegetation growth and increase slope stability. For

examining the effects of rainfall intensities, slope steepness, and geocell sizes on soil erosion, twelve physical models were built. The geocell reinforced slopes had good integrity, whereas the naked slope had horizontal fissures, according to the findings. Under 50 mm/h and 100 mm/h rainfall intensities, soil erosion was less than 40 g and more than 4000 g, respectively; the maximum slope displacement was 2.5 mm and 7.5 mm. The high slopes had the most soil erosion, with 5000 g and an 8 cm displacement, compared to 4500 g and 5.5 cm for gentle slopes; soil water contents were 40% and 30% for steep and mild slopes, respectively. The recorded soil erosion for small and large geocell reinforced slopes under 100 mm/h rainfall was 4000 g and 5000 g, respectively; the displacement of small geocell reinforced slopes was typically 1–2.5 cm smaller than big geocell reinforced slopes. The small geocell reinforced slope with a small inclination, and low rainfall intensity has the best stability, according to the findings.

2.3 MODEL TESTS

Rea and Mitchell (1978) evaluated the performance of interconnected paper cells filled with sand as a reinforced layer for use in low-cost highway construction using laboratory model testing. When enlarged, the cells were made of 0.203 mm thick paper and were square in shape. The width was fixed at 51 mm throughout. Springs were used to imitate the subgrade. The parameters that were investigated were the radius of the loaded region, cell width, cell height, subgrade stiffness, and loading repetition. Cell penetration, cell bursting, cell wall buckling, bearing capacity failure, bending failure, and excessive rutting were recognized as separate types of failure based on the test results.

J. N. Mandal et al. (1993 studied the stability of geocell-reinforced soil. The influence of geocell configuration (i.e., geocell opening size, height) on the bearing capacity and failure settlement of a two-layer system was investigated experimentally on the stability of a geocell-reinforced soft soil structure. To research load-settlement characteristics and the increase of bearing capacity and reduction of settlement, laboratory model experiments for ultimate bearing capacity of marine clay overlain by a sand layer with and without the geocell are conducted. These studies have revealed

the true behaviour of the geocell structure under various external loading conditions. Because of the usage of geocell reinforcement, load-settlement properties have been reported to improve. On the basis of the experimental results, an increased bearing capacity factor has also been proposed. With increasing layer thickness, the stiffness of the upper elastic layer over soft marine clay rises. Up to a settlement ratio of 5-10%, the geocell layer exhibits beam action. The geocell layer exhibits membrane action after a settlement ratio of 20%. The application of geocell reinforcement improved load-settlement characteristics. Because of the employment of a geocell layer, the initial stiffness of the higher sand layer is greatly increased. When the geocell opening size is smaller, and the geocell depth is bigger, the initial stiffness is greater. The bearing capacity of a geocell increases as the aperture size and thickness of the geocell increases. The settlement ratio rises as the geocell opening size increases but falls as the geocell depth grows.

N. R. Krishnaswamy et al. (2000) described model studies on Geocell supported embankments constructed over a soft clay foundation and by detail the results of laboratory model testing on geocell-supported earth embankments constructed over a soft clay foundation. In a huge test tank, the soft clay foundation was prepared to a depth of 600 mm. On this clay foundation, a single geocell layer of various thicknesses was produced, and embankments were built above it. The geocell layer was constructed using four different types of geogrids. On the top, the embankments were subjected to uniform surcharge pressure until they failed. During the test, the vertical and horizontal deformations, as well as the strains created within the geocell layer, were measured. Through a series of laboratory tests, the impact of various parameters on the behaviour of the embankments was investigated, including the tensile stiffness of geogrids used to fabricate the geocell material, the height and pocketsize of the geocell layer, the length of the geocell layer, and the type of fill material inside the geocell. The improvement was quantified in terms of increased surcharge capacity and reduced deformations at the embankment's crest. The findings of this study demonstrated the relative impact of various parameters on the performance of geocell supported embankments built on soft foundations. The addition of a layer of geocells at the embankment's base increases the embankment's load capacity and deformation response. Geocell pocket aspect ratio (height to diameter ratio) was also discovered to have a significant impact on the performance of geocell-supported embankment models. The ideal aspect ratio was discovered to be 0.5. The installation of a geocell layer made with both clayey sand and clay soil infill resulted in a

considerable improvement in performance benefit. As a result, even low-grade soils can be used as infill.

Jie Han et al. (2008) looked at how Geocell-Reinforced sand behaved when subjected to a vertical load. The behaviour of geocell-reinforced sand under a vertical load is investigated using both experimental and computational methods. A sand-filled geocell was subjected to a vertical load until it failed. To examine the mechanics of geocell and sand interactions, this test procedure was modelled using the FLAC3D numerical software. The geocell boosted the final bearing capacity and modulus of the sand, according to both experimental and numerical findings. The distributions of displacements in the sand and geocell walls, as well as the distributions of tensile and shear stresses acting on the geocell walls, are all included in the numerical results. The numerical findings for geocell-reinforced sand and sand without geocell are compared. Geocells were found to increase the bearing capacity and elastic modulus of reinforced sand by confining the infill material in both experimental and computational tests. The load deformation curve is linear up to a deformation of 1.25 mm, according to the experimental data. With the addition of the geocell, the load increased by about 65 percent for this deformation. The modulus of the base also increased similarly. Because of the modest height of the geocell employed in this investigation, numerical analysis revealed that the largest displacement and maximum stress within the cell occurred near the bottom of the cell. The maximum compression force and maximum interface shear stresses on the geocell walls were impacted by the position of the load plate. At the geocells welding joints, it's critical to have enough strength. Because of the modest height of the geocell employed in this investigation, numerical analysis revealed that the largest displacement and maximum stress within the cell occurred near the bottom of the cell. The maximum compression force and maximum interface shear stresses on the geocell walls were impacted by the position of the load plate. At the geocells welding joints, it's essential to have enough strength.

Emersleben et al. (2008) Bearing Capacity Improvement of Asphalt Paved Road with Geocells. Large-scale static load studies were conducted to assess the impact of a geocell layer on the load-deformation behaviour of the soil. Geocells with various aspect ratios, manufactured of various materials and filled with sand, were tested. An artificial mixed soil named "Glyben" was utilized to replicate soft subgrade material. When compared to an unreinforced soil, the test findings showed that a geocell layer increased the bearing capacity of the infill materials and reduced

vertical loads on the subgrade by around 30%. Geocell reinforced, unreinforced, and hydraulic bounded base (HBB) in-situ test fields were carried out within various asphalt paved road structures to verify the results of model testing. Following the completion of the road construction, a 40-ton truck was used to conduct vehicle crossing tests and falling weight deflectometer measurements, while earth pressure cells were used to monitor vertical stresses on the subgrade. Stresses beneath the geocell layer were lowered by around 30% when compared to an unreinforced test segment. The deflections measured in the geocell reinforced test portion were much lower than in the unreinforced section, according to falling weight deflectometer readings. In the geocell reinforced portion, back estimated layer modules were substantially greater than in the unreinforced part.

Pokharel et al. (2009) In an experimental investigation, assessed the behaviour of geocell-reinforced bases under static and repetitive stress. The base course materials were Kansas River sand and Quarry debris from the filling. The test results indicated that geocell confinement increased the bearing capacity and stiffness of Kansas River sand by a factor of 1.75 and 1.5, respectively, under static loading. Due to the presence of apparent cohesiveness, geocell detention had a negligible effect on the stiffness of the quarry waste. When compared to the unreinforced base, the deformation of the quarry waste base in a single geocell decreased by about a factor of 1.5. Due to poor gradation, sub-spherical particles, and little apparent cohesion, the Kansas River sand showed the lowest percentage of elastic deformation when compared to unreinforced and reinforced quarry waste. Due to the involvement of the geocell, the reinforced quarry waste had a larger percentage of elastic deformation than the unreinforced quarry waste. Another experiment to assess the influencing variables for single geocell-reinforced sands discovered that geocells placed in a circular shape had a higher bearing capacity and stiffness of the reinforced base than geocells placed in an elliptical shape.

Tafreshi and Dawson (2010a, 2010b) investigated a series of laboratory model tests on strip footings supported on 3D geocell and planar geotextile-reinforced sand beds under static and repetitive loads. Overall, the findings show that the 3D geotextile reinforcement system performs better than the planar reinforcement system for the same quantity of geotextile material utilized in

the testing. As a result, when compared to planar geotextile, a specified improvement in footing settling can be accomplished with a smaller amount of 3D geotextile material (i.e., geocell).

Amarnath Hegde et al. (2013) To assess the appropriateness of geocell cellular confinement as a foundation technology, experimental and numerical research on geocell reinforced sand beds was conducted. The results of the 1-g model tests on the geocell reinforced sand substrate supporting the square footing are presented in this study. The addition of geocell boosts the sand bed's final bearing capacity by four times, according to the findings. The addition of a planar geogrid to the base of the geocell mattress not only improves load carrying capacity but also prevents surface heave and rotational failure of the foundation. In addition to the experimental tests, a numerical study was conducted to demonstrate the rudimentary approach to modelling geocells in FLAC2D. The numerical study revealed the simplistic method to modelling the 3D nature of geocell in the 2D finite difference software FLAC2D. According to test results, adding geocell to the sand bed boosts its final bearing capacity by 4 times. The installation of a planar geogrid at the bottom of the geocell stops the surface from heaving and prevents rotation failure of the footing. As a result, using a planar geogrid layer at the bottom of the geocell mattress is always a good idea. Thus, preliminary static experiments indicate that the geocell and basal geogrid combination can be successfully used for the construction of foundations subjected to heavy loads.

M. N. Asha et al. (2014) provide experimental results from laboratory repeated plate load testing on unreinforced & reinforced model sections of unpaved road produced in a steel test tank with a plan dimension of 750 mm 750 mm and a height of 600 mm. A 150 mm diameter loading plate was used to apply the load. In the tests, geocell reinforcement was used to keep the granular sub-base contained. In the experiments, the effects of various parameters such as geocell layer height and position on the performance of these model road sections were investigated. The reinforced systems demonstrated less permanent settlements and more elastic settlements than the unreinforced systems at higher settlements, according to the experimental data. The secant modulus of reinforced systems was higher than that of unreinforced systems at all strain levels. Increases in the height of the geocell layer increased performance up to a certain point, after which, due to insufficient granular overlay thickness, additional increases in the height lowered load

resistance. In order to reap the benefits of geocell reinforcement, the location of the geocell layer within the granular sub-base was crucial. The geocell layer should be placed at the subgrade-granular sub-base contact for best benefit, with sufficient granular overlay thickness above the geocell layer.

Bojan Zlender et al. (2017) Modeling a geocell-reinforced pavement was investigated. In order to measure the permanent deformation due by cyclic stress, a pavement structure was built in the lab. Permanent deformation was decreased by roughly 53% in a laboratory test thanks to the geocell reinforcement. When geocells are employed in the pavement structure, the horizontal strain in the asphalt layer is reduced dramatically, according to the results of the computer model. As a result, the asphalt layer's fatigue life is extended. Geocells greatly improve the stability of unpaved roads with sand bottoms and lower the amount of permanent deformation, according to the test results. The infill material has an effect on the resilience modulus of the geocell. When geocell reinforcement is used, the results reveal a significant increase in bearing capacity.

2.4 STRENGTH-STIFFNESS BEHAVIOR

Rajagopal et al. (2005) discovered the role of geocell layers in improving the nature of flexible pavement. For this reason, stress examination programmes and both fields, as well as lab tests, were conducted. The pavement serviceability was assessed after a preliminary construction for a specific length of 2m. The results showed that compacting the sub-base layer over the geogrid layer resulted in a higher dry density.

Latha and Murthi (2007) studied through triaxial compression experiments and determined how several types of reinforcement, such as horizontal layers, geocells, and randomly distributed discrete fibres, affected the enhancement of sand's strength. While discrete fibre was discovered to be less successful than the other two forms of reinforcement, namely geocell and planar, the cellular form of reinforcement was determined to be the most effective one in increasing strength.

Wang et al. (2008) used large-scale direct shear testing to determine the shear characteristics of geocell reinforced soils. The researchers investigated three different specimens: silty gravel, geocell reinforced silty gravel soil, and geocell reinforced cement stabilizing silty gravel soil. Geocell reinforced soils' shear stress-displacement behaviour, shear strength, and strengthening mechanism were studied. In order to investigate the influences of testing method on shear strength, comparisons of large-scale shear test responses with those from triaxial compression tests were done. The test results indicate that the shear-strain behaviour of both unreinforced and geocell reinforced soil is nonlinear. When the normal stress was in the range of 1.0 Gpa, the geocell reinforced cement stabilized soil showed quasi-elastic characteristics. The geocell reinforcement resulted in a 244 percent increase in sand cohesion, whereas it resulted in a 10 fold increase in cohesion in the cement stabilized soil. The friction angle does not alter significantly.

Khedkar and Mandal (2009) studied the behaviour of geocell-contained sand under triaxial loading conditions. Peak deviator stress is seen to increase as the height of cellular reinforcement increases, which is due to the cellular reinforcement's generated confining effect. The reinforced samples' horizontal displacement pattern revealed multi-zoned failures. Furthermore, cellular reinforcement was observed to improve performance more than planar reinforcement.

Wesseloo et al. (2009) reported the results of uniaxial compression tests on soil-filled geocell packs of various sizes. As the test progressed, the packs were instrumented to record the strength and deformations. The test findings show that the strength of the geocell composite structure is related to the size of the individual cells in an indirect manner, and that the strength decreases as the number of cells in the structure increases.

J. Han et al. (2010) are a group of researchers who have worked on a variety of effects of infill material on geocell-reinforced base performance. Geocell's three-dimensional structure effectively provides lateral confinement to infill material, increasing base course stiffness and bearing capacity while reducing permanent deformations under repeated loading. However, only few research have looked into the impact of infill material on the performance of geocell-reinforced bases so far. Three types of infill materials were used in this study: poorly graded Kansas River

sand, quarry waste (QW), and well-graded AB-3 aggregate. The experiment looked at the bearing capacity, stiffness, permanent deformation, and percentage elastic deformation of several infill materials in geocell-reinforced bases. The benefit of geocell in the bearing capacity and stiffness of the reinforced base under static loading is more apparent when a weaker infill material was utilized, according to the test results. Under repeated loads, however, the benefit of stronger infill materials became increasingly apparent. Permanent deformations of reinforced bases were greatly reduced, and the percent of elastic deformations was significantly increased for all infill materials when compared to unreinforced bases under the same magnitude of repeated loading. Under repeated loads, the reinforced and unreinforced base courses with various infill materials were tested. From this experiment, the following conclusions are taken. Regardless of whether the infill material was weak or strong, geocell reinforcement considerably reduced permanent deformation after 150 cycles of loading. The permanent deformation of the reinforced section after 150 loading cycles at 345 kPa was equal to the permanent deformation of the unreinforced section after the first cycle of 230 kPa loading in Kansas River sand. In the case of QW, the permanent deformation on the unreinforced portion after 150 loading cycles was 1.5 times that on the reinforced part. In the case of AB-3, this factor was 1.33. Single geocell reinforcement reduced plastic deformation in all situations, but the percentage of elastic deformation was higher in stronger infill materials (QW and AB-3) than in weaker materials (sand). The improvement over the unreinforced case was more noticeable during the early loading cycles.

Sanat Kumar Pokharel et al. (2015). Validation of Geocell Design for Unpaved Roads by Neoloy Geocell, which was employed in the projects under examination, had the flexibility of HDPE at low temperatures and the elasticity of an engineering thermoplastic. Neoloy Geocell is a polyethylene matrix that contains a composite alloy of polyester/polyamide Nano-fibers. The elastic modulus at 2% strain was 620 MPa, and the tensile strength was 21.5kN/m. Over a shaky subgrade, laboratory cyclic plate loading tests and full-scale moving wheel tests were carried out on Neoloy-based Geocell-reinforced granular bases. The pavement thickness is determined, and a maximum permissible rutting is set in the design technique. Real-time testing revealed that the design formula functioned effectively within and beyond Pokharel's 2010 laboratory and moving wheel test limits. The design appeared to function better than expected in some regions. This can be attributed in part to enhancements made by the construction layers, particularly in terms of CBR

value. In all of the double layer examples, the construction or bottom layer increased the subgrade, resulting in a design with a greater margin of safety due to the subgrade strength used in the design. Finally, the design method that was used for the first time in the real application proven to be legitimate and dependable.

M. Mengelt et al. (2016) studied resilient modulus and plastic deformation of soil confined in a geocell. In a large-size cell with and without confinement in a geocell, resilient modulus experiments were done on two coarse-grained soils (gravel and sand) and a fine-grained soil (lean silty clay). The infill had an effect on the geocells robust modulus (soil in the geocell). When the infill was coarse-grained, the resilient modulus increased by just 1.4–3.2 percent, but when the infill was fine-grained, it increased by 16.5–17.9%. When the fine-grained infill was compacted wet of optimum water content, the influence on resilient modulus was greater. The fine-grained soil experiments produced larger deformations, which most likely contributed to the higher increase in resilient modulus when confined in a geocell. Analysis of permanent strains during resilient modulus tests on gravel and sand revealed that confining coarse-grained materials in a geocell decreases accumulated plastic deformation. This effect could be significant during a pavement's lifetime.

Avinash Shastri et al. (2019) Experiment on soil properties using geocell-shredded tyres reinforced sand was carried**.** The tests included the Triaxial Compressive Test and thus the Shear Test, which were used to investigate the soil's stiffness and load carrying capacity. The triaxial experiments reveal that providing shredded tyres reinforcement in content 10% and 20% improves stiffness and load carrying capacity of the soil significantly; however, tyre content 30% and 40% results in less stiffness and load carrying capacity of the soil. When geocells are used to reinforce soil using shredded tyres, the outcomes are better in terms of 10%, 20%, and 30% tyre content when compared to geocell reinforcement of soil without shredded tyres. When compared to the reduced contents of shredded tyres, 40 percent of tyre content reveals inferior weight carrying capacity. A soil sample with a relative density of 70% exhibits greater rigid behaviour and strength than samples with relative densities of 30% and 50%. Due to fewer voids, soil samples with a relative density of 70% show abrupt or brittle failure at lower axial strain, whereas samples with a

relative density of 30% and 50% show ductile failure. In comparison to the unreinforced examples, the shredded tyres reinforced soil at 10% and 20% tyre content exhibits substantially stronger and stiffer behaviour. The results demonstrate that a tyre content of less than 20% provides 1.2 times the strength of unreinforced sand. When tyre composition exceeds 20%, the strength carrying capacity is reduced. Although the friction angle of the soil-shredded tyre mixture is lower than that of soil alone, the total strength of the reinforced soil is higher due to greater particle cohesiveness. When soil is reinforced by shredded tyres, failure occurs at a higher axial strain than when the soil is not reinforced. When we increase the amount of tyre in a soil-tyre mix, the axial strain at failure increases by 1.3 times when compared to soil alone. When compared to unreinforced soil, geocell reinforced soil is significantly stronger and stiffer. The results demonstrate that adding geocell to the soil for reinforcement gives it around 2.75 times the strength of unreinforced sand. The friction angle remains same when geocells are used as reinforcing material. The geocell encasement is discovered to generate apparent sand cohesiveness, resulting in increased load carrying capability. The apparent cohesiveness of the geocell material increases as the relative density of the soil and the strength of the geocell material increases. The geocell encasement is discovered to generate apparent sand cohesiveness, resulting in increased load carrying capability. The apparent cohesiveness of the geocell material increases as the relative density of the soil and the strength of the geocell material increases.

Mohsen Kabiri Kouchaksaraei et al. (2020). The impact of geocell dimensions and layout on the strength properties of reinforced soil was explored. The layout-dependent and dimensional impacts of geocell on the shear strength of reinforced soil in various parts of a reinforcing element were investigated using both laboratory experiments and numerical calculations in this research. The finite element method was used to extend the experimental outputs using numerical simulation. The results showed that using a geocell with a smaller pocket opening width increased the soil's shear strength by 31%. Despite the fact that the pocket opening diameter increased by up to 80%, the value of shear strength decreased by just 4%. The interface shear strength between soil and the geocell edge increased as the aspect (height-diameter) ratio of the geocell rose. In comparison to the state when the geocell edge is tangential to the failure plane, the shear strength rose by 11% when the failure plane crossed through the middle of the geocell height. However, when geocell moves away from failure plane, the shear stress-horizontal displacement curves had

a similar trend to that of the unreinforced soil. The result shows that in the reinforced soil tested at 196 kPa overhead pressure, shear strength increase by more than 30%. The amount of the increase depend on the opening size of the geocell and the position of geocell placement.

Xiaowei Li et al. (2020) investigated how to improve the performance of a new geocell reinforced asphalt mixture. A new type of geocell is employed to reinforce an asphalt mixture in order to increase its performance in this paper. As a result, an experimental evaluation of the influence of high temperature resistant geocell reinforcement on compressive strength, tensile strength, shear property, water stability, and fatigue performance in an asphalt mixture was created. So, under various temperature settings, uniaxial compressive test, splitting test, uniaxial penetration test, freeze-thaw splitting test, and splitting fatigue test were performed. The results show that after geocell reinforcing, asphalt mixture's compressive and tensile strengths are improved, shear performance is improved due to the high-temperature flow deformation being restrained, and the strength reduction rate after a freeze-thaw cycle is less than that of an unreinforced asphalt mixture, as well as the fatigue life. This shows that the geocell increases the asphalt mixture's performance in a variety of ways. With its three primary reinforcement methods, high temperature resistant geocell reinforced asphalt mixture has improved compressive strength, splitting tensile strength, and shearing property of asphalt mixture. Furthermore, when the temperature rises, the compressive and splitting strengths of the asphalt mixture increase. This suggests that the geocells reinforcement effect on the asphalt mixture is more noticeable at high temperatures, whereas the geocells lateral restraint effect can better control the asphalt mixture's flow deformation. Because of the geocell, the unrecoverable deformation of the asphalt mixture is reduced in each cyclic load cycle, resulting in less cycles being required for the asphalt mixture to reach the limit deformation, hence improving the fatigue life. A composite layer structure with the same height of geocell is formed by a geocell reinforced asphalt mixture. The composite layer has stronger strength and rigidity, which is a key factor in improving the bearing capacity and deformation resistance of asphalt mixtures, and so can significantly improve their performance.

2.5 GAP IN LITERATURE REVIEW

The past literature review reveals that studies on geocells had been carried out using various model tests, laboratory research, and geocell performance evaluation. The previous studies had focused on the properties geocell pocket size, geocell aspect ratio, multiple and single geocell and on the type of loading. Some research had worked on the variety of infill material used in geocells. However minimal research is present on the effect of geocells used on field. It was found common that geocells were mainly used in improving the bearing capacity and strength of the layers. But in case of this research, the focus is on generation of modulus improvement factor using geocells based on the laboratory testing and evaluation which is compared and validated based on the field tests done with the same type and size of geocells using same gradation of aggregates. The tests will be conducted using the light weight deflectometer a non-destructive technique to check the characteristics of the prepared GSB layer. Further numerical modelling is proposed and strain values are compared with the strain values generated using the conventional IITPave software to obtain the benefits of installing geocells in the pavements.

CHAPTER 3
EXPERIMENTAL METHODOLOGY

3.0 GENERAL

The material selection, experimental design, and laboratory evaluation method are all covered in this section. To achieve the above mentioned goal, the performance of the geocell reinforced layer is assessed by simulating the geocell reinforced pavement system in finite element software and comparing the test results obtained from laboratory testing. The properties of the different materials used in the current study, as well as the sample preparation processes used, are discussed in this chapter. The material characteristics are stated first, followed by a detailed discussion of the sample preparation techniques.

The evaluation of laboratory, field, and FEA study will depend on a number of parameters that were developed for the performance of pavement reinforced with geocell based on the literature review. Because the study's focus was on both high and low-volume roadways, it was decided not to include an asphalt concrete surface layer in the investigation. The modelling analysis is therefore consisted of a subgrade layer at the bottom and a geocell reinforced layer (geocell layer with infill subbase material) at the top (bottom to top). The analysis was also carried out for pavement systems without geocell reinforcement by building a layer of the same thickness without the geocell reinforcement, in order to show the advantages of geocell reinforcement. Although the geocell installation technique proposes laying fabric between geocell and the subgrade to prevent any contamination, no separation layer is installed in this project between the proposed layers to minimize any possible additional effects.

Based on the literature and preliminary research, the three following factors influence performance:

- The thickness of the geocell layer
- The modulus of the infill material (in the geocell)
- Modulus of subgrade.

Finally, the following performance parameters were evaluated to measure the impact of Geocell:

- Vertical strain and stress distribution at the top of subgrade or below the subbase layer,
- Vertical deformation above the subgrade or below the subbase layer, and
- Modulus of the unreinforced and reinforced granular subbase layer.

The following materials were used in this investigation:

- Clayey sand (to prepare a subgrade).
- Granular Sub-base (GSB) as a subbase course.
- Geocell mattress as a subbase layer reinforcement.

This chapter is divided into two sections based on the evaluation done on field and in laboratory.

3.1 LABORATORY EVALUATION (PROTOTYPE SECTION)

In this section the properties of the different materials used in the current study, as well as the sample preparation processes used, are discussed. The material characteristics are stated first, followed by a detailed discussion of the sample preparation techniques.

3.2 MATERIALS

The section covers the properties of all the materials (geocell, granular subbase and subgrade), used in the study discusses various tests performed in the thesis.

3.2.1 CHARACTERISTICS OF SUBGRADE SOIL

The subgrade soil was prepared and compacted at its required density, and placement water content was in a test tank measuring inner dimensions of tank. On the top of the subgrade soil, a granular

subbase layer, with and without geocell reinforcement, was prepared. The test bed configuration and the densities maintained will be discussed in the subsequent sections below.

3.2.1.1 SIEVE ANALYSIS

The particles size distribution of the soil was examined using a dry sieve analysis according to IS-2720 (Part4-1985). The particle size distribution of clayey soil, which contains around 40% fines (particles smaller than 75 micron sieve size), is shown in Fig. 3.1. Atterberg's limits test were used to classify the soil even further.

Figure 3.1(a) Sieve Shaker

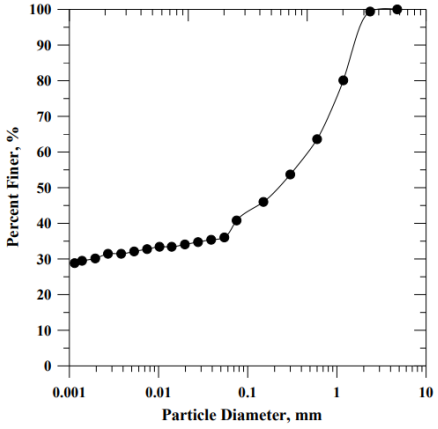

Figure 3.2 Sieve Analysis of the Subgrade soil

3.2.1.2 ATTERBERG'S LIMITS

IS-2720 (Part4-1972) was used to test Atterberg's limits, which included the liquid limit (LL) and the plastic limit (PL). Fig.3.2a shows images of apparatus used during tests. The soil flow curve is shown in Fig. 3.3b. The soil's liquid and plastic limits were found to be 47 and 21 percent, respectively. The soil's Plasticity Index, which is difference between Liquid limit and Plastic limit, was found to be 26%. Soil graded sand with clay, as per the Indian standard soil classification system (SC).

Figure 3.3 (a) Appararus used in Experiment

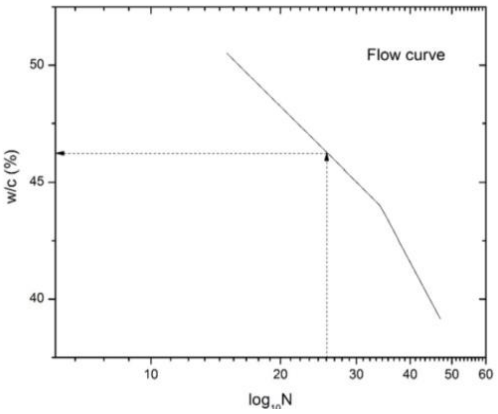

Figure 3.3 (B) Flow Curve of Soil

3.2.1.3 SPECIFIC GRAVITY

The specific gravity test is carried out in accordance with IS-2720 (Part3-1980), and the specific gravity is found out to be 2.655. The density bottle method is used to conduct this test, and the specimens used are shown in Fig.3.4.

Figure 3.4 Specific Gravity test by the density bottle method

3.2.1.4 COMPACTION CHARACTERISTICS (AUTOMATIC COMPACTOR TESTING)

The Standard Proctor compaction test used automatic compactor, which is conducted in accordance with IS-2720 (Part7-1980), is one of the laboratory methods of determining the maximum dry unit weight (MDU) and optimum moisture content (OMC). The soil is compacted in three layers in a 2200 cc compaction mould, with each layer receiving 25 blows from a conventional hammer weighing 2.6 kg and landing at a height of around 310 mm, according to the procedure.

Figure 3.5 Equipment used in the Automatic Compaction Test

Fig.3.5 shows pictures of the apparatus that is used during the test, whereas Fig.3.6 shows the relationship between unit weight and moisture content. According to the graph, the optimum moisture content (OMC) is 13.9 %, and the maximum dry unit weight (MDU) is 1.857 g/cc.

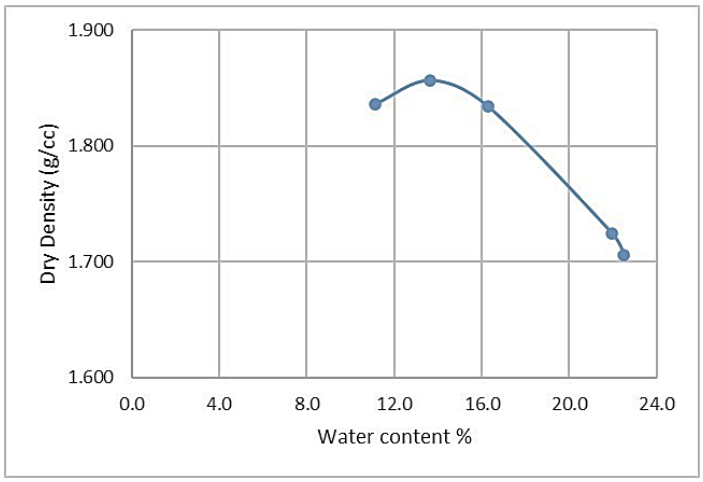

Figure 3.6 Relationship between unit weight and moisture content

3.2.1.5 CALIFORNIA BEARING RATIO

To measure the bearing resistance of subgrade soils, the California bearing ratio (CBR) test is conducted. As per the Indian Roads Congress (IRC) standards the design of flexible pavement design is based on this value. On the subgrade clayey soil, this test was carried out according to IS-2720 (Part16-1987). Figure 3.7a shows the CBR setup.

In soaked and unsoaked conditions, the CBR values are 4.9 percent and 7.8 percent, respectively. CBR of around 5.6% was considered for further analysis and design of the pavement section. The findings are presented in Fig.3.7b.

Figure 3.7a

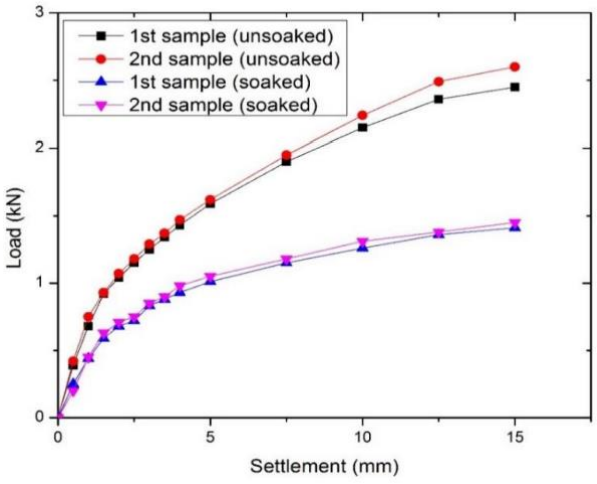

Figure 3.7b

Figure 3.7 CBR Testing of Soil

3.2.2 CHARACTERISTICS OF THE GEOCELL

High-density polyethylene (HDPE) strips are used to create the three-dimensional geo-synthetic material known as Geocell, which is then stretched on location to create a honeycomb structure. The infill material is bound by Geocell, which also acts as a lateral constraint for loading. The Geocell mattress utilized in this study is comprised of an HDPE polymer with a density of 0.935 to 0.965 gm/cm^3 and a 356 mm weld spacing. Throughout the test series, the cell height or depth was changed as 100 mm, 125 mm, and 200 mm, with a minimum cell strength of 2.1 KN. Figure 3.8 shows a typical geocell mattress adopted in the research.

Figure 3.8: Geocell used in this project.

3.2.3 CHARACTERISTICS OF GRANULAR SUBBASE

Granular Subbase (GSB) tests are conducted in compliance with MORTH specification 406.2.1.2. (Table 400-11). According to the MORTH, the aggregate must match the grading specified in Table 3.1 in order to be accepted as a subbase course material for the pavement. Aggregate material was obtained from a nearby retailer to regrade and bin the material in accordance with the MORTH's standards.

Table 3.1 Gradation of GSB as per MORTH

IS Sieve Size (mm)	Percentage Passing					
	Grading-I	Grading-II	Grading-III	Grading-IV	Grading-V	Grading-VI
75	100	-	-	-	100	-
53	80-100	100	100	100	80-100	90
26.5	55-90	70-100	55-75	50-80	55-90	75-85
9.5	35-65	50-80	-	-	35-65	55-75
4.75	25-55	40-65	10-30	15-35	25-50	30-55
2.36	20-40	30-50	-	-	10-20	10-25
0.85	-	-	-	-	2-10	-
0.425	10-15	10-15	-	-	0-5	0-8
0.075	<5	<5	<5	<5	-	0-3

3.2.3.1 COMPACTION CHARACTERISTICS

In accordance with IS-2720 (Part8-1980), the Modified Proctor compaction test which is a laboratory procedure for evaluating the maximum dry unit weight (MDU) and the optimum moisture content (OMC) are conducted. According to the process, the material was compacted in 5 layers using a 2250 cc compaction mould. Each layer received 56 blows from a 4.9 kg standard hammer that was dropped from a height of 450 mm. Figure 3.9 shows the relationship between unit weight and moisture content. The OMC is calculated to be around 6 percent and the MDU to be around 2.29 g/cc based on the graph.

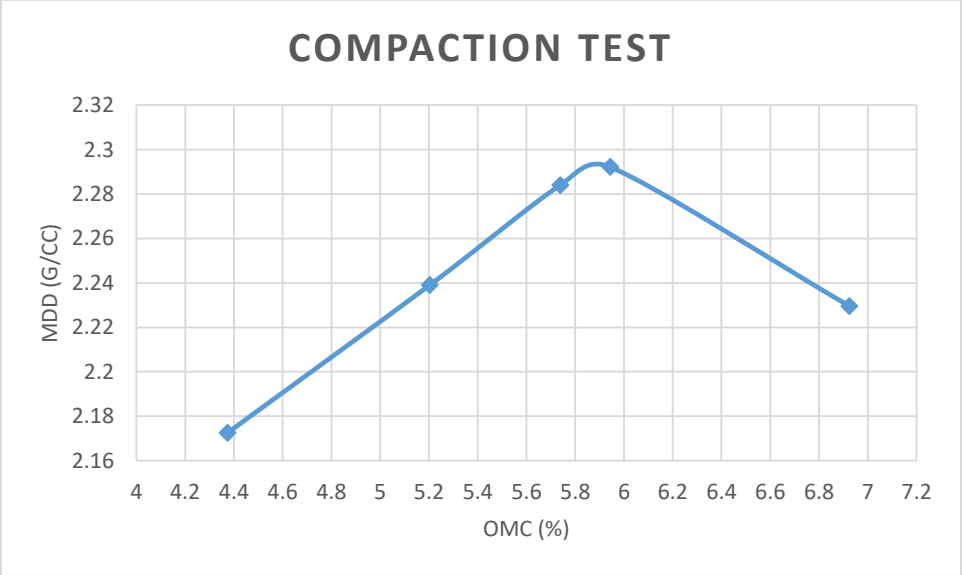

Figure 3.9 Relationship between unit weight and moisture content.

3.2.4 STONE DUST

Stone dust, often known as crusher sand, is a fine aggregate produced by stone crushers. Stone dust is predicted to be produced by each crusher unit at a rate of 15%–20%. Stone Dust consists of angular particles having more interlocking strength and improving density. By replacing soil with stone dust at varied mix proportions, it can be employed as a soil stabilizer to enhance the geotechnical qualities of the local soil. It is referred to as a mechanical stabilizer because it aids in the stabilization of the soil by improving its gradation, plasticity, and compaction properties. Stone dust is non-plastic and has a lower fraction of soil passing through a 0.075 mm sieve. When combined with stone dust, this improves the gradation and fluidity of the soil.

3.2.5 PROPERTIES OF AGGREGATES

Aggregates are a necessary part of every pavement. Aggregates are employed as stabilized or unstabilized sub-base material for each layer of pavement. The aggregates were evaluated to see if they could obtain basic property values that matched MORTH criteria and IRC codes. The aggregates used in the investigation came from the construction site of NHAI, Patiala.

The qualities of the aggregates employed in this study are evaluated using the following tests.

3.2.5.1 AGGREGATE IMPACT VALUE (AIV)

This test method was carried out in accordance with IS: 2386 Part 4. The AIV test yields a value for the aggregates' strength attribute when subjected to a sudden load. AIV represents the toughness of aggregates, which determines the material's ability to withstand a load or impact. The maximum impact value allowed is to be 18 percent. The Aggregate Impact Value is calculated using the average of the two test sample trials, and the resultant value of the test is calculated using the average of the two trials. Table 3.2 shows the findings of the Aggregates Impact Value Test.

Table3.2 Results of Aggregate Impact Value Test

Description	Trial 1	Trial 2
(a) Weight of Aggregates before testing , (gm)	420	420
(b) Weight of Aggregates that retained on sieve size of 2.36 mm, gm	374	370
(c) Weight of Aggregates that pass through sieve size of 2.36 mm, gm	51	58
Aggregate Impact Value (%), (c/a * 100)	12.14	13.8
Average Aggregate impact value; % (Max 18 %)	**12.97**	

3.2.5.2 SPECIFIC GRAVITY TEST

This test was carried out in accordance with IS: 2386 Part 3. The aggregate's specific gravity indicates material's strength. Aggregates with a higher specific gravity value appear to be more powerful than those with lower specific gravity values. At the specified temperature, it is the mass of a unit volume divided by mass of the equal volume of gas-free distilled water. It can also be

described as the difference between the densities of water and aggregate particles. The table below shows the results of the specific gravity test.

Table 3.3 Specific Gravity Result Value for Aggregates

S.No	Aggregate Size	Bulk Specific Gravity
1.	Coarse	2.635
2.	Fine	2.620
3.	Filler	2.580

3.2.5.3 WATER ABSORPTION TEST

This test procedure was carried out in accordance with IS: 2386 Part 3. This test identifies the porosity and strength property value of the aggregates. Aggregates with a lower water absorption test value are stronger, whereas those with a higher value have the property of being more porous and should not be used to build highways unless they pass the strength, impact, and hardness tests and are deemed acceptable. For the water absorption test, a maximum value of 2 % is permitted. The table below show the water absorption test result value.

Table 3.4 Water Absorption Test result value

Description	**Trial 1**	**Trial 2**
(a) Weight of saturated surface dry weight, g	2021	2025
(b) Weight of oven dry sample, g	2000	2000
(c) Water Absorption, 100*(a-b)/b	1.05	1.25
Average Absorption (%)	**1.15**	

3.2.5.4 FLOW CHART FOR THE CONSTRUCTION OF GRANULAR SUBBASE

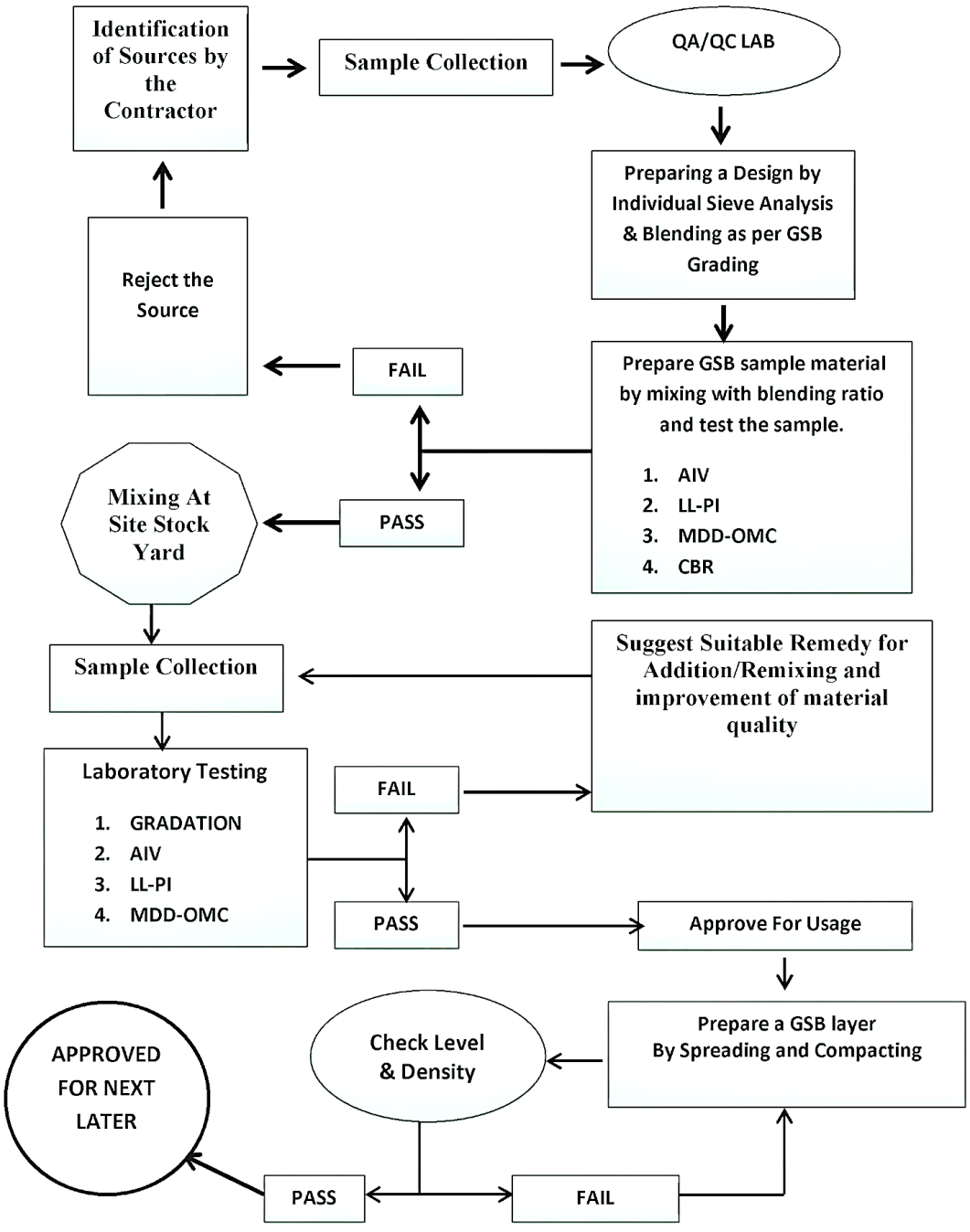

Figure 3.10 Flow Chart for the construction of Granular subbase

3.3 MIX DESIGN DATA

According to MoRTH guidelines, the GSB (Grade-I) mix's gradation has been adopted. Table 3.5 presents the adopted gradation for the GSB (Grade-I) mix, and Figure 3.12 shows the gradation graph. The midpoint gradation was selected because it showed excellent characteristics to the lower and higher point gradations.

Table 3.5 Gradation for GSB (Grade-I) as per MoRTH

Sieve Size (mm)	**Weight Retained (Kg)**	**Percentage Retained (%)**	**Cumulative Percent Retained (%)**	**Percent Passing (%)**	**Grade**	**Mid-point**
75	0	0.00%	0	100.00%	100	100
53	0	0.00%	0	100.00%	80 - 100	90
26.5	0.572	28.60%	0.286	71.40%	55 - 90	72.5
9.5	0.336	16.80%	0.454	54.60%	35 - 65	50
4.75	0.29	14.50%	0.599	40.10%	25 - 55	40
2.36	0.12	6.00%	0.659	34.10%	20 - 40	30
0.425	0.38	19.00%	0.849	15.10%	10 to 15	12.5
0.075	0.23	11.50%	0.964	3.60%	< 5	2.5

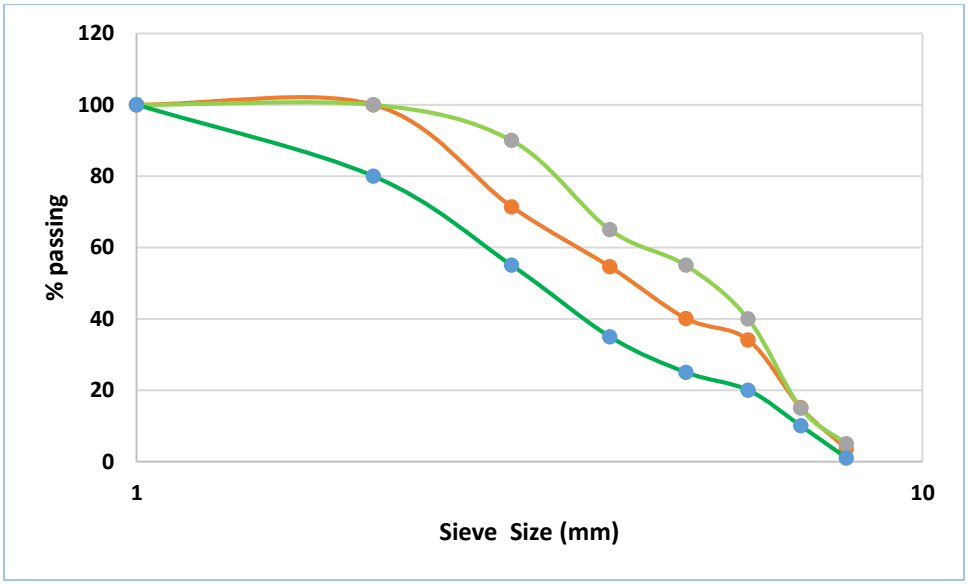

Figure 3.11 Design Gradation for GSB (Grade-I) mix as per MoRTH guidelines

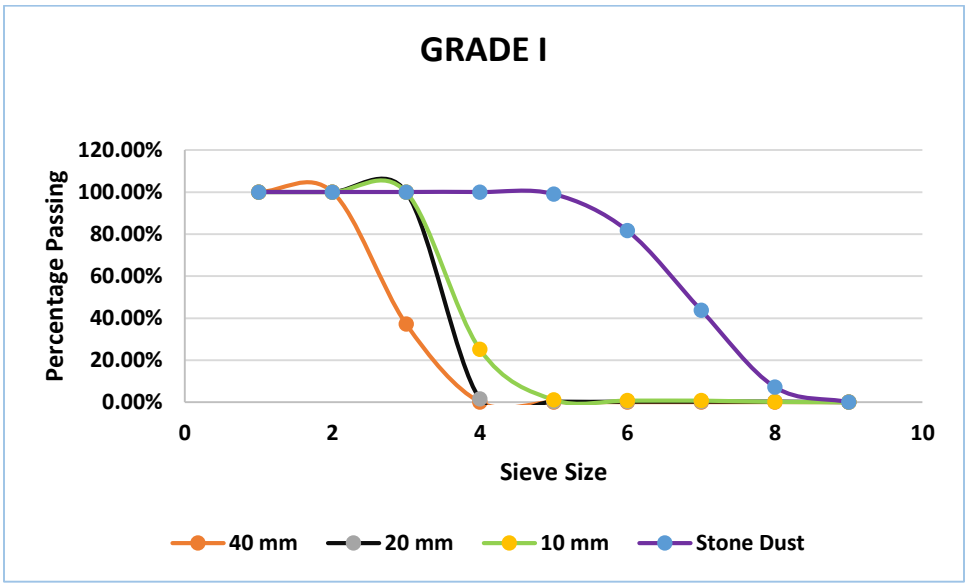

Figure 3.12 GSB (Grade-I) Sieve Analysis

Table 3.6 Design Details of Granular Subbase Material

S.no	Size of Aggregate	Blending Ratio
1	40 mm	30%
2	20 mm	10%
3	10 mm	25%
4	Stone Dust	35%

INDIVIDUAL GRADING OF 40 MM AGGREGATE

Table 3.7 Individual grading of 40 mm aggregate

40 mm Aggregate	Total Weight = 5 Kg			
Sieve Size (mm)	Weight Retained (Kg)	Percentage Retained (%)	Cumulative Percent Retained (%)	Percent Passing (%)
75.000	0.00000	0.00%	0	**100.00%**
53.000	0.00000	0.00%	0.00%	**100.00%**
26.500	3.14000	62.80%	62.80%	**37.20%**
9.500	1.86000	37.20%	100.00%	**0.00%**
4.750	0.00000	0.00%	100.00%	**0.00%**
2.360	0.00000	0.00%	100.00%	**0.00%**
0.425	0.00000	0.00%	100.00%	**0.00%**
0.075	0.00000	0.00%	100.00%	**0.00%**
Pan	0.00000	0.00%	100.00%	**0.00%**
Total	5.00000	100.00%		

INDIVIDUAL GRADING OF 20 MM AGGREGATE

Table 3.8 Individual grading of 20 mm aggregate

20 mm Aggregate	**Total Weight = 5 Kg**			
Sieve Size (mm)	**Weight Retained (Kg)**	**Percentage Retained (%)**	**Cumulative Percent Retained (%)**	**Percent Passing (%)**
75.000	0.00000	0.00%	0	**100.00%**
53.000	0.00000	0.00%	0.00%	**100.00%**
26.500	0.00000	0.00%	0.00%	**100.00%**

9.500	4.92500	98.50%	98.50%	**1.50%**
4.750	0.06200	1.24%	99.74%	**0.26%**
2.360	0.00000	0.00%	99.74%	**0.26%**
0.425	0.00000	0.00%	99.74%	**0.26%**
0.075	0.00000	0.00%	99.74%	**0.26%**
Pan	0.01300	0.26%	100.00%	**0.00%**
Total	5.00000	100.00%		

INDIVIDUAL GRADING OF 10 MM AGGREGATE

Table 3.9 Individual grading of 10 mm aggregate

10 mm				
Sieve Size (mm)	**Weight Retained (Kg)**	**Percentage Retained (%)**	**Cumulative Percent Retained (%)**	**Percent Passing (%)**
75.000	0.00000	0.00%	0	**100.00%**
53.000	0.00000	0.00%	0.00%	**100.00%**
26.500	0.00000	0.00%	0.00%	**100.00%**
9.500	3.74000	74.80%	74.80%	**25.20%**
4.750	1.20300	24.06%	98.86%	**1.14%**
2.360	0.01900	0.38%	99.24%	**0.76%**
0.425	0.00000	0.00%	99.24%	**0.76%**
0.075	0.03000	0.60%	99.84%	**0.16%**
Pan	0.00800	0.16%	100.00%	**0.00%**
Total	5.00000	100.00%		

INDIVIDUAL GRADING OF FINE AGGREGATE (STONE DUST)

Table 3.10 Individual grading of fine aggregate

Stone Dust				
Sieve Size (mm)	**Weight Retained (Kg)**	**Percentage Retained (%)**	**Cumulative Percent Retained (%)**	**Percent Passing (%)**
75.000	0.00000	0.00%	0	**100.00%**
53.000	0.00000	0.00%	0.00%	**100.00%**
26.500	0.00000	0.00%	0.00%	**100.00%**
9.500	0.00000	0.00%	0.00%	**100.00%**
4.750	0.04800	0.96%	0.96%	**99.04%**
2.360	0.87000	17.40%	18.36%	**81.64%**
0.425	1.89500	37.90%	56.26%	**43.74%**
0.075	1.82700	36.54%	92.80%	**7.20%**
Pan	0.36000	7.20%	100.00%	**0.00%**
Total	5.00000	100.00%		

BLENDING FOR GRANULAR SUBBASE MATERIAL (GSB I)

Table 3.11 Blending of Granular Subbase Grade-I

Rate of Blending (%)	**40 mm**	**20 mm**	**10 mm**	**Stone Dust**	**Total**	
	30%	10%	25%	35%	100%	
Sieve Size (mm)	**Weight Retained (Kg)**	**Percentage Retained (%)**	**Cumulative Percent Retained (%)**	**Percent Passing (%)**	**Grade**	**Mid-point**
75	0	0.00%	0	100.00%	100	**100**
53	0	0.00%	0	100.00%	80 - 100	**90**
26.5	0.572	28.60%	0.286	71.40%	55 - 90	**72.5**
9.5	0.336	16.80%	0.454	54.60%	35 - 65	**50**
4.75	0.29	14.50%	0.599	40.10%	25 - 55	**40**
2.36	0.12	6.00%	0.659	34.10%	20 - 40	**30**
0.425	0.38	19.00%	0.849	15.10%	10 to 15	**12.5**
0.075	0.23	11.50%	0.964	3.60%	< 5	**2.5**

3.4 LIGHT WEIGHT DEFLECTOMETER

During construction, light weight deflectometers (LWDs) are used to assess the stiffness of unbound materials such as subgrade/subsoils and base layers, granular layers, and backfilling materials. In the case of quality control and quality assurance of pavement construction, light weight deflectometer (LWD) devices are extremely useful. LWD devices are widely used because they provide the soil modulus mechanically through a simple device. LWD can determine both the vertical settlement value and the deflection modulus at the same time. In this study, the influence of LWD design variables on measured deflection and calculated modulus was investigated. According to the available literature, the use of LWD is expanding day by day in construction, both during construction and in service, all over the world. The device calculates a modulus value (Evd) based on the force required to cause a specific deflection in that soil type. Modulus is the most precise and independent method for determining deformation (stiffness) and, as a result, the material's compaction level. The Light Weight Deflectometer (LWD) establishes a direct link between the design specification (modulus value) and the actual site condition by measuring the modulus value.

Sub-grade materials are often classified according to (1) their resistance to deformation under load, also known as stiffness, or (2) their bearing capacity, also known as strength. In general, the more load a subgrade can support before reaching a critical deformation value, the more resistant it is to deformation.

3.4.1 LWD WORKING PRINCIPLES

The Light-Weight Deflectometer (LWD), dynamic plate loading test that was made to determine the modulus of soils and unbound fill materials (E_{LWD}). A typical LWD arrangement is shown in Annexure-1.

The test involves applying a pulse load to the soil using a disk-shaped plate of steel or aluminium plate. The loading mechanism consist of a drop weight which, when released, drops along a rod until it comes into contact with a spring dashpot unit. On a plate that rests on the ground, the spring

dashpot unit is installed. When the drop weight hits the spring dashpot unit, the LWD and ground begin to move together in a coupled mode. The two-degree-of-freedom (DOF) mass-spring-damper system behaviour of the LWD-ground system during loading and rebound lasts until the impact load is zero, at which point the system decouples.

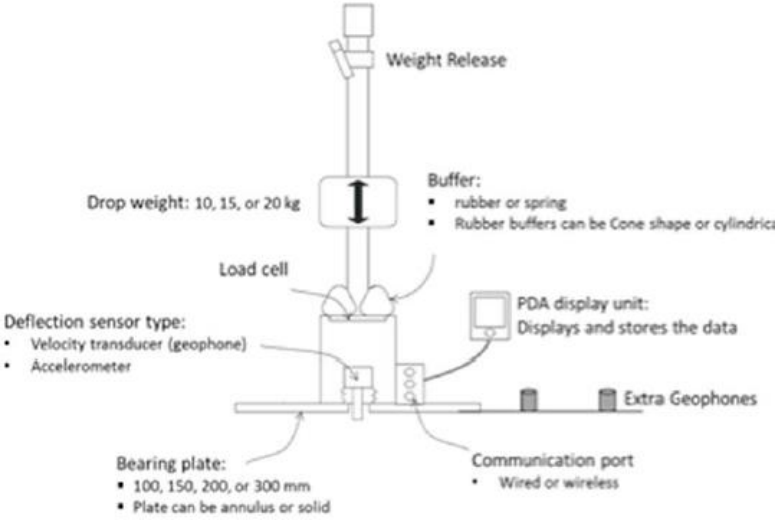

Figure 3.13 Diagram of LWD and its parts

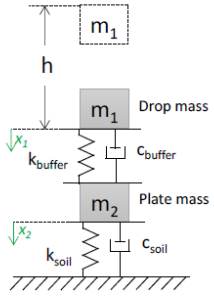

Figure 3.14 Schematic of the LWD-ground movement 2 DOF system

Based on the position of the sensors, accelerometer or velocity sensor captures the speed or acceleration of the plate or ground motions. Different LWD devices have different positions and types of deflection sensors. Using double/single acceleration/velocity integrations, the maximum displacement is calculated when the test is complete. A load cell is used to either estimate or

measures the load history and peak load. Additional geophones are provided on some models of LWDs to measure the surface deflection at various radial distances from the load's center.

Figures 3.15 and 3.16 show a deflection and peak time history and hysteresis example. The region in the hysteresis loop represents the energy loss resulting from material damping in the soil.

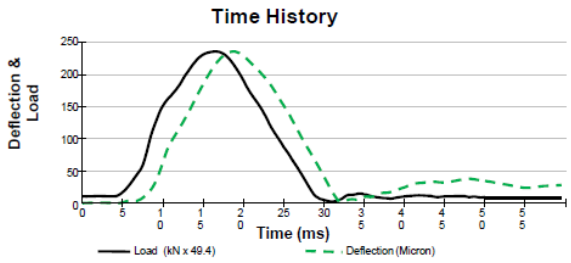

Figure 3.15 Example of load and deflection time history (from LWDmod software-Dynatest)

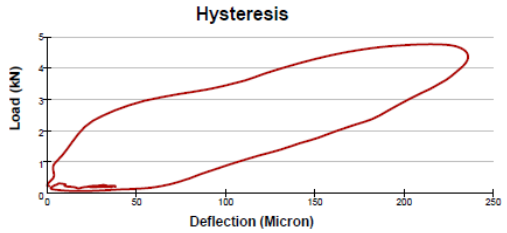

Figure 3.16 Example of load versus deflection hysteresis (from LWDmod software- Dynatest)

The modulus of subgrade or subbase layers is usually determined using LWDs. In other words, as portrayed in Figure 3.17, these are used to analyze 1 or 2-layer systems.

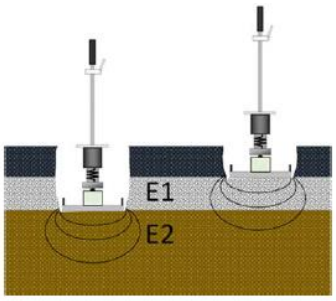

Figure 3.17 LWD testings on 1 layer and 2 layer systems

The Boussinesq equation is used to compute modulus:

$$E = \frac{2Ks\ (1 - v\text{^}2)}{Aro}$$

Where ks = $|F_{peak}/W_{peak}|$

A = is a stress distribution factor.

v = is the Poisson's ratio, and r_o is the plate radius.

In this equation, the test medium is taken to be a linearly elastic, isotropic, homogeneous semi-infinite continuum. The shape factor for the distribution of the contact stress between the plate and the soil (A) and Poisson's ratio (v), two of the parameters required for computing the modulus, are assumed.

The stress distribution coefficients (A) for various types of soils under the LWD plate are shown in Table 3.12

Table 3.12 Stress distribution factors for different soil types

Soil type	Factor (A)	Stress distribution Shape
Uniform (mixed soil)	π	
Granular material (parabolic)	3π/4	
Cohesive (inverse-parabolic)	4	

Burmister (1945) proposed the following formula for a two-layer system, here E_1 represents the modulus of the top layer with the thickness of h and E_2 represents the modulus of the underneath layer.

$$w_{0,0} = w_{0,h_c} + \left(w_{0,0} - w_{0,h}\right) = \frac{2\left(1-\upsilon^2\right)F_{peak}}{\pi r_0}\left\{\frac{1}{E_2\sqrt{1+\left(\frac{h}{r_0}\sqrt[3]{\frac{E_1}{E_2}}\right)^2}} + \frac{\left[1-\frac{1}{\sqrt{1+\left(\frac{h}{r_0}\right)^2}}\right]}{E_1}\right\}$$

Equation 3.1

3.4.2 CHARACTERISTICS OF THE STUDIED LWD

Table 3.13 Characteristics of the studied LWD

LWD	Total weight with 10 kg falling weight and plate				Falling weight	Max height
	100 mm	150 mm	200 mm	300 mm		
	(kg)	(kg)	(kg)	(kg)	(kg)	(cm)
Dynatest 3031	19.8	20.1	20.5	23.3	5, 10, 15. 20	83.8

Table 3.14 Dynatest 3031 (LWD) Specifications

LWD	Load Cell	Deforation sensor		Plate Type	Type of Buffer
		Type	Range		
	(-)	(-)	(mm)	(-)	(-)
Dynatest (3031)	Yes	Geophone + 2 additional	0 – 2.2 (+_ 0.002)	Annulus	Flat Rubber-adjustable

Figure 3.18 Shows Dynatest LWD (3031), including LWD set up with the optional geophone (picture courtesy of Dynatest Consulting Inc.)

3.5 MOISTURE CONTENT MEASUREMENT DEVICES

One of the most vital factors determining soil modulus is moisture content (MC). An appropriate rapid method of moisture content measurements must be used in field compaction QA procedures. The moisture content should be measured during placement just before compaction in order to manage variability and make sure it is within the approved specification range. After compaction, moisture content testing should be done in conjunction with LWD modulus measurement.

3.5.1 SPEEDY MOISTURE TESTER (SMT)

SMT evaluates the moisture content of a geomaterial by observing the change in gas pressure inside an airtight tank containing a mixture of soil sample and a calcium carbide reagent. There is no need for the external power source because it is portable. Many materials can be measured over a wide range of moisture content.

Figure 3.19 Rapid Moisture meter

3.6 TEST METHODOLOGY

To simulate field section in the laboratory, 0.9m x 0.9m X 0.9m rectangular tank was fabricated in the transportation lab of the Thapar Institute of Engineering and Technology. The tank could accommodate pavement layers subgrade and unreinforced and geocell reinforced subbase. Though the standard of the subgrade layer was maintained, the thickness of subgrade layer was maintained at 0.5 m; similarly, thickness of the Subbase layer varied depending on the height of the geocell selected. Different laboratory factors were investigated based on the combination proposed are shown in the table 3.15

Table 3.15 Factors Investigated in the experiment methodology

S.no	Factor	Mechanism	Means
1	Stress	Stresses at various locations on subgrade top will be examined.	The stress in the layers will be documented with the LWD testing
2	Height of reinforced subbase	The influence of Geocell reinforced subbase height on various properties will be studied.	Three different geocell heights (100 mm, 125 mm, and 200 mm) will be investigated.
3	Deflection and Modulus (LWD)	Stresses on the subgrade and GSB surface will be examined	Investigated with LWD testing machine.

3.6.1 PREPARATION OF TEST BEDS FOR DIFFERENT SIZES OF GEOCELLS

- Preparing of Calibration Charts
- Preparing Subgrade
- Preparing Granular Subbase layer

3.6.1.1 PREPARING OF CALIBRATION CHARTS

Initially of size 0.9m x 0.9m x 0.9m was used to calculate the number of blows required to obtain the maximum dry unit weight in the test tank. The pulverised soil was blended with the necessary amount of moisture before being placed into the tank to a thickness of 50 mm, where it was compacted using a hammer that weighed 5 kg and dropped from a free height of 50 mm. Three, five, and nine strikes were administered in several trials, and at each trial, two core cutters of various diameters were used to measure the unit weights. The relationship between the number of blows and the resulting unit weight was then determined using a graph. In Fig. 3.20, the calibration curve is displayed. From the graph, it can be easily inferred that 8 blows are needed to achieve a required unit weight (MDU) of 1.857 g/cc.

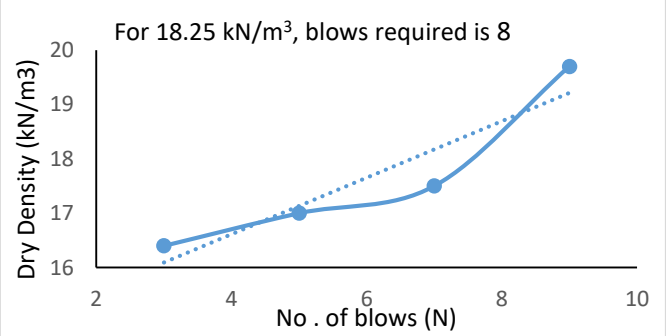

Figure 3.20 Calibration curve for subgrade

3.6.1.2 TEST BED PREPARATIONS

In a test tank with interior dimensions of 0.9 m x 0.9 m x 0.9 m, the subgrade soil is prepared and compacted to the required density and water content (length x width x height). The soil was placed in the large test tank and compacted in 5 cm thick layers until the desired height was obtained. The

required amount of soil to achieve the specified unit weight of 1.857 g/cc was weighed and placed in the tank for each layer. A 15 kg drop hammer was used to compress the soil for a predetermined number of strikes until the desired unit weight was achieved (8 blows). After each layer was compacted, the level was checked.

3.6.1.3 SUB-BASE COURSE PREPARATION

The subbase material is then dumped in test tank and compacted in 50 mm thick layers till the required height was obtained to construct unreinforced test bed. The required amount of aggregate for each layer was weighted out, mixed in the drum mixer (Figure 3.22), and placed in the test tank using a metal scoop to achieve the desired bulk unit weight of 2.29 g/cc. A hammer was then used to carefully level and compact the granular subbase course. The level was tested after each layer compaction. A drop hammer with a weight of 15 kg, a height of fall of 50 cm, and a plate size of 100 mm was used to compact the Geocell reinforced test bed to achieve a layer height of 50 mm, and so on. The level was verified again following the compaction of each layer.

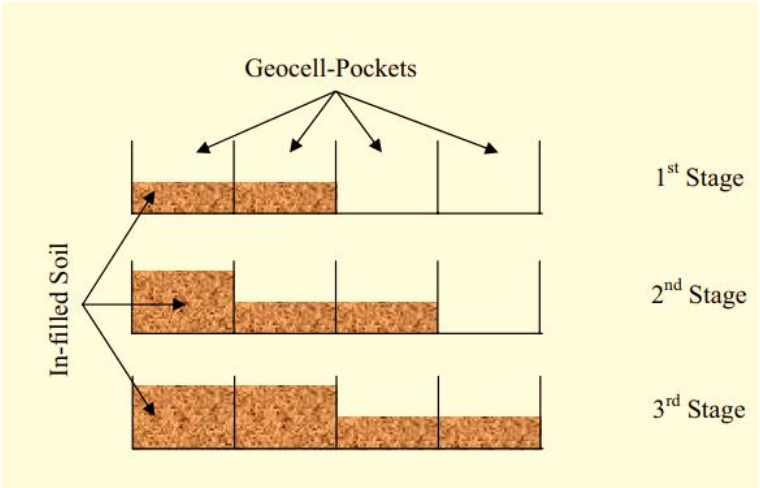

Figure 3.21 Sequence of soil in-filling

The test bed is prepared in five stages, as shown in Fig. 3.21; the first image is of an empty test tank with a volume of 0.729 m^3; the second stage involves compacting the soil for the subgrade bed; the third stage involves placing geocells on top of the subgrade; the fourth stage involves adding infill material to the geocell mattress; and the fifth stage includes compacting the subbase layer until the desired density is achieved.

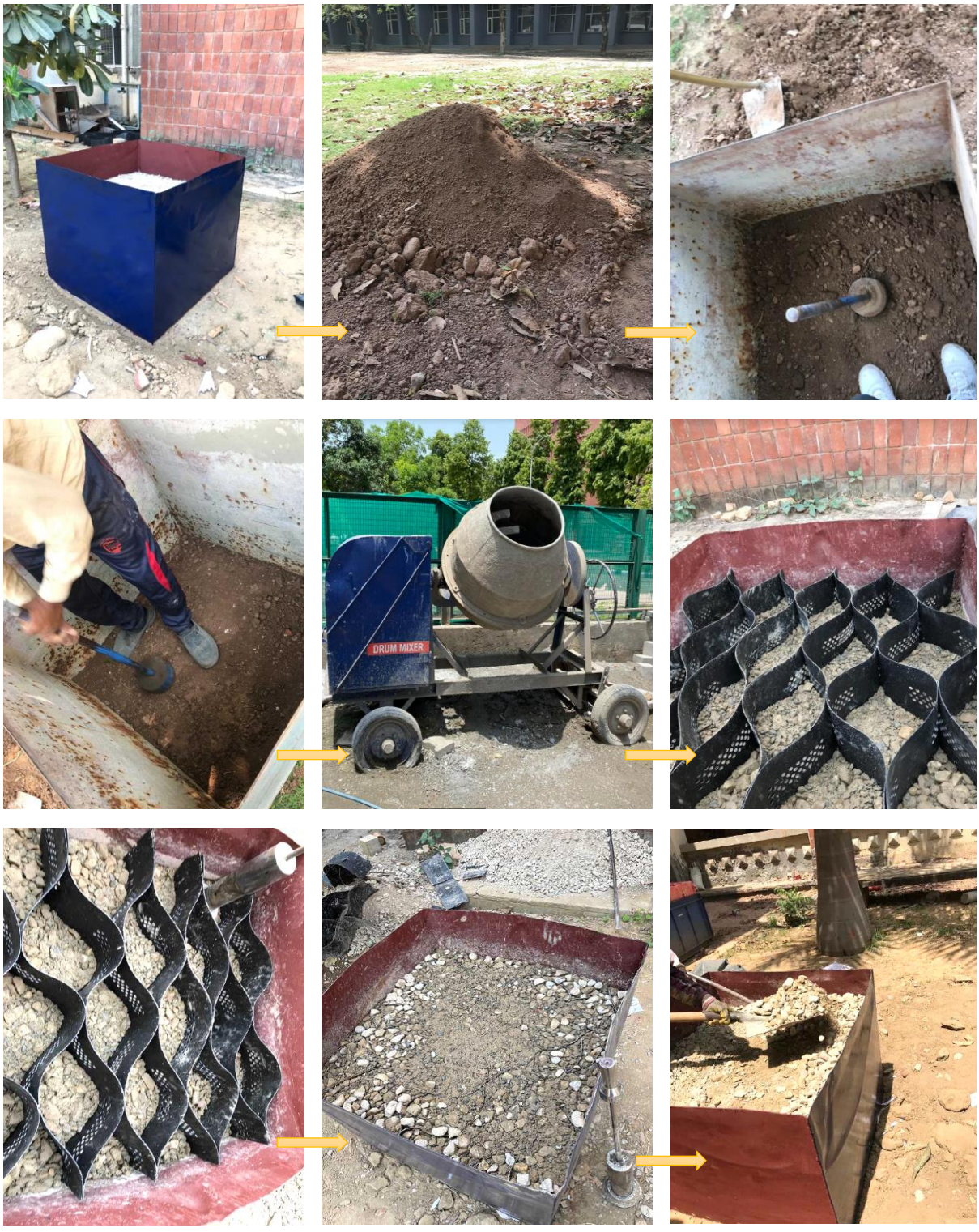

Figure 3.22 Staged Preparation of Test Bed

Figure 3.23 LWD Testing on GSB

3.7 PERFORMANCE MEASURES

Several performance indicators are offered to assess each reinforced test configuration's effectiveness in comparison to its similar unreinforced bed. The following sections discuss these variables in detail.

EQUIVALENT MODULUS IMPROVEMENT FACTOR

The ratio of the total elastic modulus of a reinforced test section (Er) to the total elastic modulus of an unreinforced test section (Eu) with the similar test setup is known as the equivalent modulus improvement factor (EMIF). The equivalent modulus improvement factor is utilised in the pavement test section to measure the effects of geocell reinforcement. This parameter is crucial when analyzing and designing pavement sections.

$$EMIF = \frac{Ereinforced}{Eunreinforced}$$

LAYER COEFFICIENT RATIO

The concept of layer coefficient ratio (LCR) is the ratio of reinforced to unreinforced layer coefficients. It serves as a gauge for the reinforced pavement layer's increased structural strength. It is determined by reinforcing subbase layers as follows:

$$\mathrm{LCR} = \frac{0.249\ log_{10}(EMIF.M_{r2}/0.0069) - 0.977}{0.249 log_{10}(M_{r2}/0.0069) - 0.977}$$

SUMMARY

Overall, a complete experimental programme has been analyzed and presented in this chapter to construct a practical pavement section for known CBR value of the subgrade.

3.8 FIELD EVALUATION

The project was expanded, and the installation of geocells along a section of NHAI Bughlada, Patiala Punjab, was included in the ongoing project. Instrumentation was used to demonstrate the benefits of geocell in pavements. The pavement was divided into 7 sections: a) 3 geocell reinforced, b) 3 unreinforced, and one section was left for subgrade testing. In addition, at the completion of the project, Light Weight Deflectometer (LWD) testing was carried out to check that the instruments were in functioning order. This section contains the location of the test section as well as construction-related information. The goal of the outdoor field tests was to investigate the possible effect of the following factors on the strength of the subbase layer: (1) Subbase course composition and (2) geocell reinforcement. The test was continued for a day, and all the observations were considered. To eliminate uncertain factors, human activities were restricted as much as possible, and the nearby activities involved were taken down.

3.8.1 SITE LOCATION AND MATERIAL PROPERTIES

SITE LOCATION

The geocell installation project took place on a local road in Bughlada, Punjab, which is a part of the NHAI construction work. Figure 3.24 depicts the position of the route within Punjab.

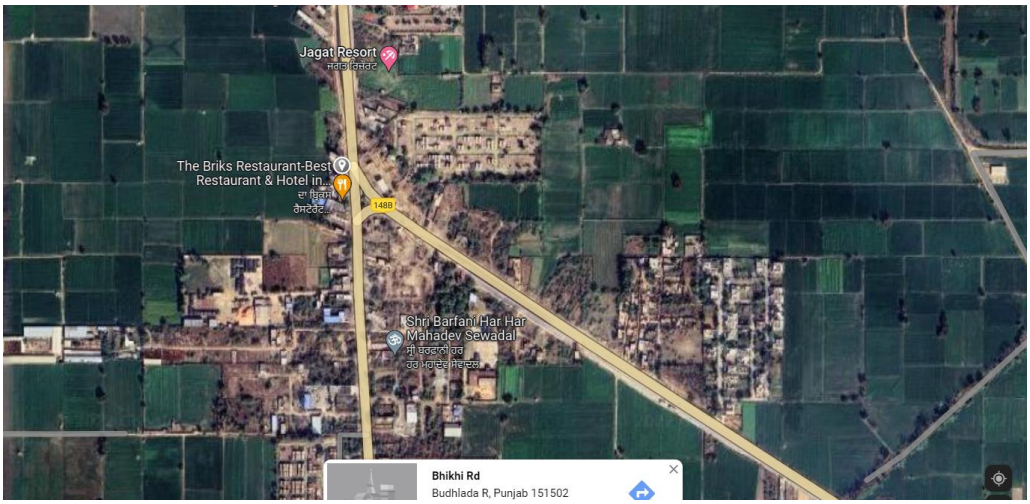

Figure 3.24 Shows the location of the site for field testing

3.8.2 SOIL CLASSIFICATION

At the construction site, subgrade and subbase material were collected and tested in the laboratory for soil classification, and the results are included in the following sections.

3.8.2.1 SUBGRADE SOIL CLASSIFICATION

The subgrade soil was classified using the proposed procedure in the Geotechnical Engineering Lab, Thapar Institute of Engineering and Technology. For the soil classification, a 500 g sample was employed. The soil is classified as poorly graded soil SP based on the gradation; 4 percent gravel, 69 percent sand, and 27 percent particles were found in the sample. The lab also determined Atterberg Limits. The liquid limit (LL) and plastic limit (PL) of the soil were 21 and 0, with a plastic limit (PL) of 21. As a result, the soil is classified as sand with clay that is poorly graded (SP-SC).

3.8.2.2 SUBBASE MATERIAL CLASSIFICATION

The gradation of the mix is satisfactory as per table 400-1 (Gradation 1). The maximum dry density and optimum moisture content are 2.185 gm/cc (avg.) and 6 % (avg.), respectively. The aggregates plasticity index indicates that it is Non-Plastic. Also, the AIV test was conducted, and 18.11% was the obtained value of the mix tests.

3.9 INSTRUMENTATION

3.9.1 GEOCELL: The geocell manufacturer used in this study is (Terrain Infratech), the same geocell used in laboratory testing analysis. Chapter 3 lists the properties of the selected geocell.

PAVEMENT SECTION

The stretch is constructed with geocell, and the pavement profile is shown in Figures 3.25. The pavement profile consisted of subgrade of 500 mm and 100 mm, 125 mm and 200 mm unbound granular subbase layer. In addition, an equal portion length of unbound unreinforced 30 m was left untreated. Approximately 30 m of the unbound section was constructed without geocell, while another 10 m was left as virgin of subgrade only for LWD testing (Figure 3.25).

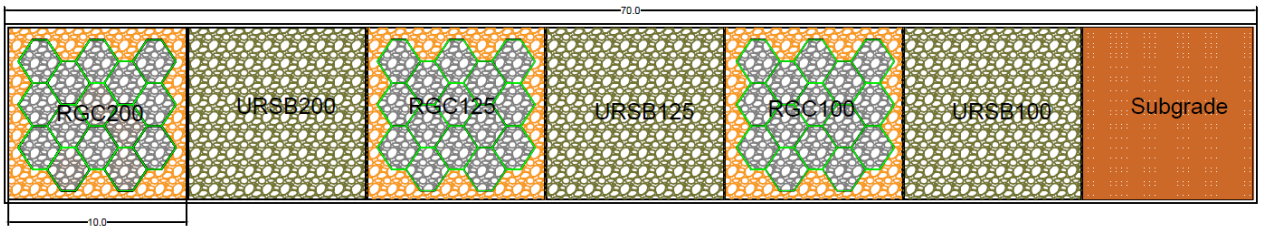

Figure 3.25 Test Section, Pavement Section of Geocell-Reinforced at Testing Site.

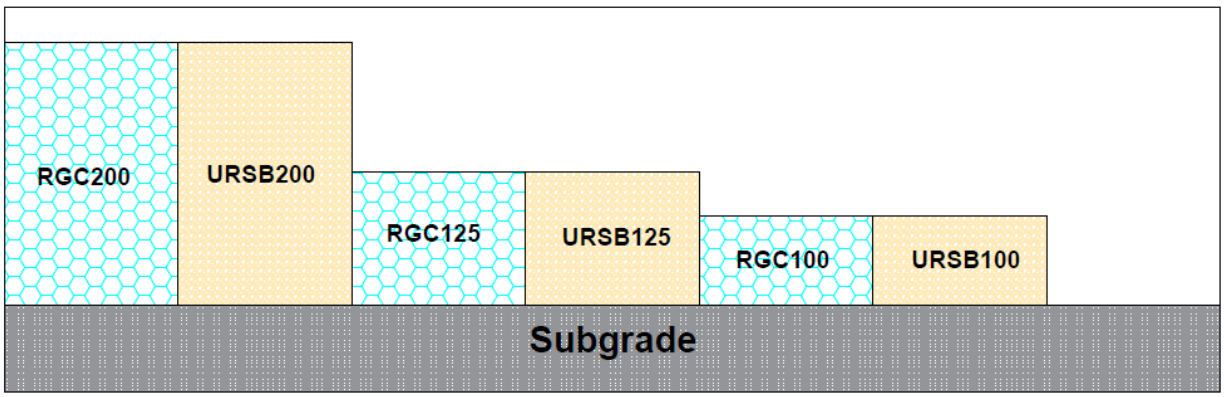

Figure 3.26 Cross section Pavement cross-section at Testing Site

Figure 3.26 shows the geocell layout arrangement in the test section and the placement of the geocell in the unreinforced section.

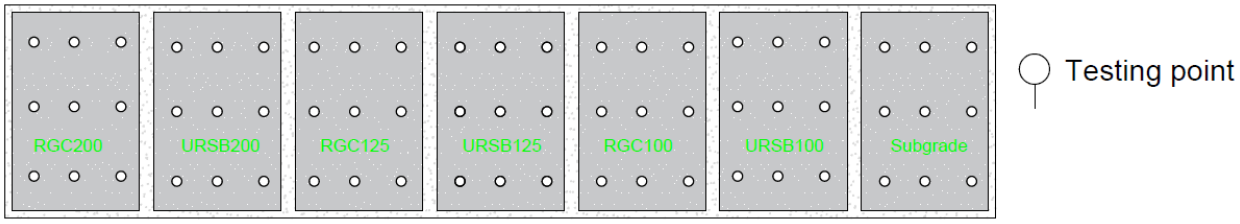

Figure 3.27 Cross Section and Instrumentation of the stretch at Testing Site for both unreinforced and reinforced Section

Figure 3.27 represents the cross-section of the geocell reinforced section of the pavements at the test site. Also, the LWD testing point's location in different sections along the entire stretch is shown in Figure 3.27

3.9.2 CONSTRUCTION OF REINFORCED AND UNREINFORCED SECTIONS

SCOPE OF WORK

- This work involves placing and compacting well-graded material on a prepared subgrade according to the specifications.
- The Grade I material shall be laid in one layer as a subbase

MATERIALS

- The material to be used as subbase coursework shall be crushed stone and stone dust
- The material is free of organic or other harmful constituents and meets grading requirements.

3.10 CONSTRUCTION WORK

3.10.1 PREPARATION OF SUBGRADE

The subgrade is prepared immediately before laying the sub-base by removing all vegetation and other extraneous debris, softly watering if necessary, and rolling with two passes of 10 Ton smooth wheeled roller. Figure 3.28 & 3.29 show the complete process of subgrade preparation.

Figure 3.28 Subgrade Preparation on site

Figure 3.29 LWD Testing on prepared Subgrade

3.10.2 UNREINFORCED SECTION INSTRUMENTATION

The construction at the field site proceeded by excavating the soil to the required depth. On an experimental basis, a nearly 70 m stretch of this road was treated with a 100 mm, 125 mm, and

200 mm thick geocell layer to evaluate the performance improvement. Field studies were carried out in a section of plan area 1.5 m X 70 m to study the influence of geocell layout and aspect ratio on the modulus of the reinforced sections.

The walls of the geocell are around 2 mm thick. The pocket size is 250 mm^2, and the c/c weld distance is 330 mm. Opening dimensions are approximately 244 & 210 mm. The tensile strength of the geocells material in the strip tension test was found to be 25 kN/m (ASTM D638-2003), and the peel strength of the weld is 20 kN/m from ASTM D6392-99 standard tensile strength tests. Also, the seam peel strength tested is 1065 N. There was no change of dimensions when pieces of the geocell were exposed to 100uC temperature in an oven for a 1-hour duration (ASTM D1204). Polyethylene strip is perforated with horizontal rows of a maximum of 10mm diameter holes. Cell perforations area is less than 12% of cell surface area. The polymer density tested provides a value of around 0.935 – 0.965 $g/cm^{3.}$

Figure 3.30 Unreinforced Section Instrumentation

3.10.3 REINFORCED SECTION

To ensure that the geocells were fully stretched, geocells were stretched, and rebar was placed to maintain the stretched condition. The rebars were removed after the geocells were installed, and pegs were used to keep the width of the geocells uniform. The contractor then started transporting material and filling geocells closer to the median, continuing until the shoulder was reached (Figure 31a, 31b, 31c, 31d, and 31e).

Figure 31(a) Laying of Geocell

Figure 31(b) Spreading and Anchoring of Geocell

Figure 3.31 (c) Filling of geocell and Spreading of GSB layer

Figure 31(d) Rolling and Compaction of the Surface layer

Figure 31(e) LWD tesing at different locations of the stretch

3.10.4 MIXING OF MATERIAL

Each material is mechanically blended by volume. The volumetric proportion is determined by a trial in the stockyard on the job site. After which the stock of graded GSB material is prepared after determining the GSB material's mixing ratio, and after preparing the GSB material, the grading of the prescribed design must be checked to ensure a homogeneous and consistent mix. Figure 3.32 shows the mixing and filling of geocells.

Figure 3.32 Mixing and Filling of materials

3.10.5 SPREADING AND COMPACTING

The desired grading of the sub-base material specified is spread on the prepared subgrade with the support of a grader of sufficient capacity (Figure 3.33), with a blade installed with hydraulic controls suitable for initial adjustment and maintaining the required slope and grade throughout the operation. The moisture content of the granular materials is checked in accordance with IS: 2720 (Part II) and is suitably adjusted by sprinkling additional water from a truck-mounted or trailer-mounted water tank capable of applying water uniformly and at controlled quantities to variable widths of surface so that it is between 1% and 2% of the optimum moisture content (OMC) corresponding to at the time of compaction.

Rolling begins immediately, and for a compacted single layer up to 200 mm, compaction was achieved with the help of a vibratory roller with a static weight of at least 8 to 10 tonnes capable of providing the desired compaction. The rolling shall commence at the lower edge and proceed towards the upper edge longitudinally for portions having unidirectional cross-fall and super elevation and shall commence at the edges and progress towards the center for portions having cross-fall on both sides. Each roller pass covers not less than one-third of the track laid out in the previous pass. The grade is monitored during the entire rolling, and any high spots or depressions that appear were fixed by removing or adding new material. The roller's speed did not exceed more than 5 km per hour. Rolling was continued until the density was achieved at least 98 percent of the material's maximum dry density as specified by IS: 2720 (Part 7).

Figure 3.33 Filling of Geocells

Figure 3.34 Spreading of aggregate materials

Figure 3.35 Spreading and preparing geocell reinforced sections

Figure 3.36 Rolling and Compaction of Prepared GSB

Figure 3.37 Aerial View of the site

Figure 3.38 Aerial View of the Site

3.11 DATA COLLECTION AND ANALYSIS

The team went to the site to test the working of the LWD after the construction and compaction of the geocell reinforced layer. The LWD testing was performed on top of the geocell reinforced and unreinforced subbase layer. The purpose of LWD tests was to measure the response of subbase characteristics and obtain a section profile (of seven pavement sections). To measure profile, the LWD tests were performed at every 9 points in each section of 10 m by dropping three seating loads and three drops for measurement. To ensure the LWD load plate was placed at top of the geocells, the cells' locations were marked on the surfaces, and the LWD operator was guided to place the load plate on top of the cells as close as possible. Each LWD test included three seating drops and three measurements with approximately 20 Kg of the load. Additionally, the LWD tests on the top of the subgrade were conducted for analysis of subgrade compaction characteristics.

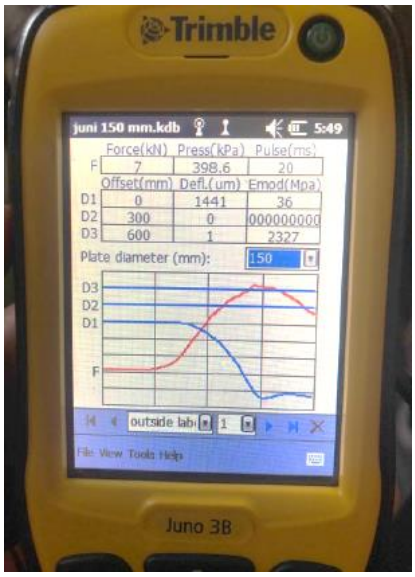

Figure 3.39 Shows a typical reading on the JUNO to a drop.

The profile data from the LWD testing was entered into the MODULUS software to estimate the modulus of the subbase, subgrade, and influence of reinforcement on the subbase modulus in order to evaluate and validate the data collected from the LWD testing device. The LWDmod software was used to identify the deflections and modulus generated at the testing points due to the applied LWD load using the modulus values acquired from the JUNO after corrections were applied to the values obtained on site.

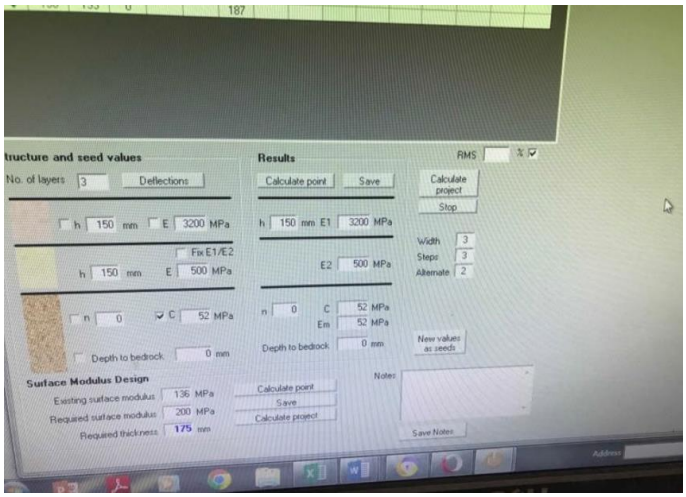

Figure 3.40 Input Data in LWDmod software

The subsequent chapter shows the modulus values generated using modulus software for unreinforced pavement, reinforced pavement, and subgrade sections in the tabular form. It can be seen that the reinforced layer exhibits a higher modulus in comparison to the unreinforced pavement section.

According to the values, the subgrade modulus is approximately 40.3 MPa for the unreinforced section, and geocell reinforced section. The load plate for the LWD was considered to be 300 mm dia., and load values were calculated by the device itself.

A comparison of no geocell and geocell sites confirmed the comparison reaction. Overall, the results indicate that the magnitude of deflections is smaller in the geocell reinforced section. In order to determine appropriate dimensions of the test pits, a three-dimensional model was established for a finite element analysis (FEA). Since the finite element model is symmetric, the finite element can be analyzed in 3-D. The material is assumed to be homogeneous and elastic. Two types of boundary conditions between the tested material and the surrounding soil were utilized in the analysis. One condition was that the vertical friction between the material and the soil was zero (frictionless), and the other one was that the material and the soil were fully bonded. The FEM model characteristics of the unreinforced and reinforced geocell layers are explained in chapter 6 of this report.

CHAPTER 4

RESULTS AND DISCUSSIONS

4.0 GENERAL

Light Weight Deflectometer testing was performed on the unreinforced and geocell reinforced pavement test sections prepared according to the design approach used to calculate the equivalent modulus improvement factor (EMIF). The results of the LWD are presented in Fig. 4.22 as modulus improvement factors for the unreinforced and geocell reinforced test sections, respectively. The load in the reinforced test section is as high as 10 N at 322-micrometer settlement, as shown in Fig. 4.8. At the settlement (541 microns), the bearing pressure in the case of an unreinforced test section is found to be 155.1 kPa. This finding indicates that the presence of geocell reinforcement increased bearing pressure by about 1.6 times that of the control section at 322-micrometer settlement.

The linear or elastic region of the stress-strain plots obtained for both the reinforced and unreinforced test sections is used to calculate the elastic modulus. As the stress-strain curves for the LWD test results obtained from the unreinforced and reinforced test sections are shown, the elastic modulus obtained in both circumstances is the equivalent module of the complete pavement test section. The EMIF is the ratio of the reinforced section's elastic modulus to the unreinforced section's elastic modulus. In comparison to the control test section, the geocell reinforced test sections had an EMIF of nearly 1.5. As a result, the inclusion of geocell reinforcement can be inferred to have improved the stiffness of the subbase course layer.

In this chapter annotations has been provided to different sections which includes URSB100, URSB125 and URSB200 for Unreinforced subbase sections and similarly RGC100, RGC125 and RGC200 for Reinforced Geocell Sections. The coding 100, 125 and 200 represents the thickness of the layers respectively followed by the type of section.

Furthermore, in order to maintain the same stiffness as unreinforced test sections, the thickness of geocell reinforced subbase layers can be reduced to the point where an EMIF greater than 1 can

be maintained. As a result, the reinforced test section's subbase course thickness was lowered from 200 mm to 100 mm, and LWD tests were performed on the test sections. As a result, the subbase course thickness of the reinforced test section was reduced from 200 mm to 100 mm, and LWD tests were conducted on all the test sections again. The experimental program is briefly divided into two stages, as shown in the table below.

Table 4.1 Experimental Program Stages

Stage	LWD Testing	Configuration
1	Lab Testing	Unreinforced test section having 100, 125, and 200 mm thick subbase course. Reinforced test section having 100, 125, and 200 mm thick subbase course
2	Field Testing	Unreinforced test section having 100, 125, and 200 mm thick subbase course. Reinforced test section having 100, 125, and 200 mm thick subbase course.

The figure 4.1 shows the pictorial representation of the experimental program performed in this entire project.

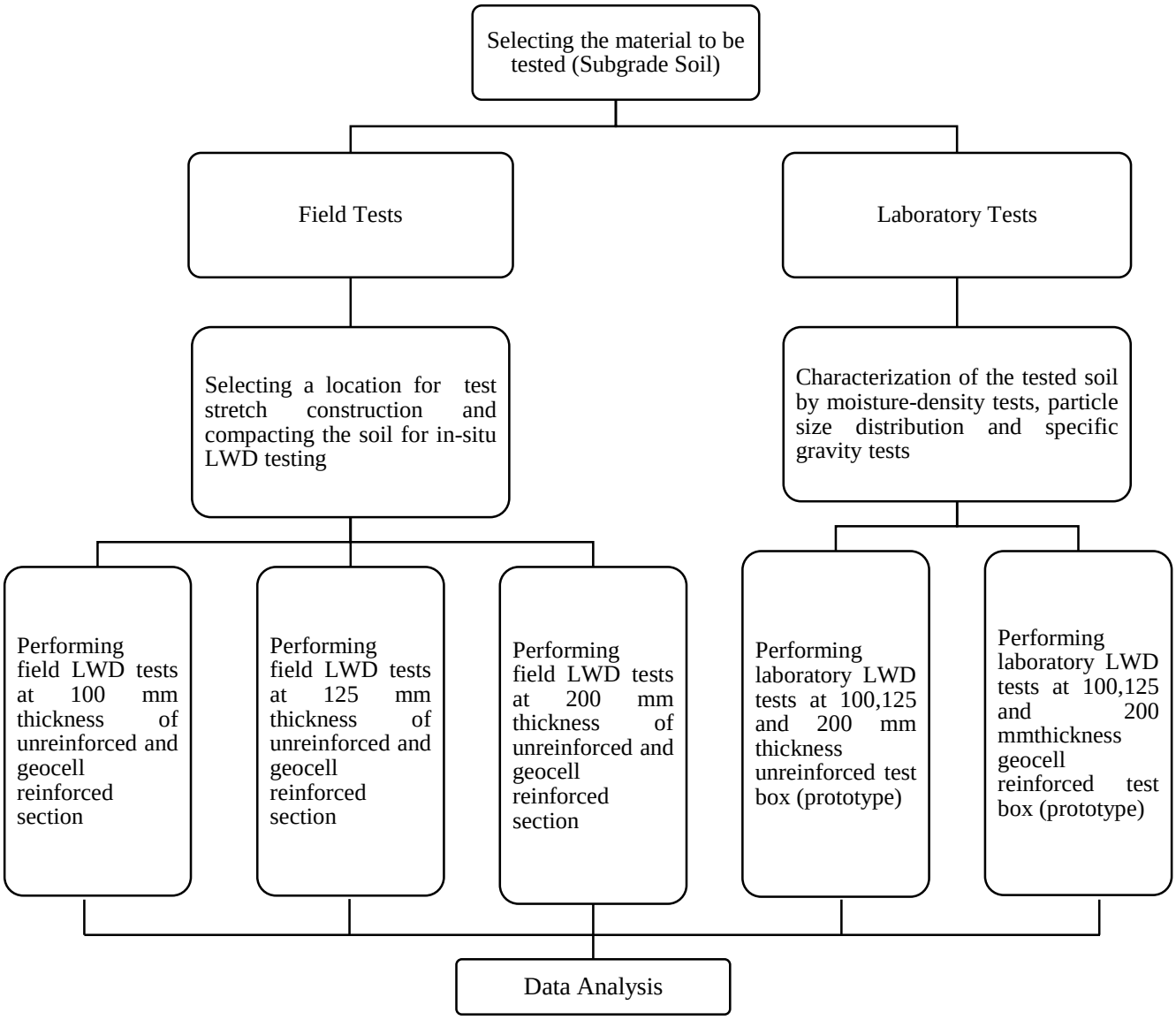

Figure 4.1: Graphical representation of experimental program

4.1 PERFORMANCE RESULTS FOR LWD TESTING

The following performance test has been carried out in this study on the different sections of unbound GSB layer. In this study, two performance tests were conducted, which included field and laboratory (prototype) sections in which moduli and deformations value were evaluated.

4.2 LABORATORY TESTING (PROTOTYPE EVALUATION)

Light Weight Deflectometer tests were conducted on an unreinforced test sections with a 100mm, 125 mm, and 200 mm thick Subbase course (Fig 4.2, 4.3, 4.4) and a geocell reinforced test section with the same thickness subbase course (Fig. 4.5, 4.6, 4.7) in the first stage to determine the effect of geocell reinforcement on subbase layer stiffness and to investigate geocell performance under loading conditions.

The loads were applied on the test sections with the help of a 20 Kg weight falling on the 300 mm dia plate, and the corresponding load applied is noted. The modulus obtained for the test sections is shown in Figures below. It can be observed that for the same level of settlement, the reinforced section is bearing more pressure than the unreinforced one.

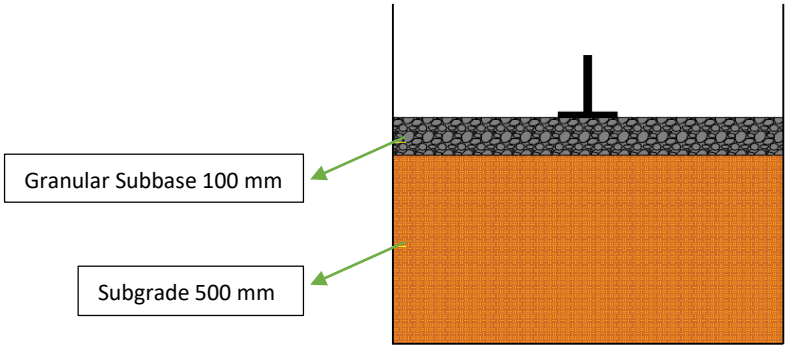

Figure 4.2. Unreinforced test section used in the study

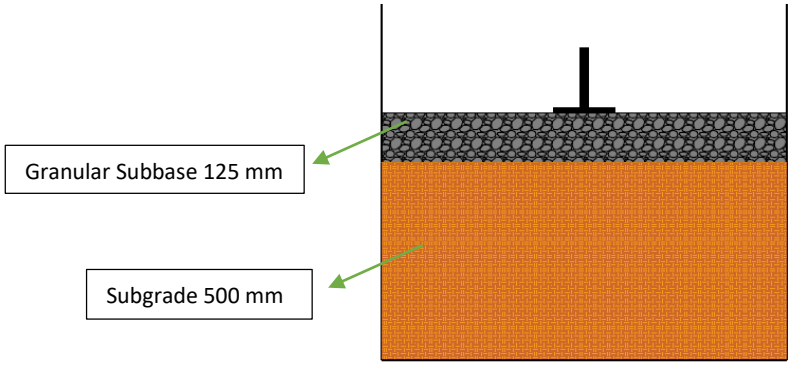

Figure 4.3 Unreinforced test section used in the study

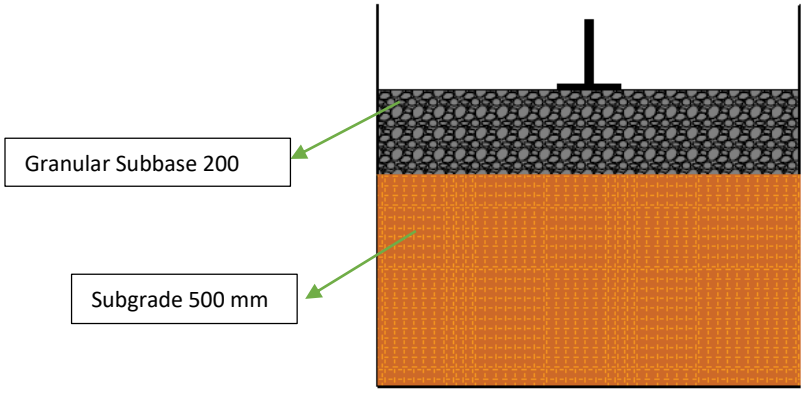

Figure 4.4 Unreinforced test section used in the study

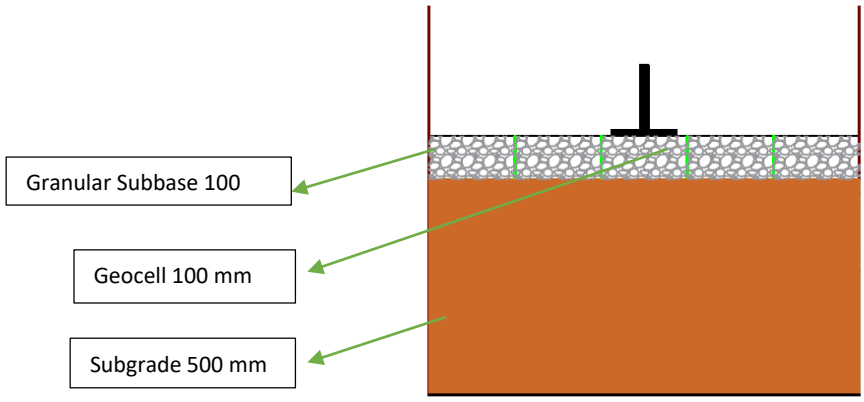

Figure 4.5 Reinforced test section used in the study

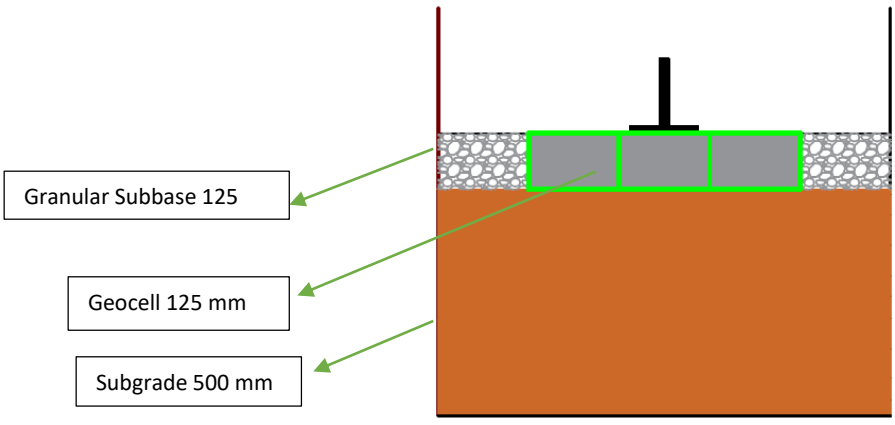

Figure 4.6 Reinforced test section used in the study

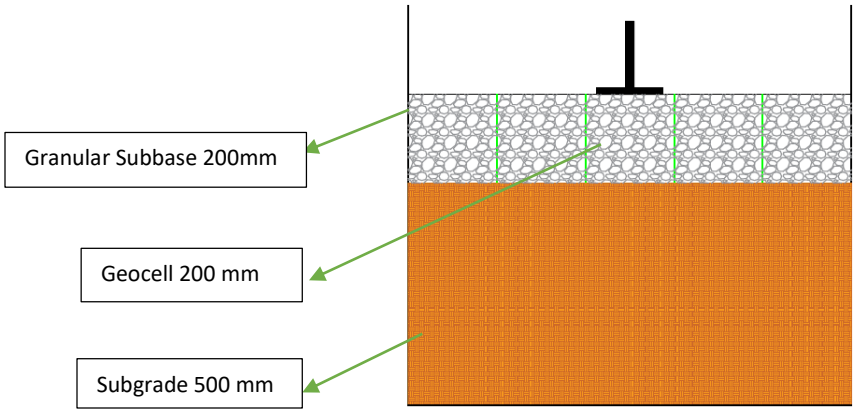

Figure 4.7 Reinforced test section used in the study

The deformation profile for both unreinforced and geocell reinforced test sections were obtained with the help of the LWD placed on the surface layers. Figure 4.8 presents the profile for the unreinforced test section in the form of bars. It can be observed from Fig. 4.8 that with the increase in the pressure applied, the deflection gets deeper, i.e., the settlement is high. However, the settlement is mainly observed below the loading region, and the settlements are observed to be very less to negligible on either sides of the loading region.

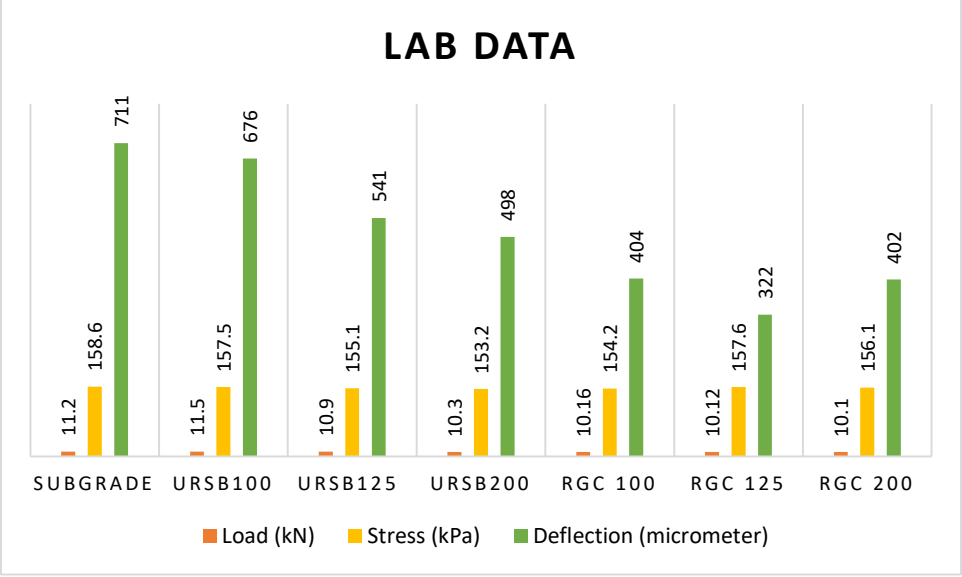

Figure 4.8 Deformation profile of Unreinforced and Reinforced Sections

Fig. 4.8 presents the deformation profile of the geocell reinforced test section. Further, with the increase in applied pressure, the settlements in the unreinforced sections have increased drastically compared to the geocell reinforced section. From this observation, it is inferred that the presence

of geocell reinforcement in the subbase layer has improved the stiffness of the subbase layer and, in turn, has reduced the surface settlements of the test section.

4.2.1 LAB TEST MODULUS RESULTS

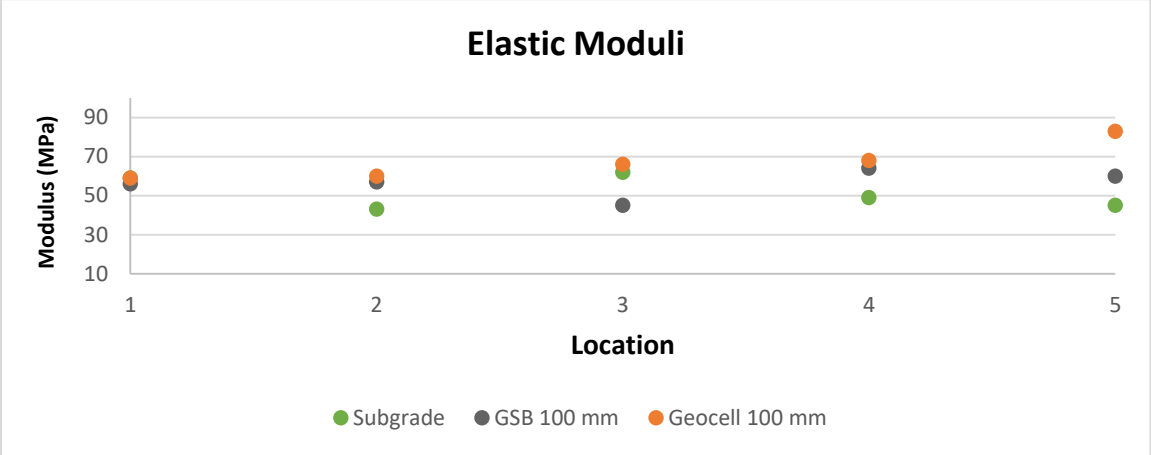

Figure 4.9 Elastic Modulus calculated at different locations of the test box for 100 mm thickness

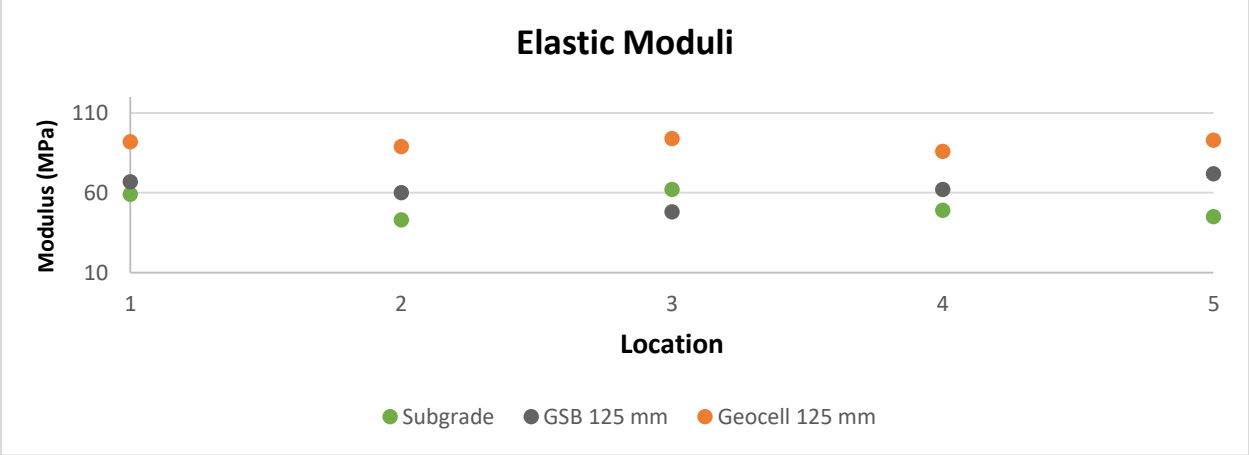

Figure 4.10 Elastic Modulus calculated at different locations of the test box for 125 mm thickness

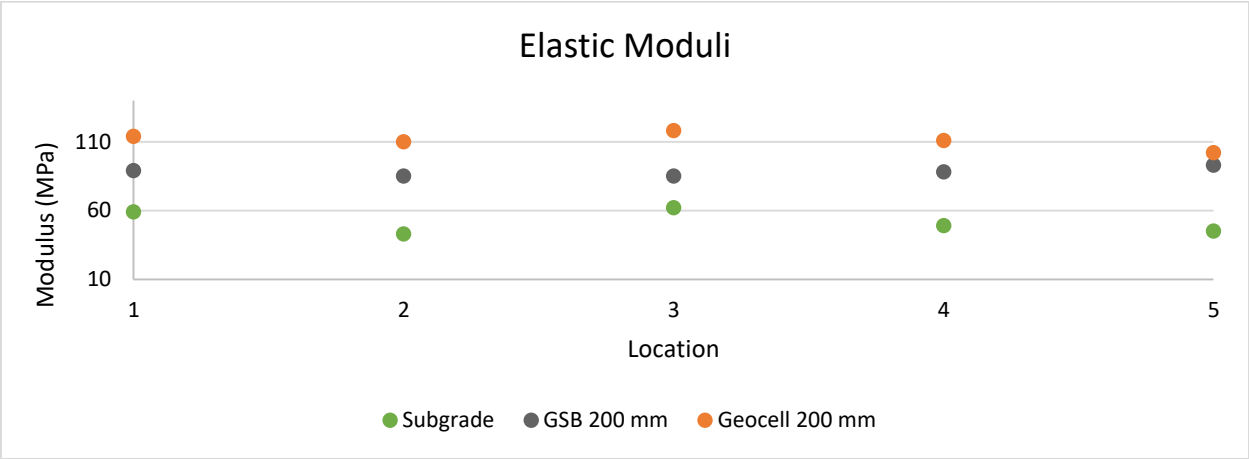

Figure 4.11 Elastic Modulus calculated at different locations of the test box for 200 mm thickness

Similarly, the pressure distribution pattern at the subgrade level for various intensities of load applied on the geocell reinforced test section shows that there is an increase in the pressure intensities recorded with an increase in the applied pressure. However, the pressure distribution patterns in the reinforced section are observed to be less narrow, unlike the pressure distribution patterns of the unreinforced section.

4.3 FIELD TEST RESULTS

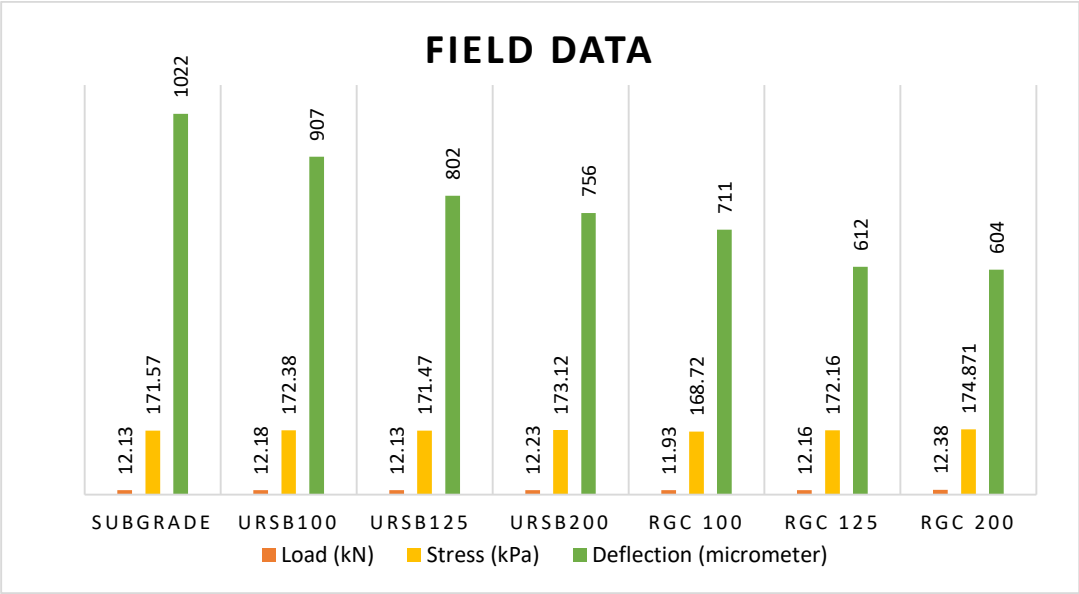

Figure 4.12 Deformation profile of Unreinforced and Reinforced Sections

From Fig. 4.12, it can be visualized that the pressure experienced at the subgrade level at all the specified locations is less in the reinforced pavement section than in the unreinforced section. It indicates that the geocell reinforcement is capable of distributing the loads to a wider area which in turn helps in reducing pressure intensities observed at the subgrade level.

4.3.1 FIELD EMOD VALUES

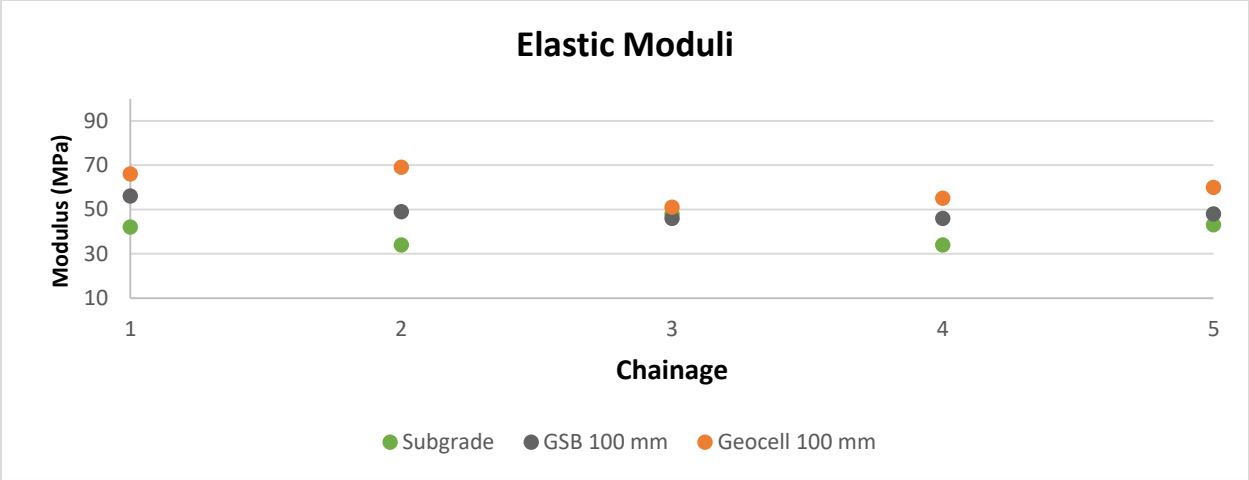

Figure 4.13 Elastic Modulus calculated at different locations of the test box for 100 mm thickness

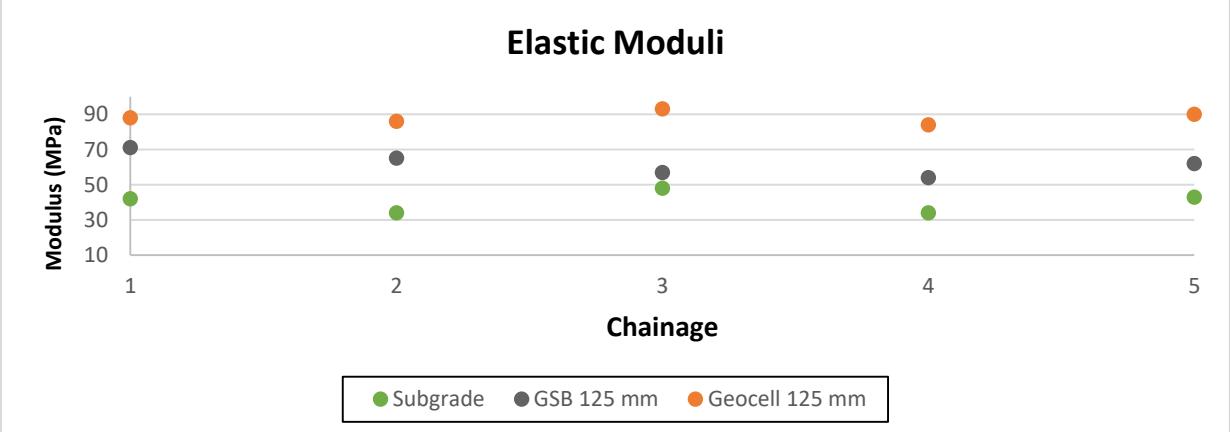

Figure 4.14 Elastic Modulus calculated at different locations of the test box for 125 mm thickness

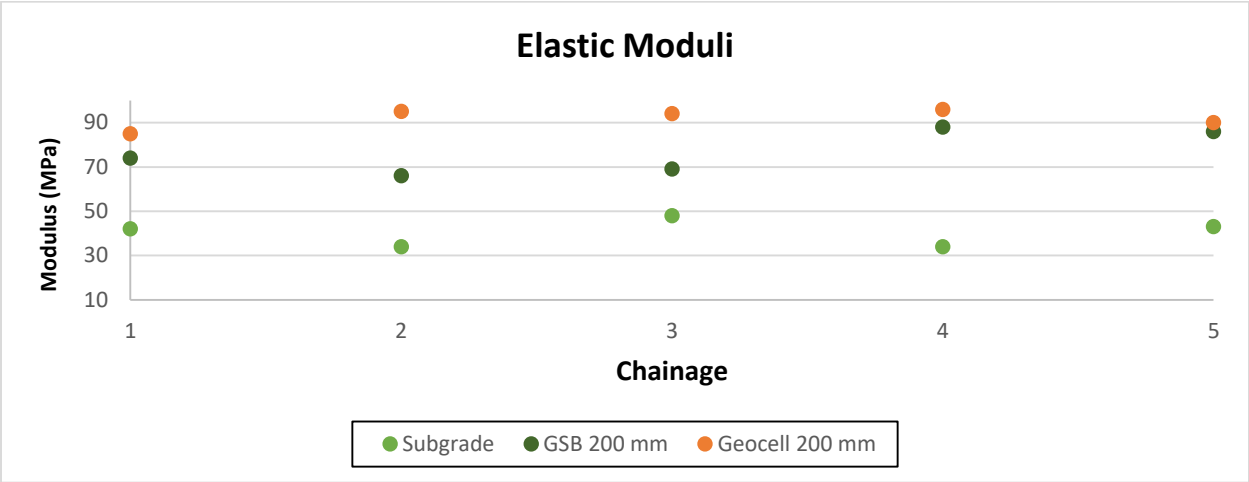

Figure 4.15 Elastic Modulus calculated at different locations of the test box for 200 mm thickness

4.4 Comparison of Modulus with respect to Thickness of unbound subbase layer

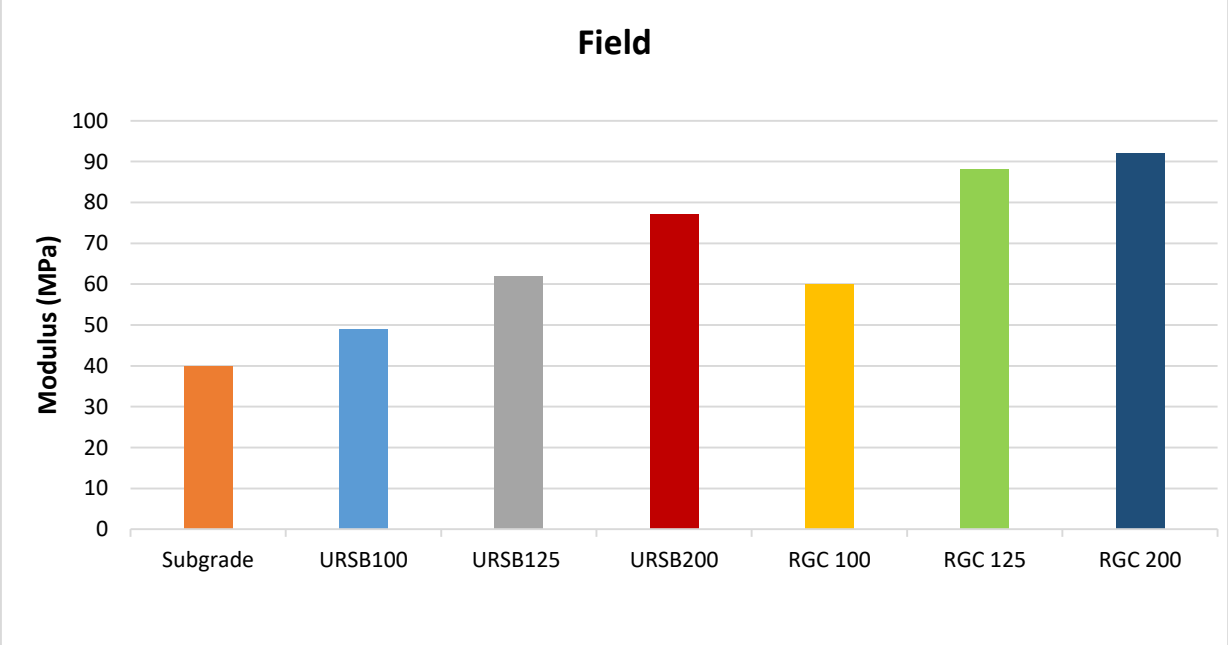

Figure 4.16 Comparison of Field Modulus with respect to thickness of unbound subbase layer

4.5 COMPARISON WITH RESPECT TO THICKNESS

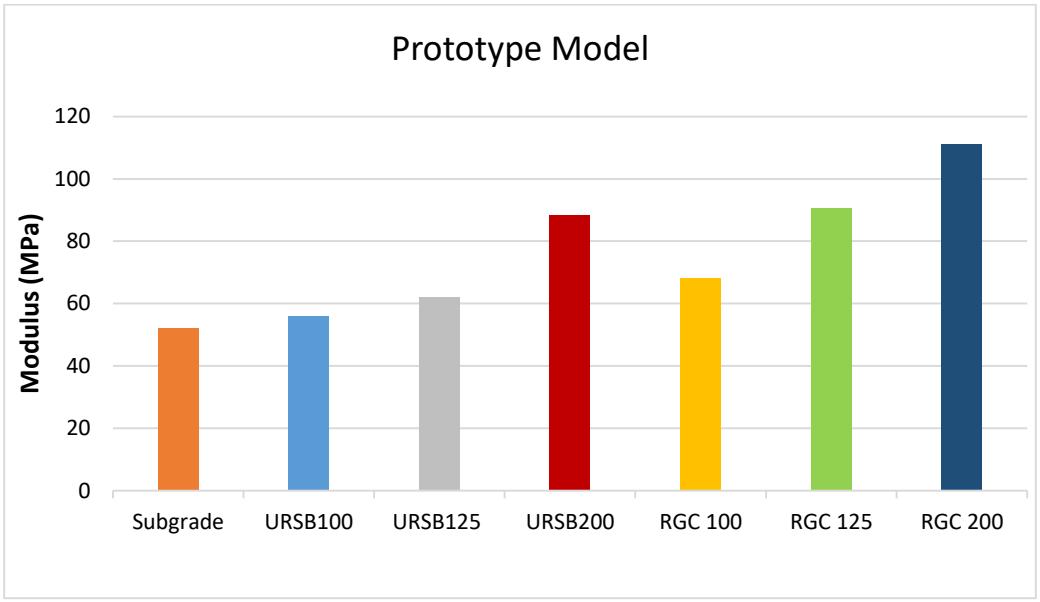

Figure 4.17 Comparison of Laboratory Modulus with respect to thickness of unbound subbase layer

4.6 COMPARISON OF FIELD AND LAB TEST MODULI

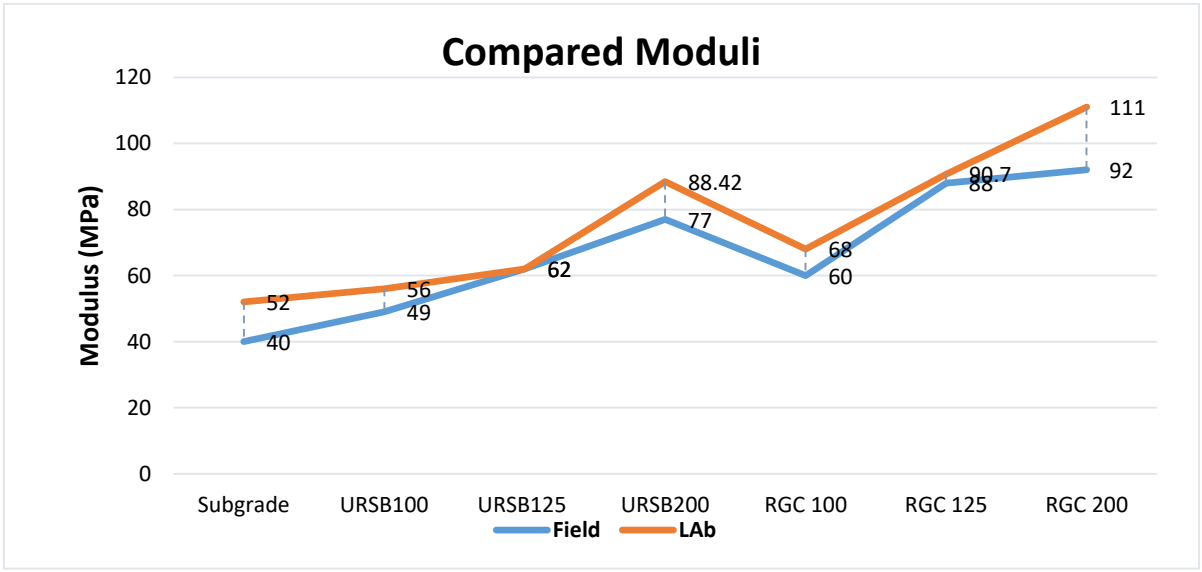

Figure 4.18 Comparison of Field and Lab test Moduli

4.7 DEFLECTION RESULTS

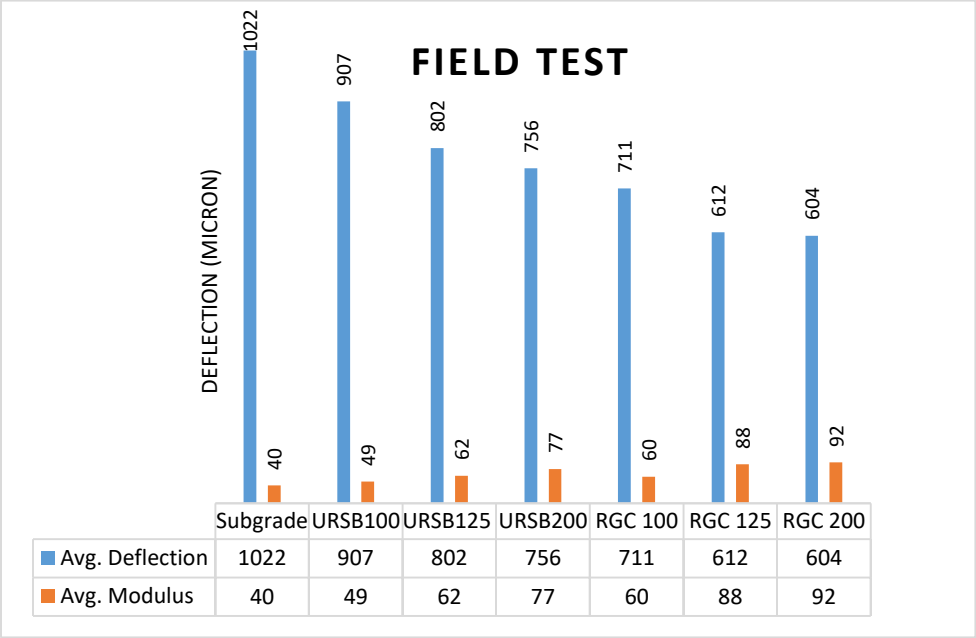

	Subgrade	URSB100	URSB125	URSB200	RGC 100	RGC 125	RGC 200
Avg. Deflection	1022	907	802	756	711	612	604
Avg. Modulus	40	49	62	77	60	88	92

Figure 4.19 Deflection calculated using LWD

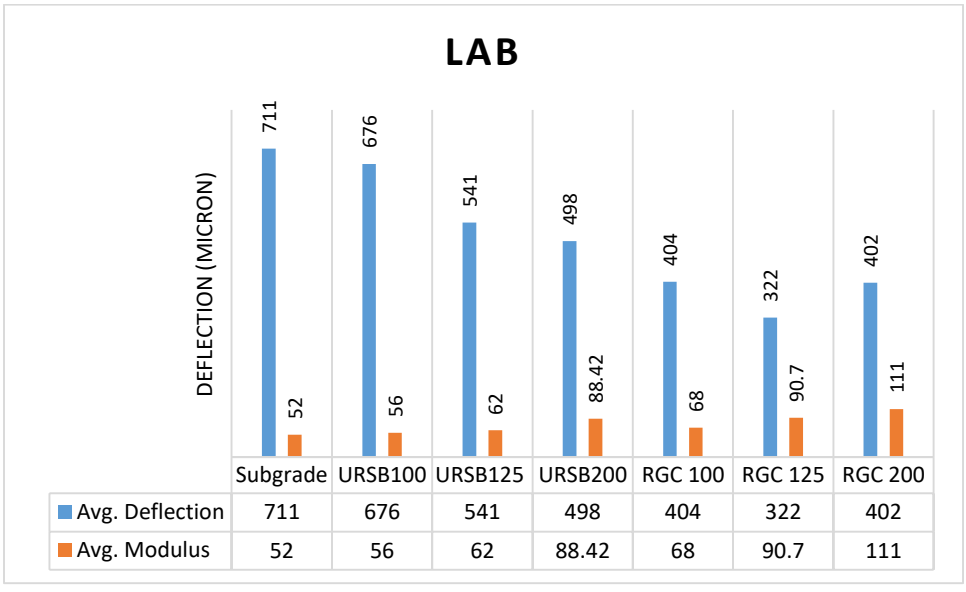

	Subgrade	URSB100	URSB125	URSB200	RGC 100	RGC 125	RGC 200
Avg. Deflection	711	676	541	498	404	322	402
Avg. Modulus	52	56	62	88.42	68	90.7	111

Figure 4.20 Deflection calculated using LWD

4.8 DEFLECTION COMPARISONS OF FIELD AND LAB TEST EVALUATIONS

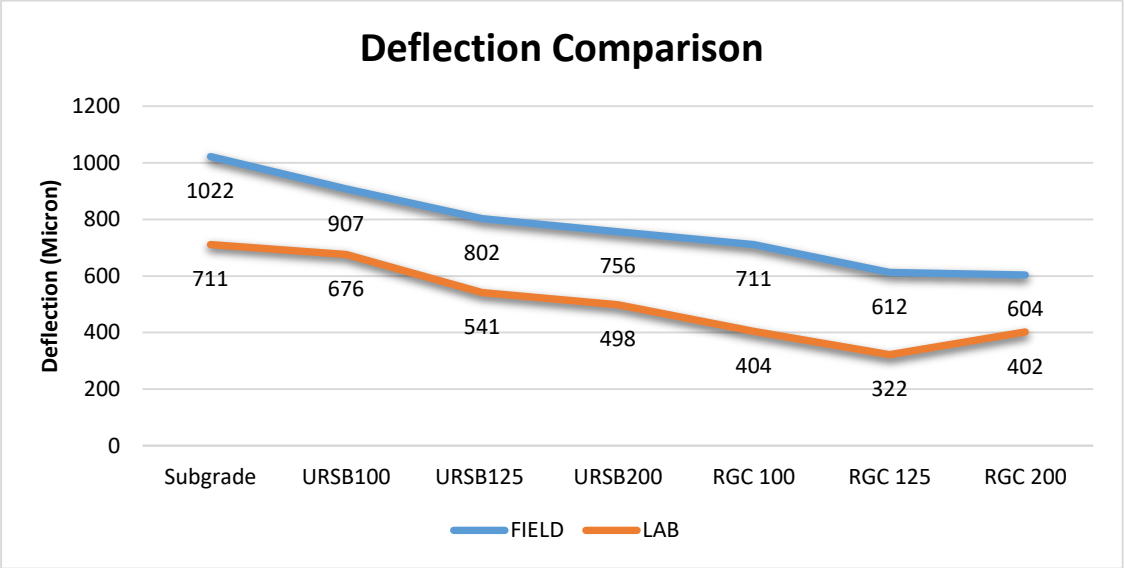

Figure 4.21 Comparison of Deflections

FIELD EVALUATION:

Table 4.2 Modulus Results of Field Testing

Layer	Modulus Calculated (MPa)
Subgrade	**40.3**
GSB 100 mm (URSB100)	**49**
GSB 125 mm (URSB125)	**62**
GSB 200 mm (URSB200)	**77**
GSB + GEOCELL 100 mm (RGC 100)	**60**
GSB + GEOCELL 125 mm (RGC 125)	**88**
GSB + GEOCELL 200 mm (RGC 200)	**92**

4.9 Modulus Improvement Factor (MIF) Calculated

1) $MIF_{(100)}$ = **1.22**
2) $MIF_{(125)}$ = **1.41**
3) $MIF_{(200)}$ = **1.1**

CALCULATIONS USING AASHTO EQUATIONS:

Table 4.3 Modified Modulus values using AASHTO

Layers	GSB	GSB + Geocell		GSB 16%	GSB + Geocell 16 %
Subgrade	51	51		59	59
100 mm	62	76.2		71	88
125 mm	75	106		87	123
200 mm	83	95		96	110

LAB TESTING:

Table 4.4 **Modulus Results of Lab Testing**

Layer	**Modulus Calculated (MPa)**
Subgrade	**52**
GSB 100 mm (URSB100)	**56**
GSB 125 mm (URSB125)	**62**
GSB 200 mm (URSB200)	**88.42**
GSB + GEOCELL 100 mm (RGC 100)	**68**
GSB + GEOCELL 125 mm (RGC 125)	**90.70**
GSB + GEOCELL 200 mm (RGC 200)	**111**

4.10 Modulus Improvement Factor (MIF) Calculated

1) $MIF_{(100)}$ = **1.2**
2) $MIF_{(125)}$ = **1.46**
3) $MIF_{(200)}$ = **1.26**

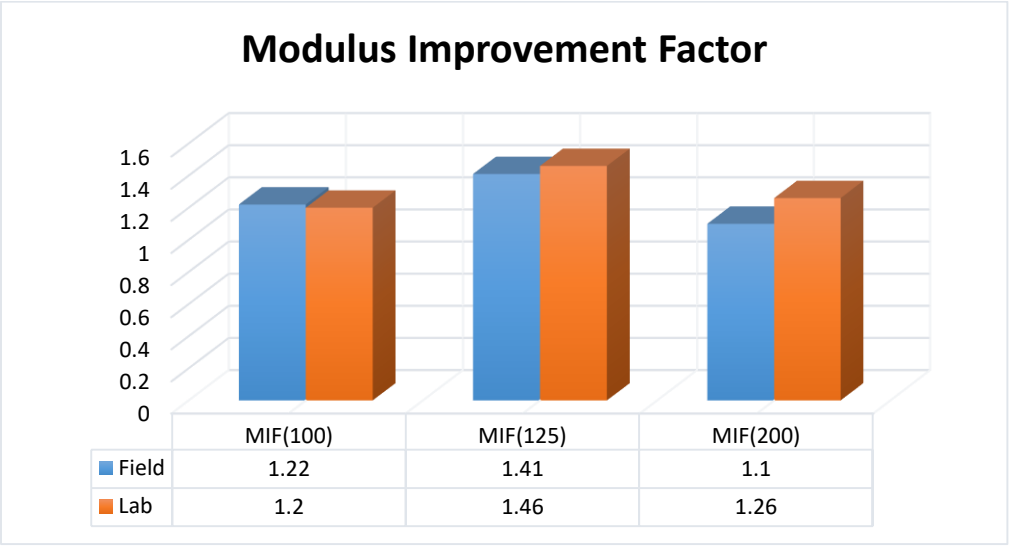

Figure: 4.22 Modulus Improvement Factor

Chapter 5

ANALYSIS AND DESIGN OF FLEXIBLE PAVEMENT

5.0 GENERAL

A highways pavement is a structure made up of processed materials that are superimposed in layers above the natural soil subgrade with the primary purpose of distributing vehicle loads to the subgrade. The pavement construction must be of sufficient strength and quality to provide a surface with adequate riding quality, favorable light reflecting properties, enough skid resistance, and minimal noise pollution. The ultimate goal is to ensure that transmitted stresses caused by wheel load are sufficiently decreased so that they do not exceed the subgrade bearing capability.

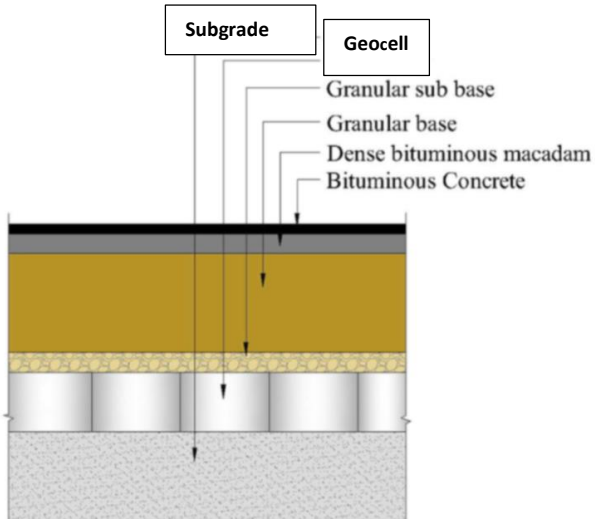

Figure 5.1 Cross Section of reinforced section

The following two performance models are considered in the design & analysis of flexible pavements:

5.1 RUTTING MODEL

Rutting is the vertical compressive strain that develops at the subgrade's top. Wheel loads are applied repeatedly, resulting in a depressed longitudinal groove along the wheel path. It happens from the bottom to the top. For design traffic less than or equal to 30 msa, a rut depth of not more than 20 mm in 20% of the length under consideration is considered critical, and for design traffic,

more than 30 msa, a rut depth of not more than 10 mm in 20% of the length under consideration is considered critical. It can be calculated using the equations mentioned below:

$$N_r = 4.1656 * 10^{-8} * (1/E_v)^{4.5337} \quad \text{(for 80\% reliability)}$$

$$N_r = 1.41 * 10^{-8} * (1/E_v)^{4.5337} \quad \text{(for 90\% reliability)}$$

Where,

Nr – rutting life of subgrade

Ev – permissible value of vertical strain at the top of the subgrade

5.2 FATIGUE MODEL

The horizontal tensile strain created at the bottom of the bituminous layer is referred to as fatigue. The application of tyre loads caused these interconnecting cracks to form along the wheel path. If 20% of the surface under examination is cracked for design traffic less than or equal to 30 msa and 10% for design traffic greater than 30 msa, the pavement is said to have failed in fatigue. It can be calculated using the following equations:

$$N_f = 2.21 * 10^{-4} * (1/E_t)^{3.89} * (1/M_r)^{0.854} \quad \text{(for 80\% reliability)}$$

$$N_f = 0.711 * 10^{-4} * (1/E_t)^{3.89} * (1/M_r)^{0.854} \quad \text{(for 90\% reliability)}$$

Or

$$N_f = 1.6064 * C * 10^{-4} * (1/E_t)^{3.89} * (1/Mr_{bitumen})^{0.854} \quad \text{(for 80\% reliability)}$$

$$N_f = 0.5161 * C * 10^{-4} * (1/E_t)^{3.89} * (1/Mr_{bitumen})^{0.854} \quad \text{(for 90\% reliability)}$$

Where,

C - adjustment factor used to account for the effect of variation in the volumetric parameters of mix & is given by:

$$C = 10^M \text{ \& } M = 4.84\,[(V_{be}/V_{be} + V_a) - 0.69]$$

N_f– fatigue life of bituminous layer

E_t – permissible value of horizontal strain at the bottom of bituminous layer

M_r – resilient modulus of bituminous layer (in MPa)

V_{be} - % volume of effective bitumen in the mix

V_a - % volume of air voids in the mix

Expressways, National Highways, State Highways, and Urban Roads, as well as other categories of roads with design traffic greater than or equal to 20 msa, are subjected to 90% reliability performance equations, while roads with design traffic less than 20 msa are subjected to 80% reliability performance equations.

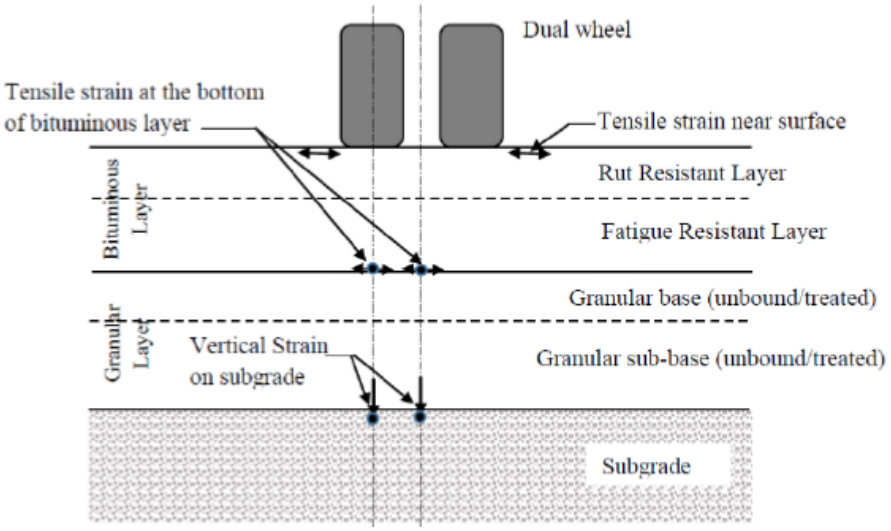

Figure 5.2 Typical cross-section of pavement with bituminous layer(s), granular base, and GSB displaying the locations of critical strains (Source: IRC: 37-2018)

5.3 ANALYSIS OF FLEXIBLE PAVEMENTS USING IIT PAVE SOFTWARE

IIT Pave software is used to build and analyse flexible pavements to ensure that they operate well both structurally and functionally. The essential inputs for the estimation of real strain values for fatigue and rutting are the thickness of individual layers, their resilient moduli, and poison's ratio, wheel load, tyre pressure, and coordinates of important places. Table 3.1 of IRC: 37-2018 details the standard conditions that must be followed while conducting the analysis.

Table 5.1 Standard conditions of pavement analysis using IITPAVE (Source: IRC: 37-2018)

Analysis Condition	
Material response model	Linear elastic model
Layer interface condition	Fully bonded (all layers)
No. of Wheels	Dual wheel
Wheel Loads	20 kN on each single wheel (two wheels)
Contact stress for critical parameter analysis	0.56 MPa for tensile strain in bituminous layer and vertical compressive strain on subgrade; 0.80 MPa for Cement treated base
Critical mechanistic Parameters	
Bituminous Layer	Tensile strain at the bottom
Cement treated base	Tensile stress and tensile strain at the bottom
Subgrade	Compressive strain at the top
Note: (a) Only the absolute value of strains/stresses (without the + or – sign) should be used in the performance equations (b) For Pavements with strong bases and/or thin bituminous layers, there may be only compressive strains at the bottom of the bituminous layer, and fatigue check may not be required for such cases.	

From the output generated, actual value of strain for fatigue can be read as the maximum of radial & tangential strains at a depth (equal to the thickness of bituminous layer) & radial distances of 0 mm & 155 mm. It is to be noted that upper line of the strains is considered from the two sets of results provided. Also, actual value of strain for rutting can be read as the maximum of the strains corresponding to the interface between granular sub-base & subgrade. It is to be noted that the lower line of the strains is considered from the two sets of results provided. Negative values represent the compressive strains & positive values represent the tensile strains.

For the purpose of comparison with the allowable strains, absolute values of these strains are considered.

5.4 PROCEDURE OF PAVEMENT DESIGN

The structural design of unreinforced flexible pavement is illustrated through the following outline:

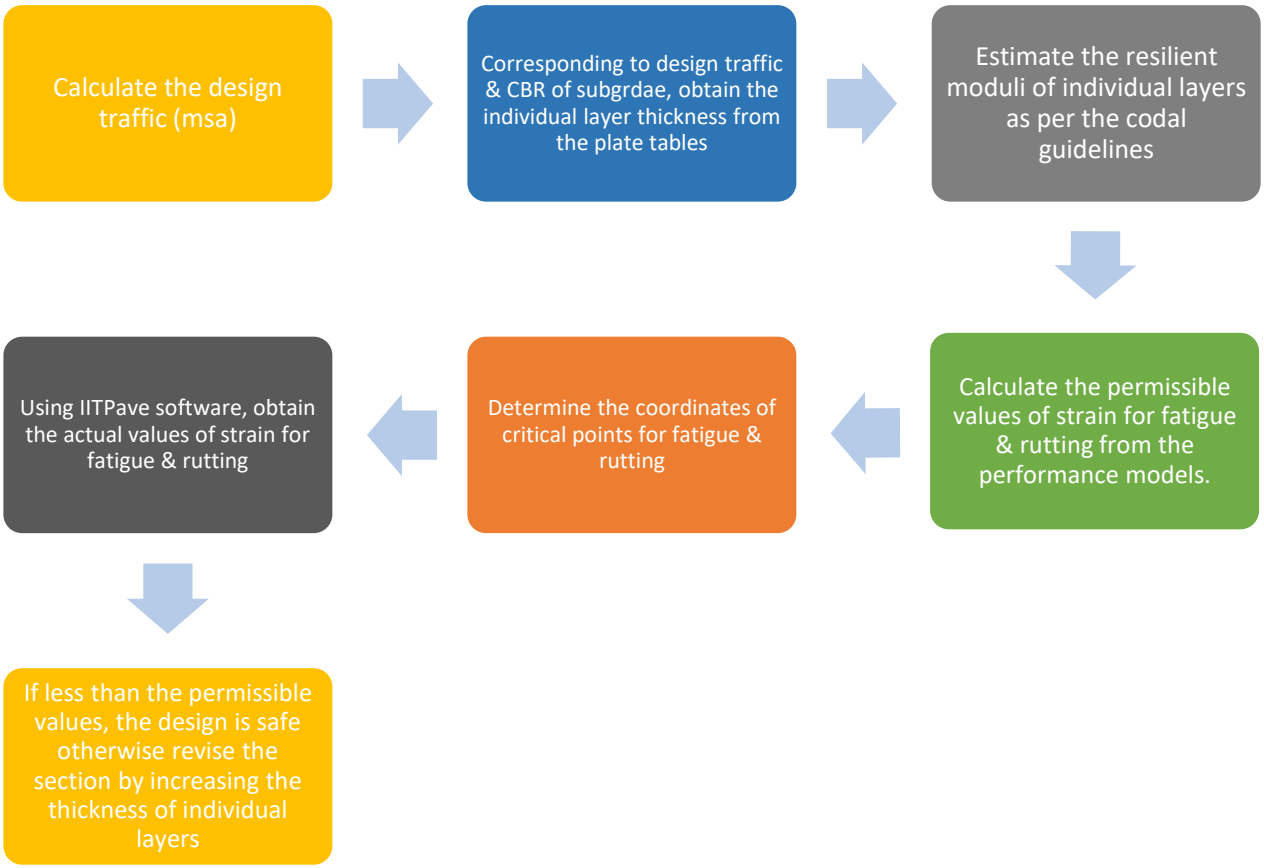

Figure 5.3 Outline of design for unreinforced section

5.5 High Volume Roads

5.5.1 DESIGN OF UNREINFORCED SECTIONS

Data Input:

Design Traffic = **50 msa**

$Mr_{subgrade}$ = **59 MPa** or **8556.77 Psi**

Corresponding to the design traffic & CBR, thickness of the different pavement layers is estimated from the pavement design catalogue (plate 2):

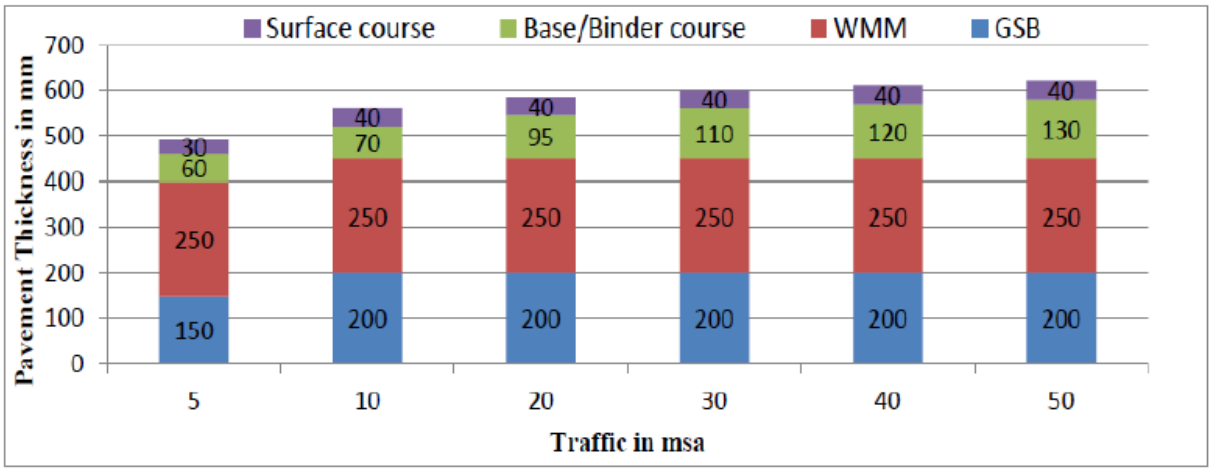

Figure 5.4 Design Catalogue (Plate-2) Effective CBR 6%

(Source: IRC: 37-2018)

Section 1: <u>For Granular Subbase with thickness 200 mm</u>

a) Thickness of granular sub-base = 200 mm

b) Thickness of granular base = 250 mm

c) Thickness of DBM = 150 mm

d) Thickness of BC = 40 mm

- Resilient modulus of GSB from LWD testing results = 96 MPa or 13922.88 Psi

- Resilient modulus of Base = $0.2 * h^{0.45} * Mr_{GSB}$ (h is thickness of Base)

  $= 0.2 * 250^{0.45} * 96 = 230.34$ MPa or 33406.58481 Psi

- **<u>Fatigue cracking criteria for bituminous layer</u>:**

$$N_f = 0.711 * 10^{-4} * (1/E_t)^{3.89} * (1/Mr_{bitumen})^{0.854} \text{ (for 90\% reliability)}$$

$$50 \times 10^6 = 0.711 \times 10^{-4} * (1/E_t)^{3.89} * (1/3000)^{0.854}$$

E_t = 156 micron (permissible value of strain for fatigue cracking)

- **<u>Subgrade rutting criteria</u>:**

$$N_r = 1.41 * 10\text{-}8 * (1/E_v)^{4.5337} \text{ (for 90\% reliability)}$$

$$50 \times 10^6 = 1.41 \times 10^{-8} * (1/E_v)^{4.5337}$$

Ev = 371.69 micron (permissible value of strain for rutting)

- ❖ Now using IIT Pave software, compute the actual strain values & compare them with the permissible values:
- a) The coordinates of critical points for fatigue are = (190,0) & (190,155)
- b) The coordinates of critical points for rutting are = (640,0) & (640,155)

- ❖ Actual value of strain for fatigue cracking:

  147 < **156**

- ❖ Actual value of strain for rutting:

  270 < **371.69**

- ➢ Since the actual strain values obtained from IIT Pave are well within the permissible limits, the design for unreinforced section is safe.

Section 2: <u>For Granular Subbase with thickness 125 mm</u>

a) Thickness of granular sub-base = 125 mm

b) Thickness of granular base = 250 mm

c) Thickness of DBM = 150 mm

d) Thickness of BC = 40 mm

- Resilient modulus of GSB = from LWD testing results = 87 MPa 12617.61 Psi

- Resilient modulus of Base = $0.2 * h^{0.45} *$ MrGSB (h is thickness of Base)

  $= 0.2 * 250^{0.45} * 87 = 208$ MPa or 30166.24 Psi

- **<u>Fatigue cracking criteria for bituminous layer</u>:**

$$N_f = 0.711 * 10^{-4\,*} (1/E_t)^{3.89} * (1/Mr_{bitumen})^{0.854} \text{ (for 90\% reliability)}$$

$$50 \times 10^6 = 0.711 \times 10^{-4} * (1/E_t)^{3.89} * (1/3000)^{0.854}$$

E_t = 156 micron (permissible value of strain for fatigue cracking)

- **<u>Subgrade rutting criteria</u>:**

$$N_r = 1.41 * 10\text{-}8 * (1/E_v)^{4.5337} \text{ (for 90\% reliability)}$$

$$50 \times 10^6 = 1.41 \times 10^{-8} * (1/E_v)^{4.5337}$$

Ev = 371.69 micron (permissible value of strain for rutting)

❖ Now using IIT Pave software, compute the actual strain values & compare them with the permissible values:

- a) The coordinates of critical points for fatigue are = (190,0) & (190,155)
- b) The coordinates of critical points for rutting are = (565,0) & (565,155)

❖ Actual value of strain for fatigue cracking:

153 < **156**

❖ Actual value of strain for rutting:

314 < **371.69**

➢ Since the actual strain values obtained from IIT Pave are well within the permissible limits, the design for unreinforced section is safe.

Section 3: <u>For Granular Subbase with thickness 100 mm</u>

a) Thickness of granular sub-base = 100 mm

b) Thickness of granular base = 250 mm

c) Thickness of DBM = 160 mm

d) Thickness of BC = 40 mm

- Resilient modulus of GSB = from LWD testing results = 71 MPa 10297.13 Psi

- Resilient modulus of Base = $0.2 * h^{0.45} *$ MrGSB (h is thickness of Base)

$= 0.2 * 250^{0.45} * 71 = 170$MPa or 24655.1 Psi

- **<u>Fatigue cracking criteria for bituminous layer</u>:**

$$N_f = 0.711 * 10^{-4} * (1/E_t)^{3.89} * (1/Mr_{bitumen})^{0.854} \text{ (for 90\% reliability)}$$

$$50 \times 10^6 = 0.711 \times 10^{-4} * (1/E_t)^{3.89} * (1/3000)^{0.854}$$

E_t = 156 micron (permissible value of strain for fatigue cracking)

- **<u>Subgrade rutting criteria</u>:**

$$N_r = 1.41 * 10\text{-}8 * (1/E_v)^{4.5337} \text{ (for 90\% reliability)}$$

$$50 \times 10^6 = 1.41 \times 10^{-8} * (1/E_v)^{4.5337}$$

Ev = 371.69 micron (permissible value of strain for rutting)

- ❖ Now using IIT Pave software, compute the actual strain values & compare them with the permissible values:

- a) The coordinates of critical points for fatigue are = (200,0) & (200,155)
- b) The coordinates of critical points for rutting are = (550,0) & (550,155)

- ❖ Actual value of strain for fatigue cracking:

155 < **156**

- ❖ Actual value of strain for rutting:

315 < **371.69**

- ➢ Since the actual strain values obtained from IIT Pave are well within the permissible limits, the design for unreinforced section is safe.

5.5.2 REINFORCED SECTION

Using the revised resilient modulus of the reinforced sections of GSB using LWD, computing the actual strain values on IIT Pave software & comparing them with the permissible values.

Section 4: For Geocell reinforced Granular Subbase with thickness 200 mm

a) Thickness of granular sub-base = 200 mm

b) Thickness of granular base = 250 mm

c) Thickness of DBM = 130 mm

d) Thickness of BC = 40 mm

- Resilient modulus of geocell reinforced section from LWD testing results = 110 MPa or 15953.3 Psi
- Resilient modulus of Base = $0.2 * h^{0.45} *$ MrGSB (h is thickness of Base)

$= 0.2 * 250^{0.45} * 110 = 263.93$ MPa or 38278.378 Psi

- **Fatigue cracking criteria for bituminous layer:**

$$N_f = 0.711 * 10^{-4} * (1/E_t)^{3.89} * (1/Mr_{bitumen})^{0.854} \text{ (for 90\% reliability)}$$

$$50 \times 10^6 = 0.711 \times 10^{-4} * (1/E_t)^{3.89} * (1/3000)^{0.854}$$

E_t = 156 micron (permissible value of strain for fatigue cracking)

- **Subgrade rutting criteria:**

$$N_r = 1.41 * 10\text{-}8 * (1/E_v)^{4.5337} \text{ (for 90\% reliability)}$$

$$50 \times 10^6 = 1.41 \times 10^{-8} * (1/E_v)^{4.5337}$$

Ev = 371.69 micron (permissible value of strain for rutting)

- Now using IIT Pave software, compute the actual strain values & compare them with the permissible values:

- a) The coordinates of critical points for fatigue are = (170,0) & (170,155)
- b) The coordinates of critical points for rutting are = (620,0) & (620,155)

- Actual value of strain for fatigue cracking:

  154 < **156**

- Actual value of strain for rutting:

  292 < **371.69**

- Since the actual strain values obtained from IIT Pave are well within the permissible limits, the design for reinforced section is safe.

Section 5: <u>For Geocell reinforced Granular Subbase with thickness 125 mm</u>

a) Thickness of granular sub-base = 125 mm

b) Thickness of granular base = 250 mm

c) Thickness of DBM = 125 mm

d) Thickness of BC = 40 mm

- Resilient modulus of geocell reinforced section from LWD testing results = 123 MPa or 17838.69 Psi

- Resilient modulus of Base = $0.2 * h^{0.45} *$ MrGSB (h is thickness of Base)

  $= 0.2 * 250^{0.45} * 123 = 295.12$ MPa or 42802.18679 Psi

- **<u>Fatigue cracking criteria for bituminous layer</u>:**

$$N_f = 0.711 * 10^{-4} * (1/E_t)^{3.89} * (1/Mr_{bitumen})^{0.854} \text{ (for 90\% reliability)}$$

$$50 \times 10^6 = 0.711 \times 10^{-4} * (1/E_t)^{3.89} * (1/3000)^{0.854}$$

E_t = 156 micron (permissible value of strain for fatigue cracking)

- **<u>Subgrade rutting criteria</u>:**

$$N_r = 1.41 * 10\text{-}8 * (1/E_v)^{4.5337} \text{ (for 90\% reliability)}$$

$$50 \times 10^6 = 1.41 \times 10^{-8} * (1/E_v)^{4.5337}$$

Ev = 371.69 micron (permissible value of strain for rutting)

❖ Now using IIT Pave software, compute the actual strain values & compare them with the permissible values:

- a) The coordinates of critical points for fatigue are = (165,0) & (165,155)
- b) The coordinates of critical points for rutting are = (540,0) & (540,155)

- ❖ Actual value of strain for fatigue cracking:
  152 < **156**

- ❖ Actual value of strain for rutting:

  343 < **371.69**

- ➢ Since the actual strain values obtained from IIT Pave are well within the permissible limits, the design for reinforced section is safe.

Section 6: <u>For Geocell reinforced Granular Subbase with thickness 100 mm</u>

a) Thickness of granular sub-base = 100 mm

b) Thickness of granular base = 250 mm

c) Thickness of DBM = 150 mm

d) Thickness of BC = 40 mm

- Resilient modulus of GSB = from LWD testing results = 88 MPa 12762.64 Psi

- Resilient modulus of Base = $0.2 * h^{0.45} *$ MrGSB (h is thickness of Base)

  $= 0.2 * 250^{0.45} * 88 = 211$MPa or 30622.70 Psi

- **<u>Fatigue cracking criteria for bituminous layer</u>:**

$$N_f = 0.711 * 10^{-4\,*} (1/E_t)^{3.89} * (1/Mr_{bitumen})^{0.854} \text{ (for 90\% reliability)}$$

$$50 \times 10^6 = 0.711 \times 10^{-4} * (1/E_t)^{3.89} * (1/3000)^{0.854}$$

E_t = 156 micron (permissible value of strain for fatigue cracking)

- **<u>Subgrade rutting criteria</u>:**

$$N_r = 1.41 * 10\text{-}8 * (1/E_v)^{4.5337} \text{ (for 90\% reliability)}$$

$$50 \times 10^6 = 1.41 \times 10^{-8} * (1/E_v)^{4.5337}$$

Ev = 371.69 micron (permissible value of strain for rutting)

❖ Now using IIT Pave software, compute the actual strain values & compare them with the permissible values:

- a) The coordinates of critical points for fatigue are = (190,0) & (190,155)
- b) The coordinates of critical points for rutting are = (540,0) & (540,155)

❖ Actual value of strain for fatigue cracking:

153 < **156**

❖ Actual value of strain for rutting:

329 < **371.69**

➢ Since the actual strain values obtained from IIT Pave are well within the permissible limits, the design for reinforced section is safe.

SUMMARY OF ABOVE RESULTS

Table 5.2 Calculated Strain Values for High Volume Roads

Layer	Height (mm)	Modulus (MPa)	Permissible value of strain for Fatigue (micron)	Permissible value of strain for Rutting (micron)	Actual Strain for Fatigue cracking (micron)	Actual Rutting (micron)
Subgrade	500	59	156	371.69	-	-
Unreinforced GSB	100	71			155	315
	125	87			153	314
	200	96			147	270
Geocell reinforced GSB	100	88			153	329
	125	123			152	343
	200	110			154	292

5.6 ANALYSIS AND DESIGN OF FLEXIBLE PAVEMENT FOR LOW VOLUME ROADS

5.6.1 Unreinforced Section

In this section the pavement analysis and results for pavement with conventional Sub-Base and geocell reinforcement on low volume roads has been conducted.

Design Input:

Design Traffic = **5 msa**

Subgrade Modulus = **59 MPa**

Corresponding to the design traffic & CBR, thickness of the different pavement layers is estimated from the pavement design catalogue (plate 2):

(Source: IRC: 37-2018)

Section 7: For Granular Subbase with thickness 200 mm

a) Thickness of granular sub-base = 200 mm

b) Thickness of granular base = 200 mm

c) Thickness of DBM = 10 mm

d) Thickness of BC = 30 mm

- Resilient modulus of GSB from LWD testing results = 96 MPa

- Resilient modulus of Base = $0.2 * h^{0.45} * Mr_{GSB}$ (h is thickness of Base)

  $= 0.2 * 200^{0.45} * 96 = 208$ MPa

- **Fatigue cracking criteria for bituminous layer:**

$$N_f = 1.6064*C*10^{-04} [1/\varepsilon t]^{3.89}*[1/M_{Rm}]^{0.854}$$

$$5*10^6 = 1.6064*2.556*10^{-04} [1/\varepsilon_t]^{3.89} * [1/3000]^{0.854}$$

Et = 465 micron (permissible value of strain for rutting)

- **Subgrade rutting criteria:**

$$N_R = 4.1656 \times 10^{-08} [1/\varepsilon_v]^{4.5337}$$

$$5*10^6 = 4.1656 \times 10^{-08} [1/\varepsilon_v]^{4.5337}$$

E_v = 784.3 micron (permissible value of strain for fatigue cracking)

- Now using IIT Pave software, compute the actual strain values & compare them with the permissible values:

- a) The coordinates of critical points for fatigue are = (40,0) & (40,155)
- b) The coordinates of critical points for rutting are = (440,0) & 440,155)

- Actual value of strain for fatigue cracking:

  353 < **465**

- Actual value of strain for rutting:

  750 < **784.3**

- Since the actual strain values obtained from IIT Pave are well within the permissible limits, the design for unreinforced section is safe.

Section 8: <u>For Granular Subbase with thickness 125 mm</u>

a) Thickness of granular sub-base = 125 mm

b) Thickness of granular base = 220 mm

c) Thickness of DBM = 35 mm

d) Thickness of BC = 30 mm

- Resilient modulus of GSB from LWD testing results = 87 MPa

- Resilient modulus of Base = $0.2 * h^{0.45} * Mr_{GSB}$ (h is thickness of Base)

$= 0.2 * 220^{0.45} * 87 = 197.07$ MPa

- **<u>Fatigue cracking criteria for bituminous layer</u>:**

$$N_f = 1.6064*C*10^{-04} [1/\varepsilon t]^{3.89}*[1/M_{Rm}]^{0.854}$$

$$5*10^6 = 1.6064*2.556*10^{-04} [1/\varepsilon_t]^{3.89} * [1/3000]^{0.854}$$

Et = 465 micron (permissible value of strain for rutting)

- **<u>Subgrade rutting criteria</u>:**

$$N_R = 4.1656 \times 10^{-08} [1/\varepsilon_v]^{4.5337}$$

$$5*10^6 = 4.1656 \times 10^{-08} [1/\varepsilon_v]^{4.5337}$$

E_v = 784.3 micron (permissible value of strain for fatigue cracking)

❖ Now using IIT Pave software, compute the actual strain values & compare them with the permissible values:

- a) The coordinates of critical points for fatigue are = (65,0) & (65,155)
- b) The coordinates of critical points for rutting are = (410,0) & 410,155)

❖ Actual value of strain for fatigue cracking:

357 < **465**

❖ Actual value of strain for rutting:

763 < **784.3**

➢ Since the actual strain values obtained from IIT Pave are well within the permissible limits, the design for unreinforced section is safe.

Section 9: <u>For Granular Subbase with thickness 100 mm</u>

a) Thickness of granular sub-base = 100 mm

b) Thickness of granular base = 260 mm

c) Thickness of DBM = 30 mm

d) Thickness of BC = 30 mm

- Resilient modulus of GSB from LWD testing results = 71 MPa

- Resilient modulus of Base = $0.2 * h^{0.45} * Mr_{GSB}$ (h is thickness of Base)

$= 0.2 * 260^{0.45} * 71 = 173.39$ MPa

- **<u>Fatigue cracking criteria for bituminous layer</u>:**

$$N_f = 1.6064*C*10^{-04} [1/\varepsilon t]^{3.89}*[1/M_{Rm}]^{0.854}$$

$$5*10^6 = 1.6064*2.556*10^{-04} [1/\varepsilon_t]^{3.89} * [1/3000]^{0.854}$$

Et = 465 micron (permissible value of strain for rutting)

- **<u>Subgrade rutting criteria</u>:**

$$N_R = 4.1656 \times 10^{-08} [1/\varepsilon_v]^{4.5337}$$

$$5*10^6 = 4.1656 \times 10^{-08} [1/\varepsilon_v]^{4.5337}$$

E_v = 784.3 micron (permissible value of strain for fatigue cracking)

- Now using IIT Pave software, compute the actual strain values & compare them with the permissible values:

- a) The coordinates of critical points for fatigue are = (60,0) & (60,155)
- b) The coordinates of critical points for rutting are = (420,0) & 420,155)

- Actual value of strain for fatigue cracking:

392 < **465**

- Actual value of strain for rutting:

768 < **784.3**

- Since the actual strain values obtained from IIT Pave are well within the permissible limits, the design for unreinforced section is safe.

5.6.2 REINFORCED SECTION

Section 10: For Geocell reinforced Granular Subbase with thickness 200 mm

a) Thickness of granular sub-base = 200 mm

b) Thickness of granular base = 190 mm

c) Thickness of DBM = 5 mm

d) Thickness of BC = 30 mm

- Resilient modulus of GSB from LWD testing results = 110 MPa

- Resilient modulus of Base = $0.2 * h^{0.45} * Mr_{GSB}$ (h is thickness of Base)

$= 0.2 * 190^{0.45} * 96 = 233.27$ MPa

- **Fatigue cracking criteria for bituminous layer:**

$$N_f = 1.6064*C*10^{-04} [1/\varepsilon t]^{3.89}*[1/M_{Rm}]^{0.854}$$

$$5*10^6 = 1.6064*2.556*10^{-04} [1/\varepsilon_t]^{3.89} * [1/3000]^{0.854}$$

E_t = 465 micron (permissible value of strain for rutting)

- **Subgrade rutting criteria:**

$$N_R = 4.1656 \times 10^{-08} [1/\varepsilon_v]^{4.5337}$$

$$5*10^6 = 4.1656 \times 10^{-08} [1/\varepsilon_v]^{4.5337}$$

E_v = 784.3 micron (permissible value of strain for fatigue cracking)

❖ Now using IIT Pave software, compute the actual strain values & compare them with the permissible values:

- a) The coordinates of critical points for fatigue are = (40,0) & (40,155)
- b) The coordinates of critical points for rutting are = (440,0) & 440,155)

❖ Actual value of strain for fatigue cracking:

296 < **465**

❖ Actual value of strain for rutting:

769 < **784.3**

➢ Since the actual strain values obtained from IIT Pave are well within the permissible limits, the design for reinforced section is safe.

Section 11: <u>For Geocell reinforced Granular Subbase with thickness 125 mm</u>

a) Thickness of granular sub-base = 125 mm

b) Thickness of granular base = 240 mm

c) Thickness of DBM = 0 mm

d) Thickness of BC = 30 mm

- Resilient modulus of GSB from LWD testing results = 123 MPa

- Resilient modulus of Base = $0.2 * h^{0.45} * Mr_{GSB}$ (h is thickness of Base)

$= 0.2 * 240^{0.45} * 87 = 289.75$ MPa

- **<u>Fatigue cracking criteria for bituminous layer</u>:**

$$N_f = 1.6064*C*10^{-04} [1/\varepsilon t]^{3.89}*[1/M_{Rm}]^{0.854}$$

$$5*10^6 = 1.6064*2.556*10^{-04} [1/\varepsilon_t]^{3.89} * [1/3000]^{0.854}$$

Et = 465 micron (permissible value of strain for rutting)

- **<u>Subgrade rutting criteria</u>:**

$$N_R = 4.1656 \times 10^{-08} [1/\varepsilon_v]^{4.5337}$$

$$5*10^6 = 4.1656 \times 10^{-08} [1/\varepsilon_v]^{4.5337}$$

E_v = 784.3 micron (permissible value of strain for fatigue cracking)

❖ Now using IIT Pave software, compute the actual strain values & compare them with the permissible values:

- a) The coordinates of critical points for fatigue are = (30,0) & (30,155)
- b) The coordinates of critical points for rutting are = (395,0) & 395,155)

❖ Actual value of strain for fatigue cracking:

186 < **465**

❖ Actual value of strain for rutting:

769 < **784.3**

➢ Since the actual strain values obtained from IIT Pave are well within the permissible limits, the design for reinforced section is safe.

Section 12: <u>For Geocell reinforced Granular Subbase with thickness 100 mm</u>

a) Thickness of granular sub-base = 100 mm

b) Thickness of granular base = 260 mm

c) Thickness of DBM = 15 mm

d) Thickness of BC = 30 mm

- Resilient modulus of GSB from LWD testing results = 88 MPa

- Resilient modulus of Base = $0.2 * h^{0.45} * Mr_{GSB}$ (h is thickness of Base)

  $= 0.2 * 260^{0.45} * 88 = 214.90$ MPa

- **Fatigue cracking criteria for bituminous layer:**

$$N_f = 1.6064*C*10^{-04} [1/\varepsilon t]^{3.89}*[1/M_{Rm}]^{0.854}$$

$$5*10^6 = 1.6064*2.556*10^{-04} [1/\varepsilon_t]^{3.89} * [1/3000]^{0.854}$$

Et = 465 micron (permissible value of strain for rutting)

- **Subgrade rutting criteria:**

$$N_R = 4.1656 \times 10^{-08} [1/\varepsilon_v]^{4.5337}$$

$$5*10^6 = 4.1656 \times 10^{-08} [1/\varepsilon_v]^{4.5337}$$

E_v = 784.3 micron (permissible value of strain for fatigue cracking)

❖ Now using IIT Pave software, compute the actual strain values & compare them with the permissible values:

- a) The coordinates of critical points for fatigue are = (45,0) & (45,155)
- b) The coordinates of critical points for rutting are = (415,0) & 415,155)

❖ Actual value of strain for fatigue cracking:

344 < **465**

❖ Actual value of strain for rutting:

767 < **784.3**

➢ Since the actual strain values obtained from IIT Pave are well within the permissible limits, the design for reinforced section is safe.

5.7 SUMMARY OF THE ABOVE RESULTS

Table 5.3 Calculated Strain Values for Low Volume Roads

Layer	Height(mm)	Modulus (MPa)	Permissible value of strain for Fatigue (micron)	Permissible value of strain for Rutting (micron)	Actual Strain for Fatigue cracking (micron)	Actual Rutting (micron)
Subgrade	500	59	465	784.3	-	-
Unreinforced GSB	100	71			392	768
	125	87			357	763
	200	96			353	750
Geocell reinforced GSB	100	88			344	767
	125	123			186	769
	200	110			296	769

PAVEMENT ANALYSIS AND RESULTS FOR PAVEMENT WITH GEOCELL REINFORCED SUB-BASE

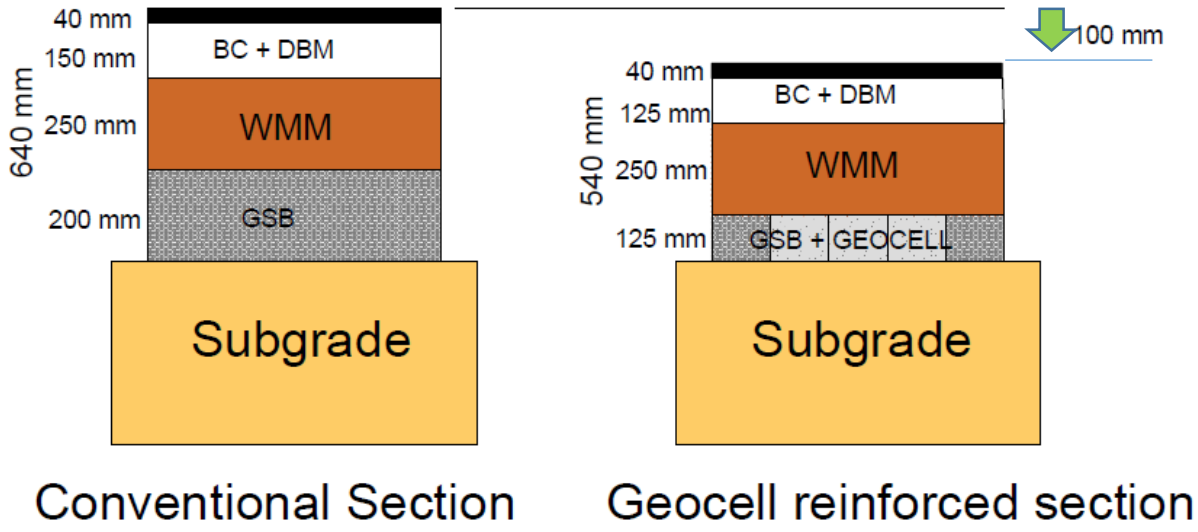

Figure 5.5 Comparison of Sections

5.8 COMPARISON OF THICKNESS

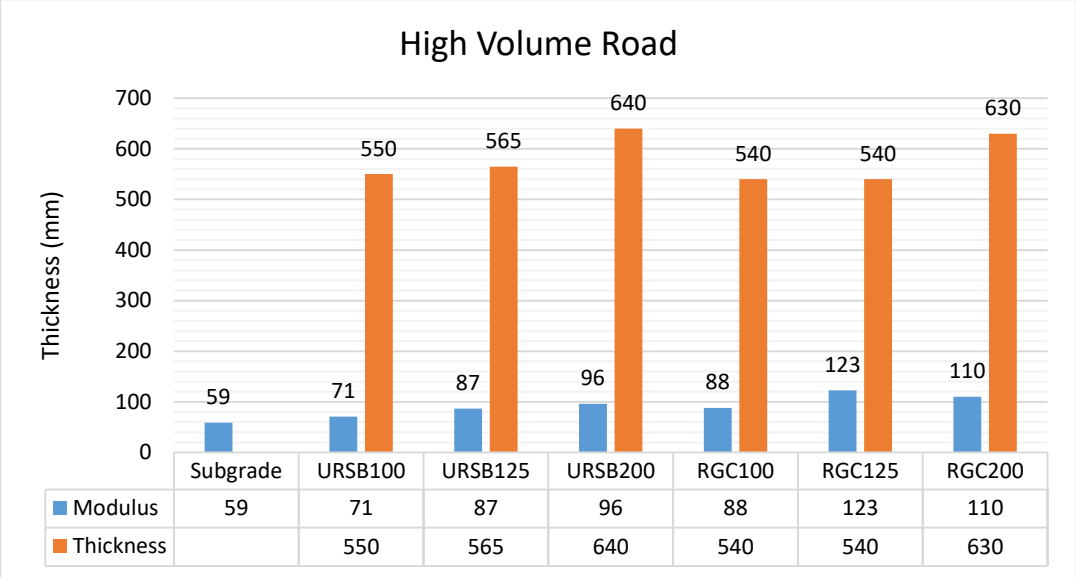

Figure 5.6 Thickness of pavements for unreinforced and reinforced Sections

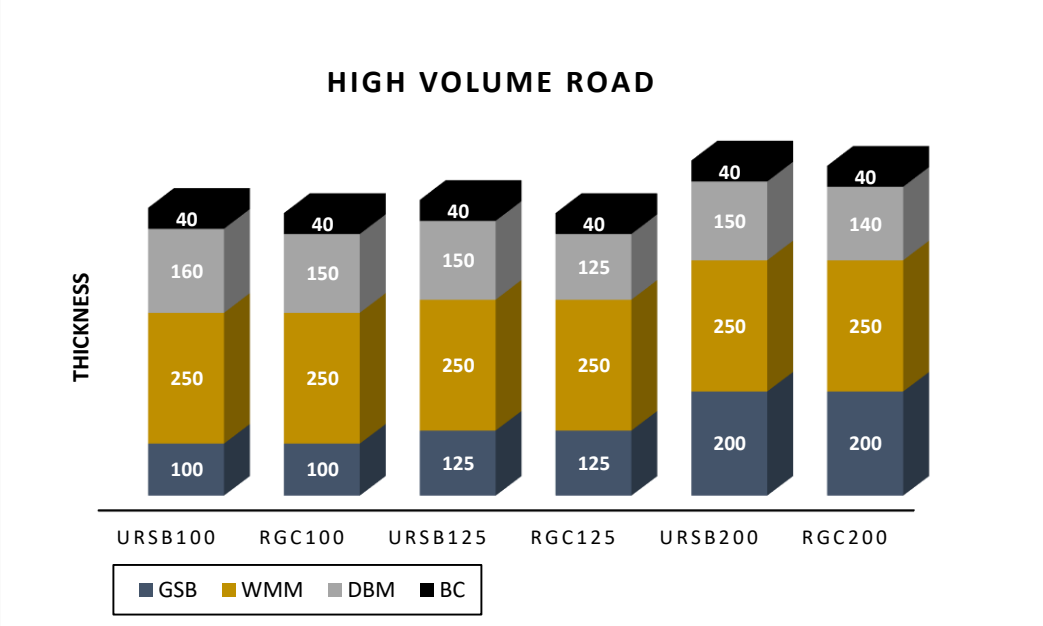

Figure 5.7 Thickness of individual layers

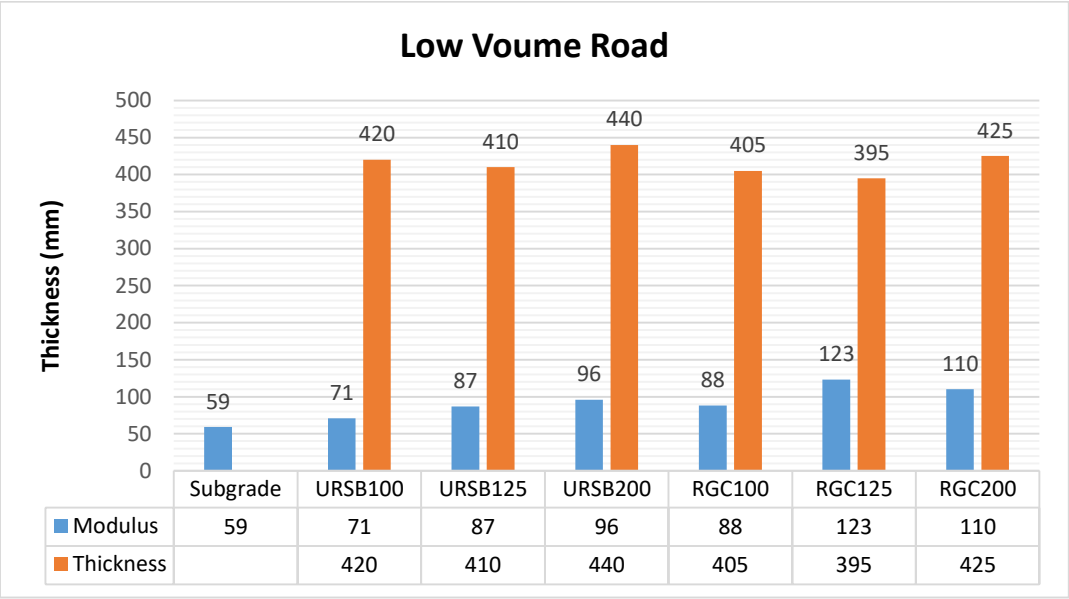

Figure 5.8 Thickness of pavements for unreinforced and reinforced Sections (LOW Vol. Road)

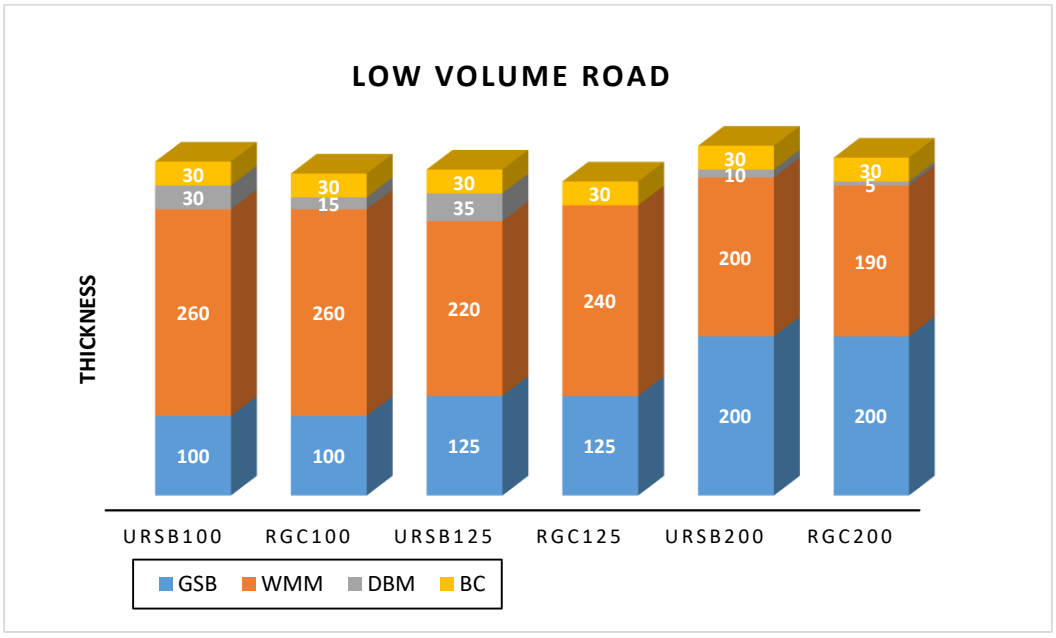

Figure 5.9 Thickness of pavements for unreinforced and reinforced Sections (LOW Vol. Road)

5.9 GENERAL

As there is such a massive investment in the transportation industry, cost analysis is one of the most important considerations. In India, where this industry is expanding, various changes are being made to make it more cost-effective. The length and width of the road, the thickness of the layer, the density of the material, and the cost of 1cumec of material are all used to estimate the cost of a roadway construction project for any section.

5.9.1 HIGH VOLUME ROADS (50 msa Traffic)

Cost comparison for a 1 km road section with a pavement width 7 m

Table 5.4 Design of Unreinforced Section 1

Section 1: A pavement section with bituminous layer(s), granular base and GSB							
Layers	Thickness (mm)	Width (m)	Length (m)	Quantity (m3)	Cost Incurred (INR)	Amount (Lacs)	Total (Lacs)
BC	40	7	1000	280	10138	28.38	215.15
DBM	150			1050	10013	1 cr, 5 lac	
WMM	250			1750	2803.65	49.06	
GSB	200			1400	2658.10	37.21	

Table 5.5 Design of Unreinforced Section 2

Section 2: A pavement section with bituminous layer(s), granular base and GSB							
Layers	Thickness (mm)	Width (m)	Length (m)	Quantity (m3)	Cost Incurred (INR)	Amount (Lacs)	Total (Lacs)
BC	40	7	1000	280	10138	28.38	201.19
DBM	150			1050	10013	1 cr , 5 lac	
WMM	250			1750	2803.65	49.06	
GSB	125			875	2658.10	23.25	

Table 5.6 Design of Unreinforced Section 3

Section 3: A pavement section with bituminous layer(s), granular base and GSB							
Layers	Thickness (mm)	Width (m)	Length (m)	Quantity (m3)	Cost Incurred (INR)	Amount (Lacs)	Total (Lacs)
BC	40	7	1000	280	10138	28.38	176.64
DBM	115			805	10013	80.60	
WMM	250			1750	2803.65	49.06	
GSB	100			700	2658.10	18.60	

Table 5.7 Design of Reinforced Section 4

Section 4: A pavement section with bituminous layer(s), granular base and Geocell reinforced GSB							
Layers	Thickness (mm)	Width (m)	Length (m)	Quantity (m3)	Cost Incurred (INR)	Amount (Lacs)	Total (Lacs)
BC	40	7	1000	280	10138	28.38	214.16
DBM	130			910	10013	91.11	
WMM	250			1750	2803.65	49.06	
GSB	200			1400	2658.10	37.21	
Geocell	200			7000 Sqm	120	8.4	

Table 5.8 Design of Reinforced Section 5

Section 5: A pavement section with bituminous layer(s), granular base and Geocell reinforced GSB							
Layers	Thickness (mm)	Width (m)	Length (m)	Quantity (m3)	Cost Incurred (INR)	Amount (Lacs)	Total (Lacs)
BC	40	7	1000	280	10138	28.38	196
DBM	125			875	10013	87.61	
WMM	250			1750	2803.65	49.06	
GSB	125			875	2658.10	23.25	
Geocell	125			7000 Sqm	110 Sqm	7.7	

Table 5.9 Design of Reinforced Section 6

Section 6: A pavement section with bituminous layer(s), granular base and Geocell reinforced GSB							
Layers	Thickness (mm)	Width (m)	Length (m)	Quantity (m3)	Cost Incurred (INR)	Amount (Lacs)	Total (Lacs)
BC	40	7	1000	280	10138	28.38	202.84
DBM	150			1050	10013	1 cr 5 lac	
WMM	250			1750	2803.65	49.06	
GSB	100			700	2658.10	18.60	
Geocell	100			7000 Sqm	90 Sqm	6.3	

5.9.2 LOW VOLUME ROADS: 5 msa Traffic

Table 5.10 Design of Unreinforced Section 7

Section 7: A pavement section with bituminous layer(s), granular base and GSB							
Layers	Thickness (mm)	Width (m)	Length (m)	Quantity (m3)	Cost Incurred (INR)	Amount (Lacs)	Total (Lacs)
BC	40	7	1000	210	10138	21.28	104.84
DBM	10			70	10013	7	
WMM	200			1400	2803.65	39.35	
GSB	200			1400	2658.10	37.21	

Table 5.11 Design of Unreinforced Section 8

Section 8: A pavement section with bituminous layer(s), granular base and GSB							
Layers	Thickness (mm)	Width (m)	Length (m)	Quantity (m3)	Cost Incurred (INR)	Amount (Lacs)	Total (Lacs)
BC	30	7	1000	210	10138	21.28	112.23
DBM	35			245	10013	24.53	
WMM	220			1540	2803.65	43.17	
GSB	125			875	2658.10	23.25	

Table 5.12 Design of Unreinforced Section 9

Section 9: A pavement section with bituminous layer(s), granular base and GSB							
Layers	Thickness (mm)	Width (m)	Length (m)	Quantity (m3)	Cost Incurred (INR)	Amount (Lacs)	Total (Lacs)
BC	30	7	1000	210	10138	21.28	111.88
DBM	30			210	10013	21	
WMM	260			1820	2803.65	51	
GSB	100			700	2658.10	18.60	

Table 5.13 Design of Reinforced Section 10

Section 10 : A pavement section with bituminous layer(s), granular base and Geocell reinforced GSB							
Layers	Thickness (mm)	Width (m)	Length (m)	Quantity (m3)	Cost Incurred (INR)	Amount (Lacs)	Total (Lacs)
BC	35	7	1000	210	10138	24.78	107.67
DBM	-			35	10013	-	
WMM	190			1330	2803.65	37.28	
GSB	200			1400	2658.10	37.21	
Geocell	200			7000 Sqm	120 Sqm	8.4	

Table 5.14 Design of Reinforced Section 11

Section 11 : A pavement section with bituminous layer(s), granular base and Geocell reinforced GSB							
Layers	Thickness (mm)	Width (m)	Length (m)	Quantity (m3)	Cost Incurred (INR)	Amount (Lacs)	Total (Lacs)
BC	30	7	1000	210	10138	21.28	99.33
DBM	-			-	10013	-	
WMM	240			1680	2803.65	47.10	
GSB	125			875	2658.10	23.25	
Geocell	125			7000	110 Sqm	7.7	

Table 5.15 Design of Reinforced Section 12

Section 12: A pavement section with bituminous layer(s), granular base and Geocell reinforced GSB							
Layers	Thickness (mm)	Width (m)	Length (m)	Quantity (m3)	Cost Incurred (INR)	Amount (Lacs)	Total (Lacs)
BC	30	7	1000	210	10138	21.28	107.7
DBM	15			105	10013	10.5	
WMM	260			1820	2803.65	51.02	
GSB	100			700	2658.10	18.60	
Geocell	100			7000 Sqm	90 Sqm	6.3	

5.10 SUMMARY

HIGH VOLUME ROADS

Table 5.16 Cost Analysis of High Volume Roads

Layer	**Thickness (mm)**	**Modulus (MPa)**	**Rate/km (lac)s**
Unreinforced GSB	**200**	**96**	**215.15**
	125	87	201.19
	100	71	176.64
Geocell reinforced GSB	200	110	214.16
	125	**123**	**196**
	100	88	202.84

LOW VOLUME ROADS

Table 5.17 Cost Analysis of Low Voume Roads

Layer	Thickness (mm)	Modulus (MPa)	Rate/km (lac)s
Unreinforced GSB	**200**	**96**	**104.84**
	125	**87**	**112.23**
	100	71	111.88
Geocell reinforced GSB	200	110	107.67
	125	**123**	**99.33**
	100	88	107.7

HIGH VOLUME ROAD - 125 MM GEOCELL COMPARISON WITH 200 MM GSB

Table 5.18 Cost Saving Using Geocell (High Volume Roads)

Cost Saving with Geosynthetic Application	196	percent
Material Saving	Saving in granular material quantity (Cum)	9 – 10 %

LOW VOLUME ROAD – 125 MM GEOCELL COMPARISON WITH 125 MM GSB

Table 5.19 Cost Saving using Geocell (Low Volume Roads)

Cost Saving with Geosynthetic Application	196	percent
Material Saving	Saving in granular material quantity (Cum)	11 – 12 %

5.10.1 The graphical representation of the above results is shown in figure below

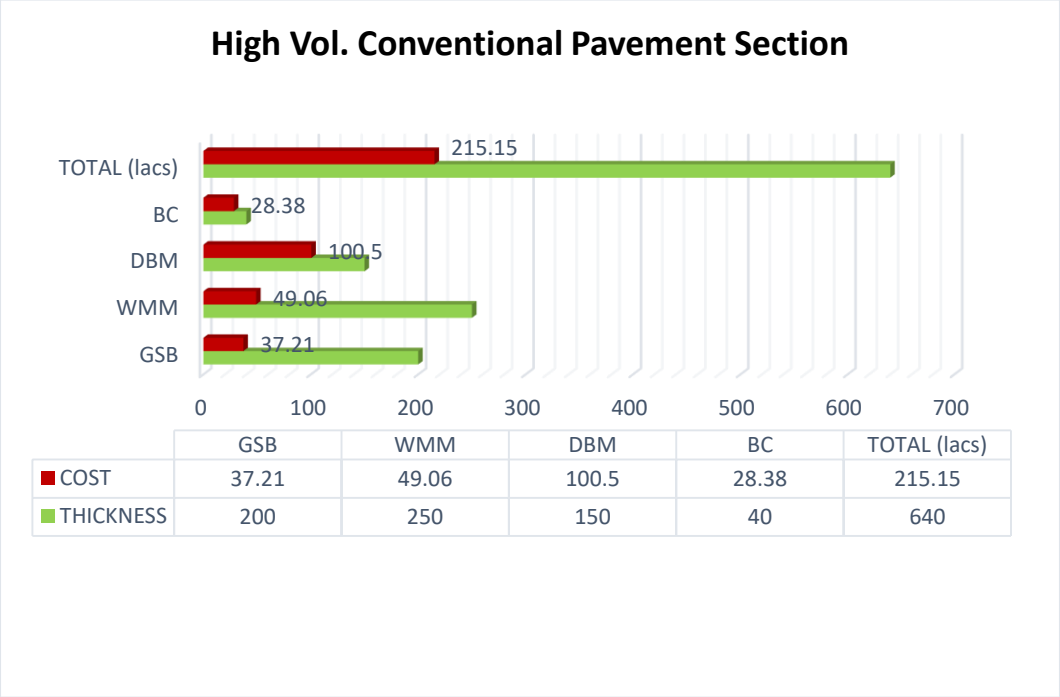

	GSB	WMM	DBM	BC	TOTAL (lacs)
COST	37.21	49.06	100.5	28.38	215.15
THICKNESS	200	250	150	40	640

Figure 5.10 Cost Analysis of High Vol. Conventional Pavement

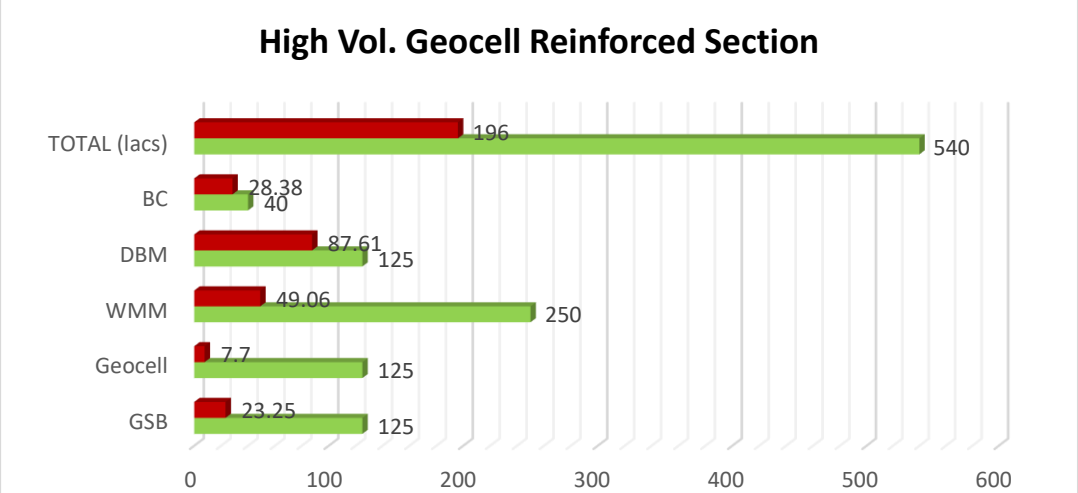

	GSB	Geocell	WMM	DBM	BC	TOTAL (lacs)
COST	23.25	7.7	49.06	87.61	28.38	196
THICKNESS	125	125	250	125	40	540

Figure 5.11 Cost Analysis of High Vol. Geocell Reinforced Section

Tabular representation and graphical representation for thickness, quantity and rate analysis of the section mentioned above is shown in table 5.11 and figure 5.12, respectively.

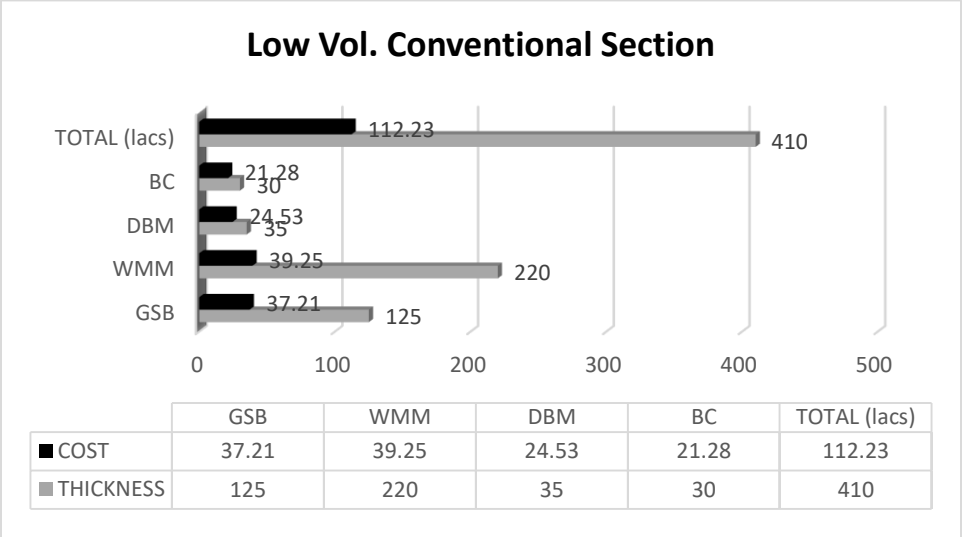

	GSB	WMM	DBM	BC	TOTAL (lacs)
COST	37.21	39.25	24.53	21.28	112.23
THICKNESS	125	220	35	30	410

Figure 5.12 *Cost Analysis of Low Vol. Conventional Pavement*

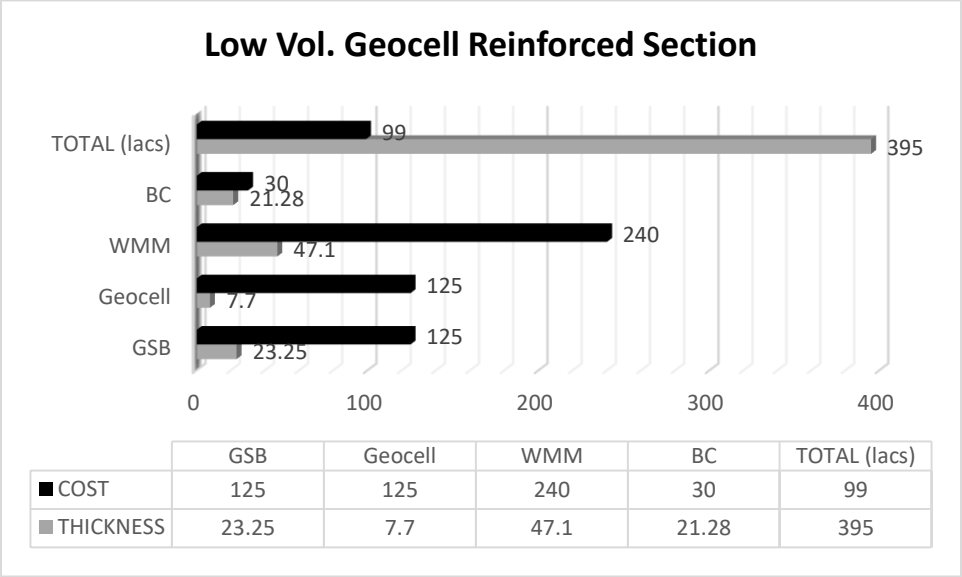

	GSB	Geocell	WMM	BC	TOTAL (lacs)
COST	125	125	240	30	99
THICKNESS	23.25	7.7	47.1	21.28	395

Figure 5.13 *Cost Analysis of Low Vol. Geocell Reinforced Section*

CHAPTER 6

FINITE ELEMENT MODELLING (FEM) AND ANALYSIS OF RESULTS

6.0 GENERAL

This chapter discusses the 3-D FEM that was created to evaluate geocell-reinforced pavement structures to evaluate the behavior of the geocell-reinforced pavement structure under loading, emulating laboratory testing, and traffic loading field situations.

Although FE analysis (FEA) can determine the level of reinforcement given by the geocell, mesh generation for FEA is influenced by several factors, including the interaction between the geocell and neighboring soil, load transfer, and confinement offered by the geocell, among others. Geocell modeling demanded a significant number of elements and nodes to model the honeycomb shape of geocell, which needed a considerable amount of processing effort. Therefore to create a 3-D FE model (FEM) that better fulfills the needs imposed by the geocell-reinforced pavement's properties, multiple FEMs with different levels of sophistication were developed before the final 3-D model was developed. These models were designed to evaluate the following factors:

- Soil material model
- Reinforced-layer boundary conditions
- Geocell Height
- Shell element type
- Geocell-soil interaction

Abaqus, a general-purpose finite element software that permits dynamic FEA and provides a comprehensive set of material and contact models/algorithms, was selected to perform FEA.

6.1 PARAMETRIC STUDY

For testing the influence of the geocell reinforced layer on pavement performance, the following parameters were selected:

1) The thickness of the geocell reinforced layer
2) Infill material modulus (GSB)
3) Subgrade modulus

The plan for conducting the parametric study is shown in Table 6.1. It also displays the material parameters, as well as the layer thicknesses. All of the cases in Table 6.1 are also done without a geocell to compare the effectiveness of the geocell. According to the laboratory evaluation plan mentioned in previous chapters, GSB of height 100 mm, 125 mm, and 200 mm was selected.

Table 6.1: Dimension and Properties of Geocell-Reinforced Pavement FE Model with Geocell Panel Simulated Using Hexagonal Shaped Cells

Pavement Structure Thickness		
Layers	Geocell Reinforced Pavement Structure	Unreinforced Pavement Structure
Top Subbase layer (mm)	Varying 100, 125 and 200	Varying 100, 125 and 200
Geocell Reinforced Subbase (mm)	Varying 100 , 125 and 200	Varying 100 , 125 and 200
Subgrade (mm)	500	500
Finite Element Model Properties (Geocell 200 mm)		
No of Solid Elements (Geocell)	4280	
Number of Thick Shell Elements (Geocell)	4280 of type S4R	
Total Number of Elements	9880	
Total Number of Nodes	11577	
Finite Element Model Size		
Longitudinal Dimension, x-axis (mm)	500	
Transverse Dimension, y-axis (mm)	1000	

The influence of the geocell reinforced layer was evaluated using the following two pavement performance criteria:

- Vertical stress distribution on the top of the subgrade
- Vertical strain distribution on the top of the subgrade

The typical quarter model used in the study, as well as the various layers in the model, are shown in Figure 6.1 below

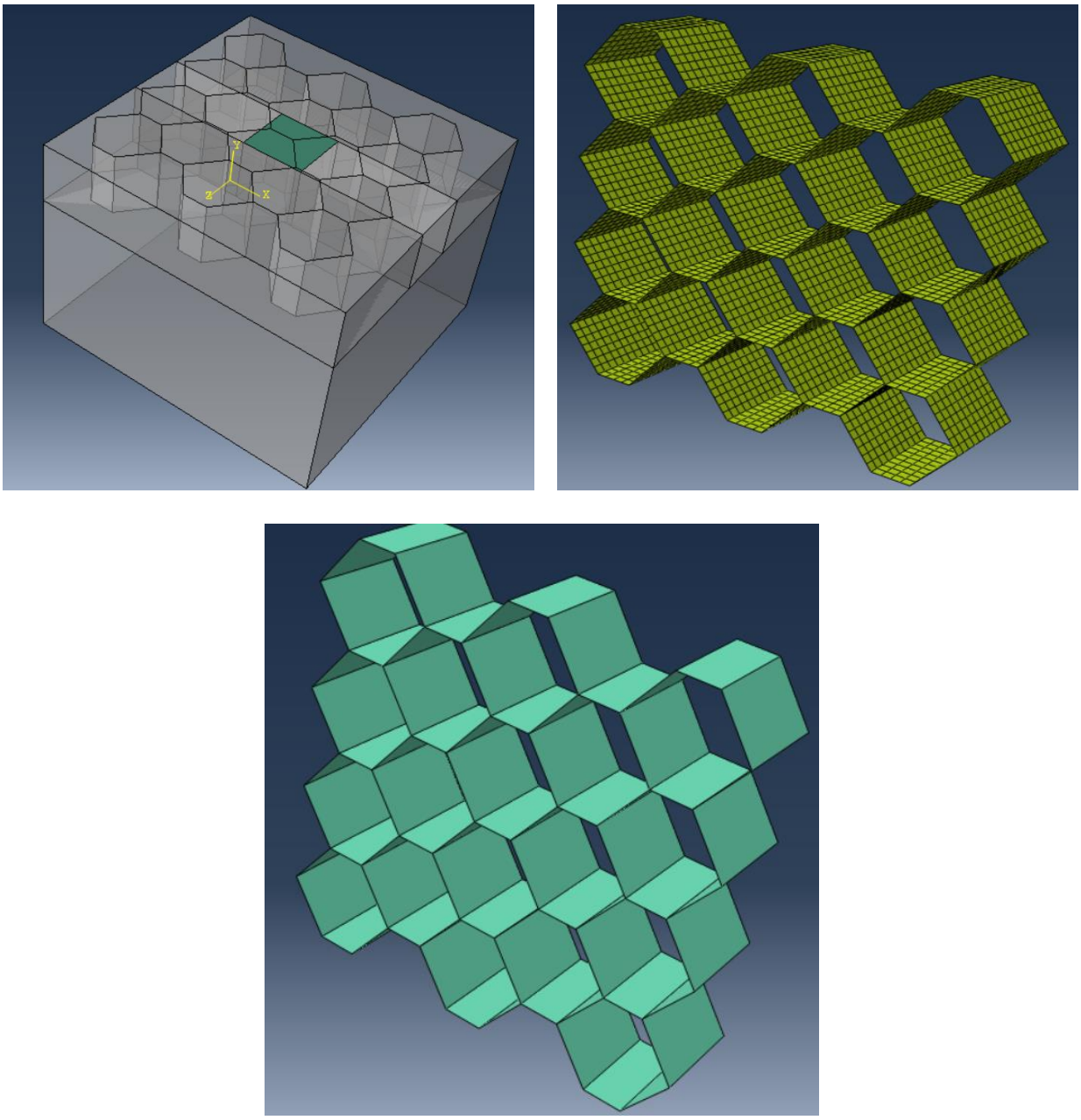

Figure 6.1 : Model used in the parametric study

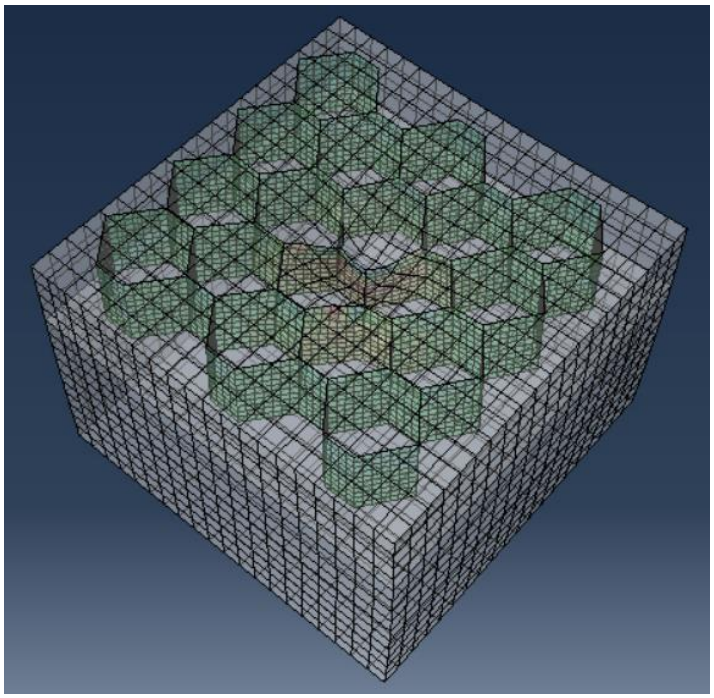

Figure 6.2 Location of output evaluated from FEA

Each model has a 500 mm subgrade layer beneath the subbase layers. The properties examined are represented by a legend that included geocell height and infill material modulus and subgrade modulus.

Instead of measuring the output on a single element, an average of three elements (nearby) was considered, which illustrates the strains measured on subgrade for both geocell and no geocell model for 100 mm, 125 mm, and 200 mm thicknesses.

Except for stresses on the geocell, all FEA results are compared to the stresses and strains obtained from IITPave software. Only one load cycle data is used to compare IITPave and FEA. The following sections discusses the impact of the geocell reinforced layer on the performance factors.

6.2 INFLUENCE OF SUBBASE MODULUS VALUES

For comparison purposes, six different cases were studied (three with 100 mm,125 mm, and 200 mm thick geocell reinforced sections and three with unreinforced sections of the same thicknesses). The subgrade is 500 mm thick and has a 59 MPa modulus.

The infill material has the same properties as the conventional subbase layer used in the unreinforced section. Figures 6.3 and 6.4 show the strain distribution on the top of the subgrade for material with different infill modulus. There is a noticeable difference in strains between geocell and no geocell cases when they are of different sizes.

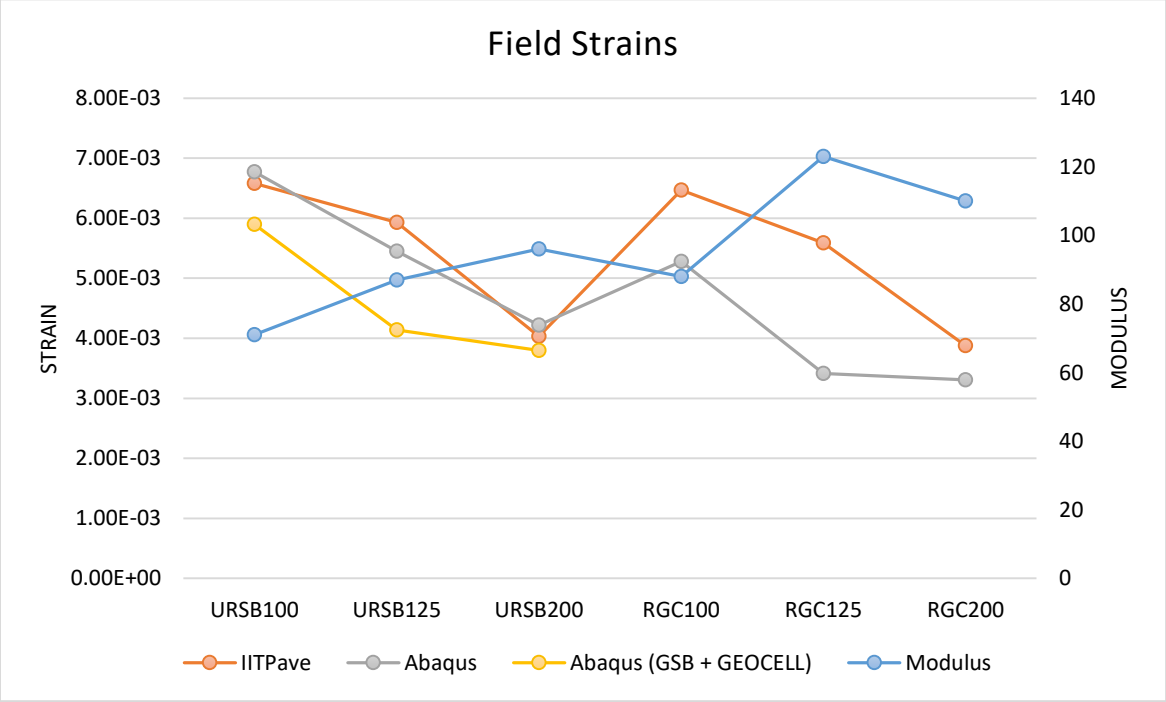

Figure 6.3 Field Strain Distribution (Unreinforced vs. Geocell Reinforced) along the Subgrade

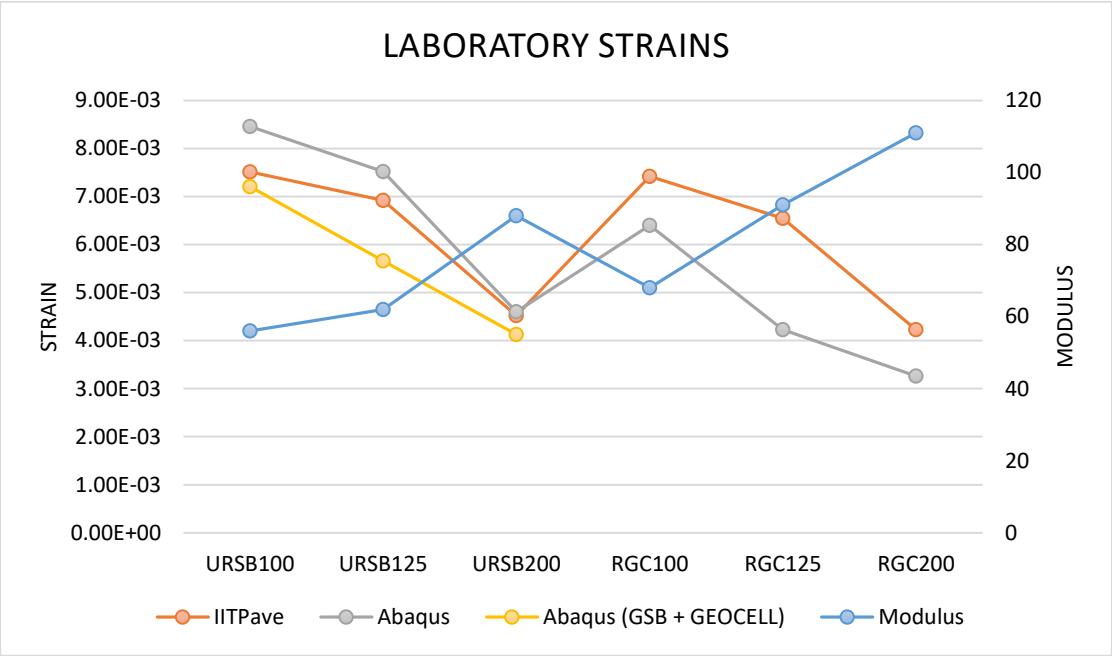

Figure 6.4 Laboratory Strain Distribution (Unreinforced vs. Geocell Reinforced) along the Subgrade

The following conclusions are drawn based on the summarized results: The stresses and strains estimated from FEA (unreinforced or reinforced geocell layer) are higher than those estimated using IITPave software. Geocell reinforced layers often produced higher deformation than the no geocell layers. This trend is like the one observed in the laboratory evaluations as well. Therefore the results obtained from the Finite Element Modelling fall well within the values obtained from the IITPave software.

6.3 INFLUENCE OF GEOCELL LAYER THICKNESS OR GEOCELL HEIGHT

This study used three geocell heights (Geocell 100 mm, 125 mm, and 200 mm) for comparison. The figures below show the results, and the analysis yields the following conclusions:

In terms of geocell height, the geocell 200 mm performance is inferior to other geocell sizes as it only reduced stresses up to 10% at from the loading. In contrast, geocell 100 mm and 125 mm reduced the stresses more as compared to Geocell 200 mm. Geocell 200 has minimal influence over the unreinforced GSB 200 mm (URSB200).

The observed trends are presented in this section, and the benefits of geocell height are summarized in the form of tables below based on the overall evaluation. The results show that geocell heights of 100 and 125 mm provide a benefit when employing geocell. The test results also suggest that tension on top of the subgrade should be considered when designing geocell pavements.

6.4 FINITE ELEMENT MODEL DEVELOPMENT

A 3-D FE model was created for this purpose in order to address better the geometry of geocell panels, which expand into a honeycomb configuration when deployed on-site, as illustrated in Figure 6.5.

Figure 6.5 Geocell and infill material

6.5 SOIL MODELS

Many researchers used FEM or finite difference methods to model the geocell and infill material as a composite material (Bathurst and Knight 1998; Latha and Somwanshi 2009; Latha et al. 2009; Mhaiskar and Mandal 1996), but only a few modeled them separately (Bortz and Hossain 2015; Evans 1994; Yang 2010, Han et al. 2008. The infill material (linear elastic or plastic) and geocell (elastic) respond to loading simultaneously in the geocell reinforced base layer, although each material's working mechanism is distinct. As a result, in order to more exactly predict a geocell reinforced subbase layer, the behavior of each material (infill and geocell) must be studied independently, as was done in this study.

Geomaterials' mechanical behavior can be modeled to varying degrees of accuracy. The most fundamental stress-strain relationship, Hooke's equation of linear elasticity, may not give appropriate responses to reflect soil behavior under traffic loading effectively. Researchers have presented many constitutive models to describe various elements of soil behavior. However, as a soil model becomes more advanced, more input parameters require further laboratory experiments. Only a few models rely on parameters derived from standard laboratory studies.

6.6 SHELL ELEMENT TYPE FOR GEOCELL MODELING

The element aspect ratio or computational constraints are one of the issues that arise while modeling the geocell and geomaterials. Although geomaterials can be modeled as solid elements of any size and shape, the geocell, due to its thickness, can only be modeled in certain shapes and sizes.

6.7 GEOCELL DIMENSIONS AND PROPERTIES

In the parametric study, three different types of geocells with different heights were simulated. The dimensions and material properties of the geocell types evaluated are shown in Table 6.2. Geocell was modeled as a material with linear elastic properties.

Table: 6.2 Geocell Dimension and Properties

Geocell Dimensions			
Longitudinal length (mm)	880		
Transversal Length (mm)	840		
Height (mm)	**100**	**125**	**200**
Thickness (mm)	2		
Material Properties			
Density (kg/m3)	950		
Modulus (MPa)	275		
Poisson's Ratio	0.35		

6.8 CONTACT MODEL

6.8.1 FINITE ELEMENT TYPES AND MESH SIZE

In ABAQUS, the 8-node continuum three-dimensional brick element (C3D8R) with reduced order numerical integration is used to model all of the model's components. This element can represent significant deformations, as well as geometric and material nonlinearities. Each node of the solid element (C3D8R) has three degrees of freedom. To maintain the continuity of nodes between successive levels, all layers are simulated with the same geometry Figure 6.6 shows the entire model.

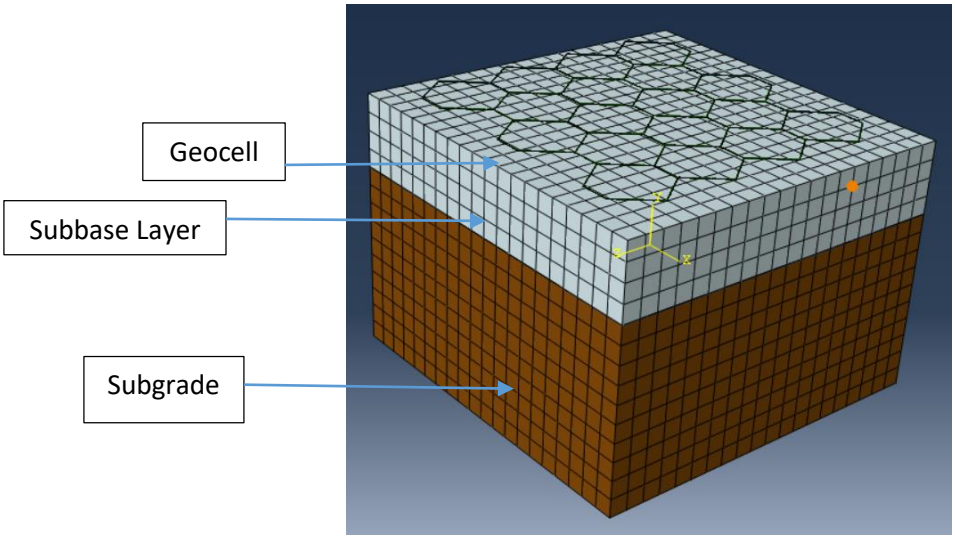

Figure 6.6 Mesh for all layers

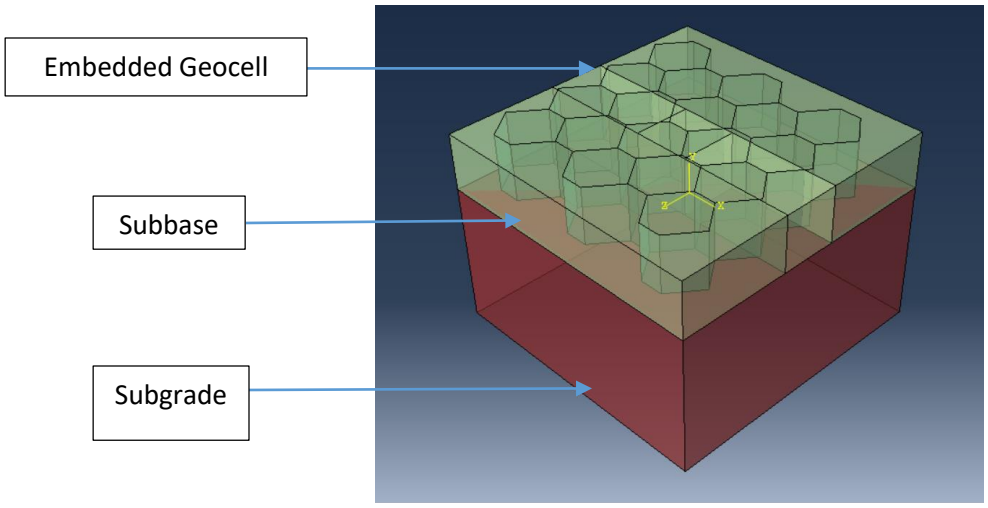

Figure 6.7 REINFORCED MODEL USED IN THE STUDY

6.8.2 BOUNDARY CONDITIONS

The model was allowed to move in the direction of the major principal stress σ1 (i.e., vertical settlement) and the minor principal stresses σ 3′ (i.e., parallel the roadway) (1 ε, 3 ε ≠ 0). The base of the model was restricted to any displacement, as shown in Fig 6.8. The type of element chosen was C3D8R (i.e. eight-node reduced integration element). The interaction between subbase and geocell strips was modelled with contact elements, including the hard normal contact as used by Leshchinsky and Ling (2013a). Given the highly random nature of particles orientations within the subbase assembly, it was assumed that angle of the shearing resistance between the aggregates and geocell mattress was isotropic, considering that the membrane texture is usually uniform. In the numerical simulation, the contact between the infilled granular soil and geocell wall was modelled as an interface element with a fixed angle of shearing resistance. The bottom surface of the subgrade and the sides of the layers are assumed to be fixed, which means that the nodes at the bottom of the subgrade and sides of layers cannot move horizontally or vertically, which has a significant effect on predicting the model's response. This is a representation of the steel box's bottom and sides. The boundary conditions used in the analysis are shown in Figure 6.8

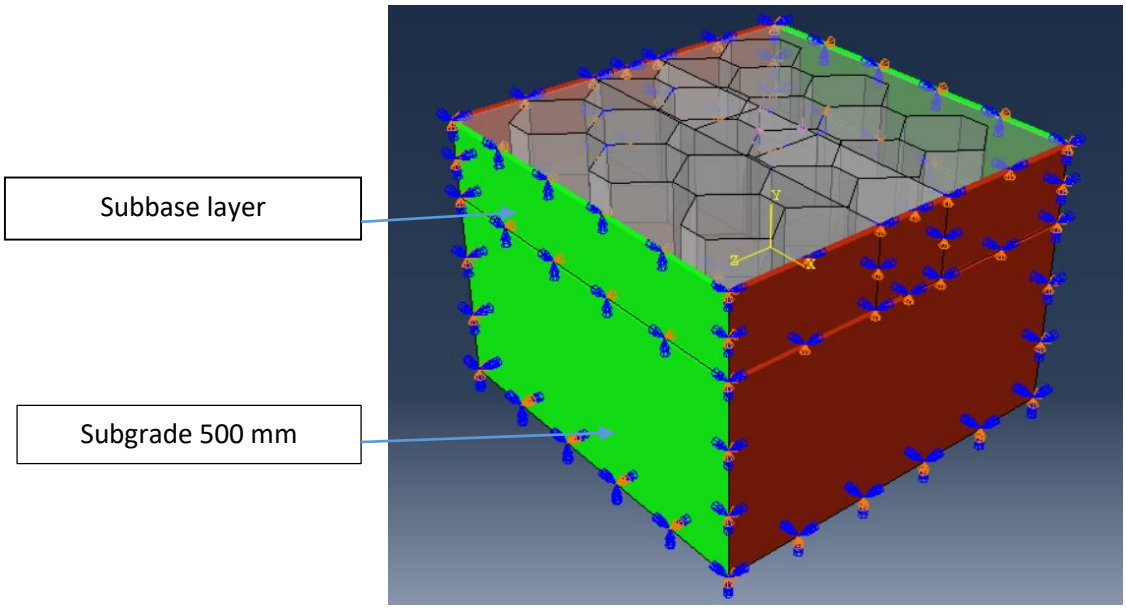

Figure 6.8 Boundary Conditions

6.8.3 LOADING CONDITIONS

In order to have uniform deformation, initially, a constant confining pressure was applied to the unit to simulate mean pressure due to the geostatic stresses inherent in a subbase. A static load with a magnitude of σ mean = 40000 N was applied to the top of the specimen in the strain-controlled model. The maximum stress pattern was chosen to provide the most possible critical stress that could be applied to the subbase as measured by Indraratna et al. (2015)

In ABAQUS, the applied wheel load is 40000 N (0.4 KN), that is evenly distributed across the whole contact area. Calculated uniform contact pressure of 0.56 MPa, which is the same as the pressure of a tyre using two parameters: longitudinal and transverse vertical pressure distribution on the loaded surface. Loading is used to simulate horizontal wheel motion at a preset pace. The loading position should be applied in a gradual manner in this procedure, as indicated in Figure 6.9, in order to have a complete wheel position 6.10. Figure 6.11 shows the model's wheel deformation position due to loading.

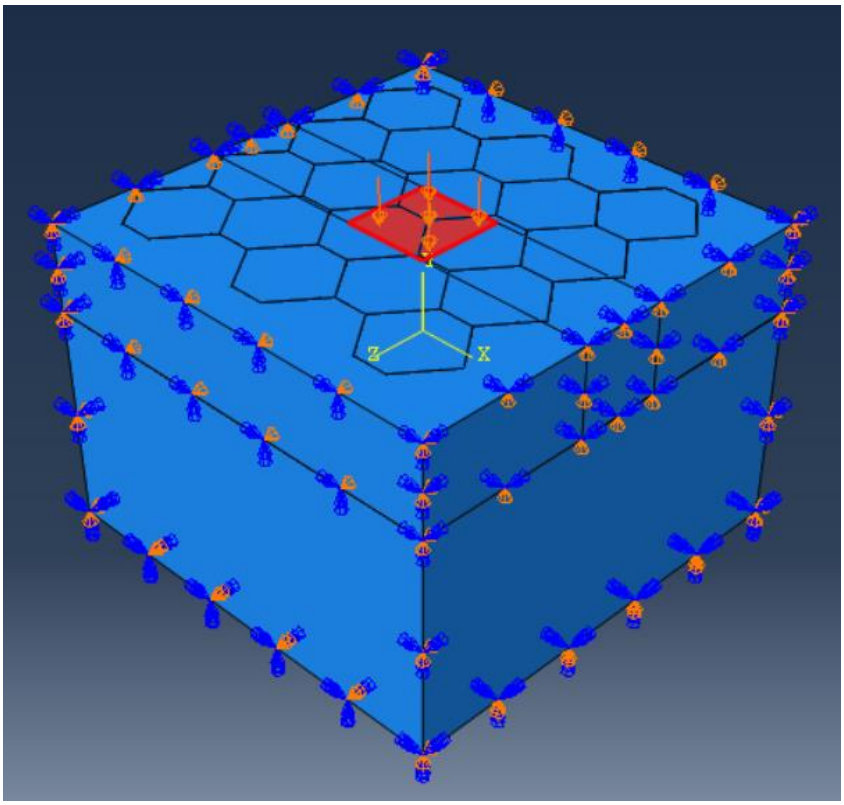

Figure 6.9 Position of Wheel/loading

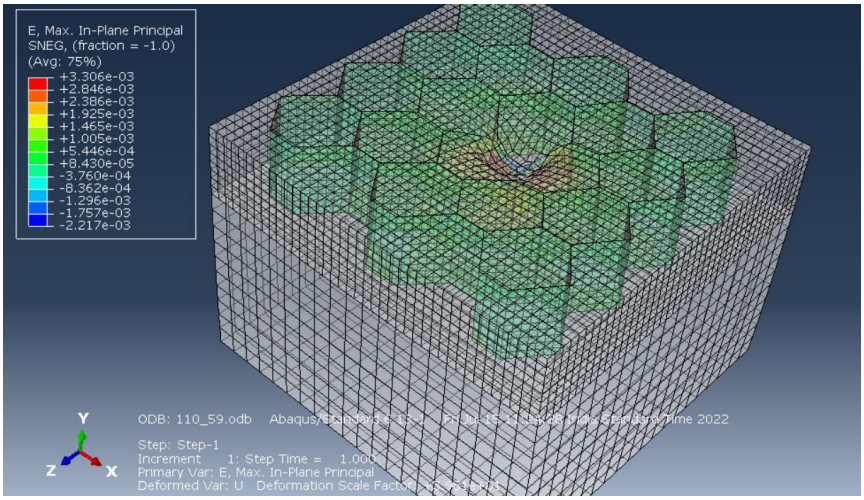

Figure 6.10 Location of output evaluated from FEA

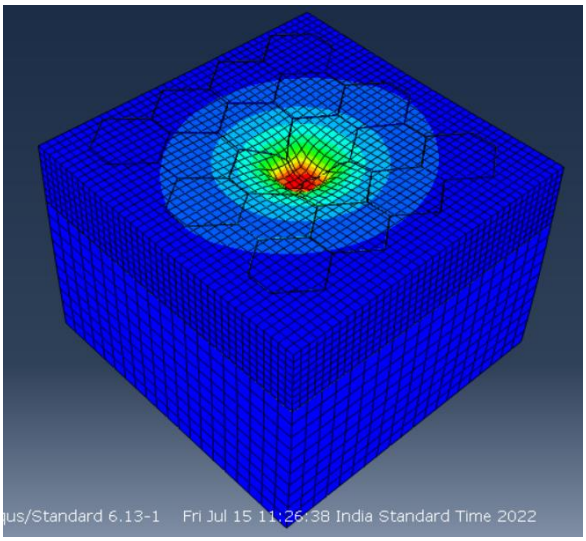

Figure 6.11 Deformation due to loading conditions

6.9 Summary

The results of the ABAQUS program are very close to the results of laboratory tests; Figure 6.3 and 6.4 show the result of Lab and ABAQUS strain values for 100 mm, 125 mm, and 200 mm geocell reinforced subbase thickness respectively. The output results of Abaqus software shows the beneficial effects of the axial stiffness of geocells in the subbase course and interface strength of materials at different thickness of subbase course layer on vertical surface deformation

6.10 FIELD STRAIN VALUES CALCULATED

Table 6.3 Strain values calculated for field evaluation using softwares

Section	MODULUS	IITPave	ABAQUS	Abaqus (GSB + GEOCELL)
URSB100	71	6.58E-03	6.77E-03	5.90E-03
URSB125	87	5.93E-03	5.45E-03	4.14E-03
URSB200	96	4.03E-03	4.22E-03	3.80E-03
RGC100	88	6.47E-03	5.28E-03	-
RGC125	123	5.59E-03	3.42E-03	-
RGC200	110	3.88E-03	3.31E-03	-

6.11 LABORATORY STRAIN VALUES CALCULATED

Table 6.4 Strain values calculated for laboratory evaluation using softwares

Section	MODULUS	LAB	ABAQUS	Abaqus (GSB + GEOCELL)
URSB100	56	7.51E-03	8.46E-03	7.21E-03
URSB125	62	6.92E-03	7.52E-03	5.66E-03
URSB200	88	4.52E-03	4.60E-03	4.13E-03
RGC100	68	7.42E-03	6.40E-03	-
RGC125	91	6.55E-03	4.23E-03	-
RGC200	111	4.23E-03	3.26E-03	-

6.12 FLEXIBLE PAVEMENT MODEL USING FEM

This section presents the entire pavement model used in the study for calculating the actual strains generated in the model at the surface using Abaqus Software (FEM). The section shows the cross section of the pavement followed by the strains calculated in the software. Increase in the thickness of flexible pavement increases the number of passes which reaches the same value of rutting (value of failure) and leads to decrease the displacement in subgrade and subbase layers. The ABAQUS program successfully simulated pavement structure models, so the ABAQUS program can be used to analyze paved and unpaved roads.

In this study, finite element modelling is analysed to examine the beneficial effects of reinforcement in pavement subbase layers at different thickness.

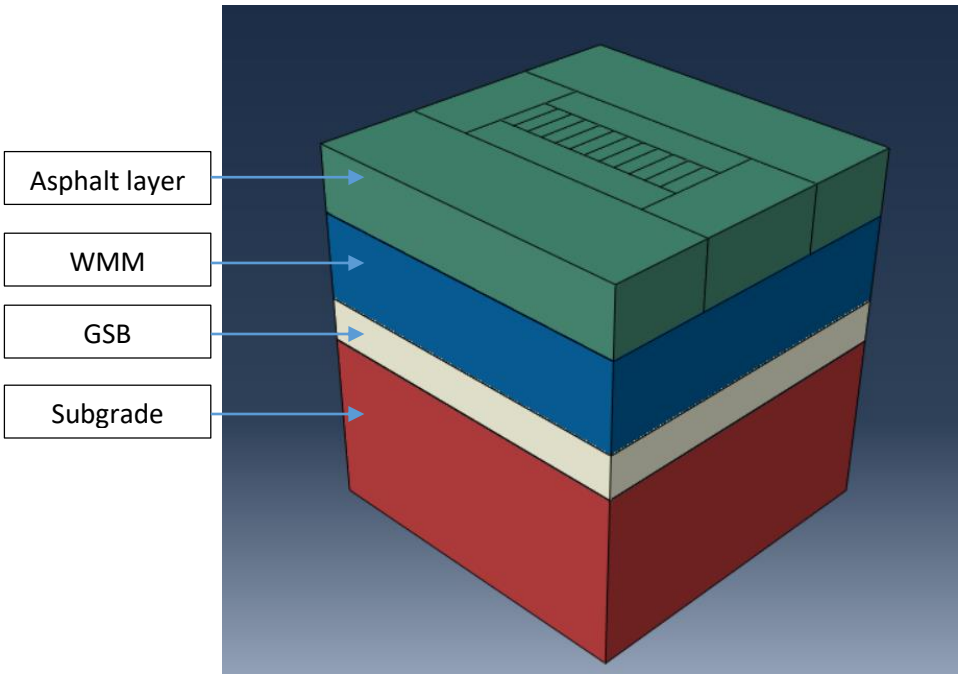

Figure 6.12 Cross section of Unreinforced Section

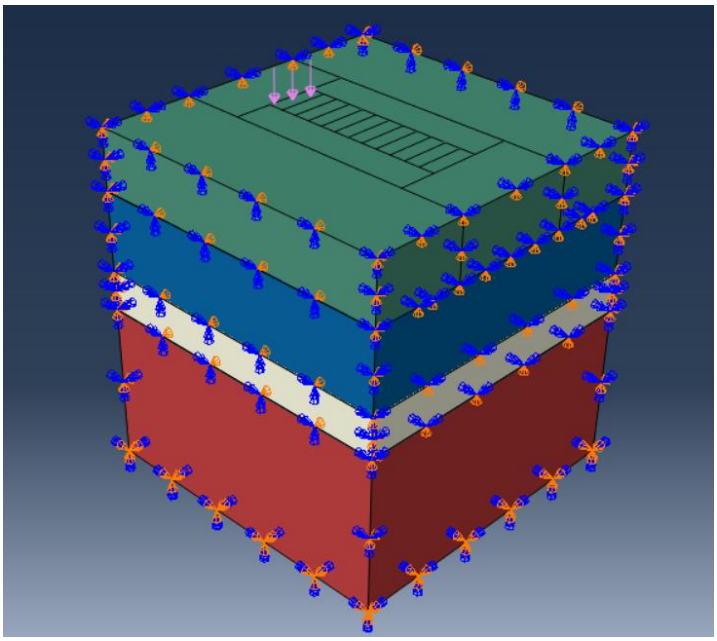

Figure 6.13 Boundary Conditions

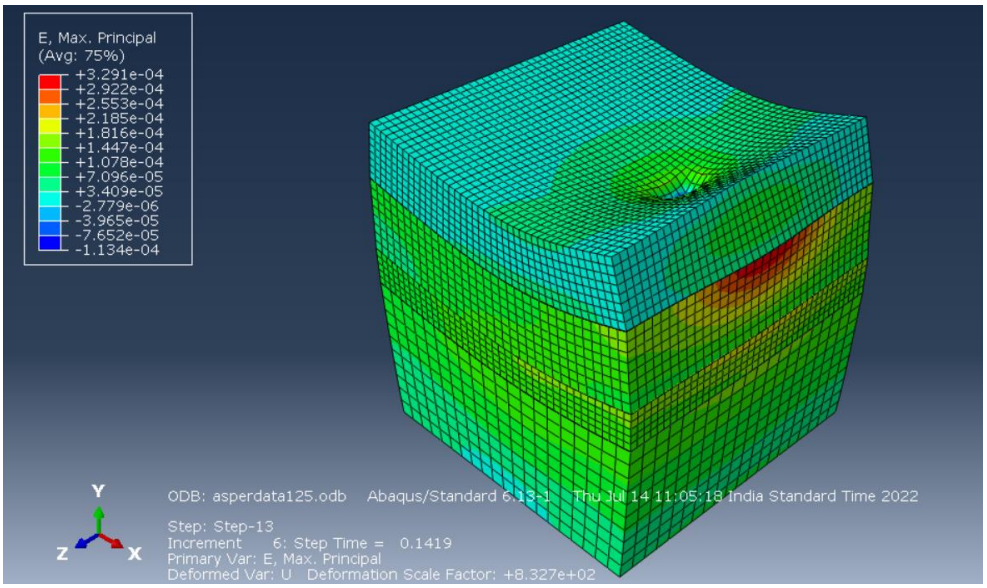

Figure 6.14 Effect due to loading on the surface layer

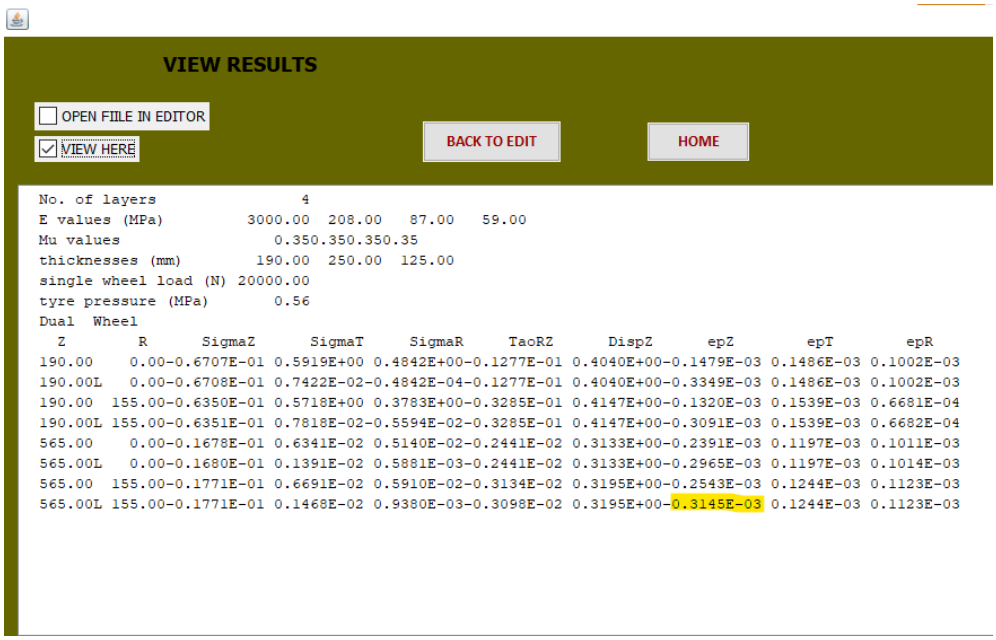

Figure 6.15 Screenshot of output strain values from IITPave

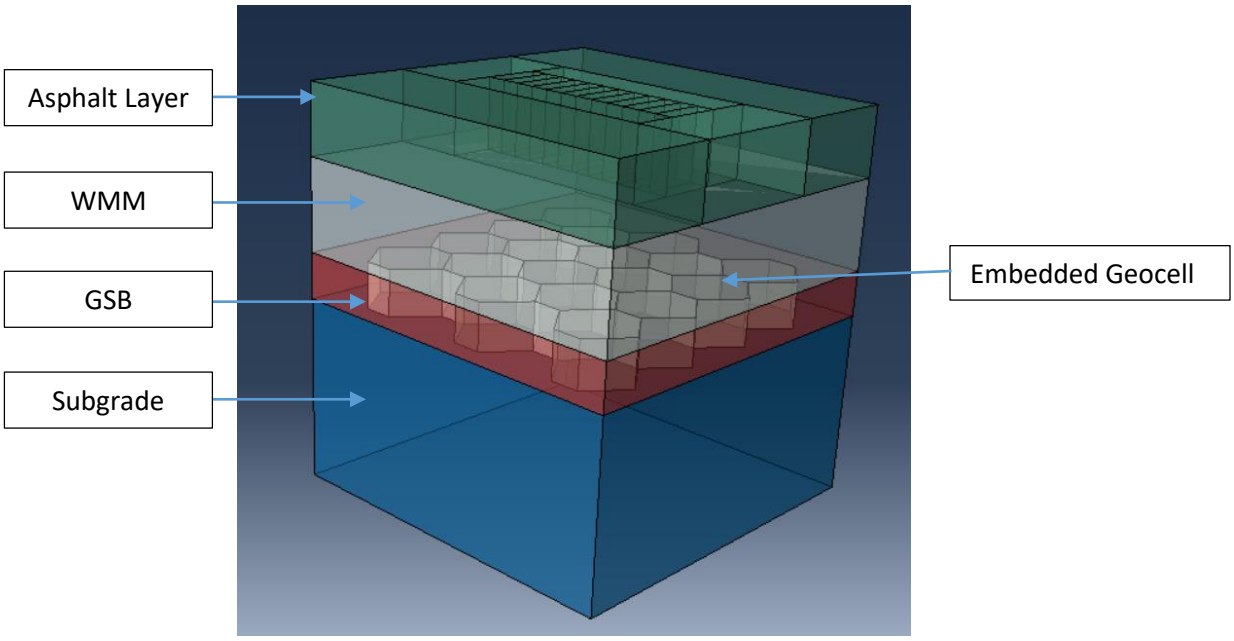

Figure 6.16 Cross section of geocell reinforced section

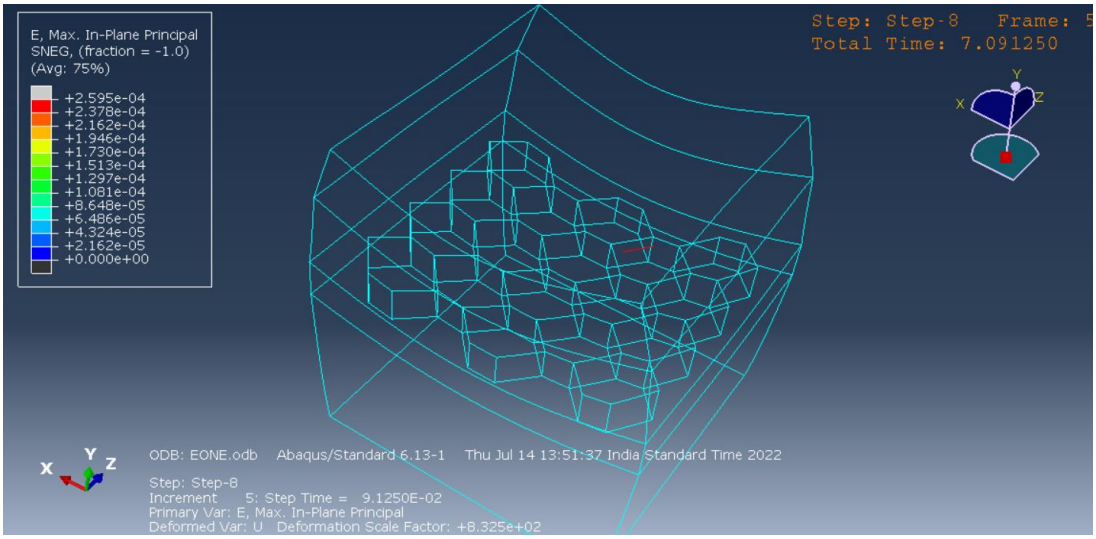

Figure 6.17 Deformation sketch of the section model

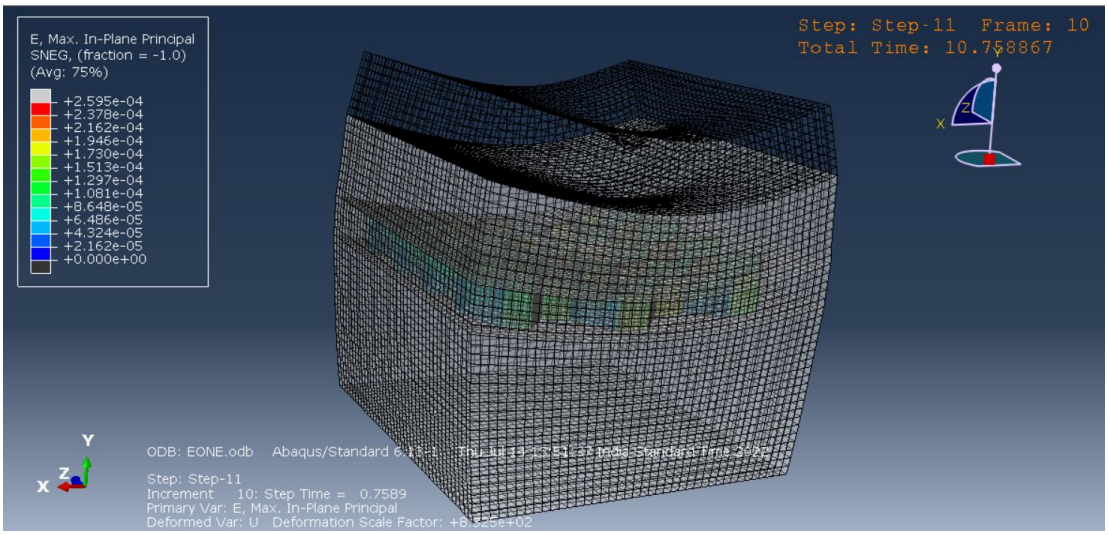

Figure 6.18 Shows effect of cyclic loading on the entire pavement section

Table 6.5 Comparison of strain values using software's

Section	IITPave Value	Abaqus Value	Abaqus GSB+Geocell
125 mm GSB	3.14E-04	3.53E-04	2.60E-04

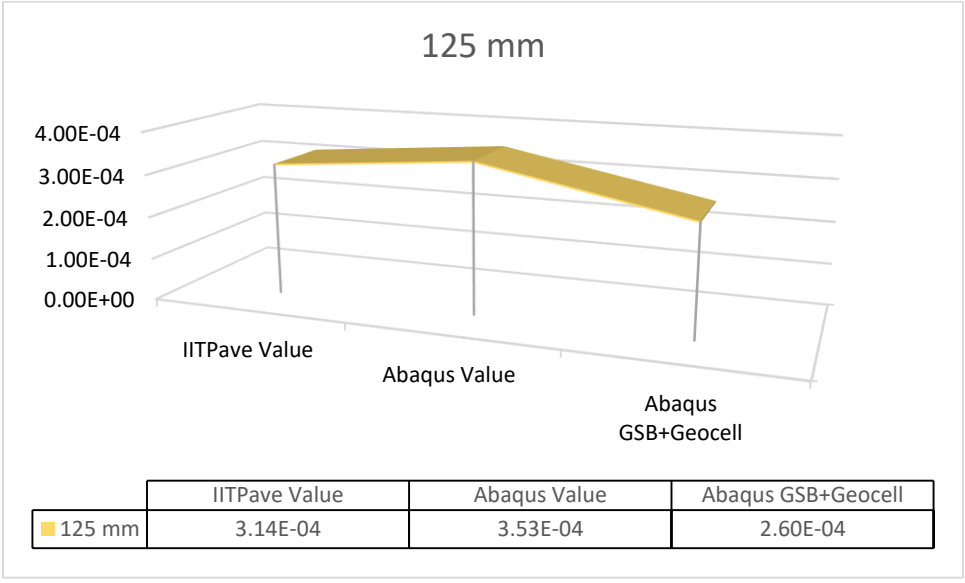

Figure 6.19 Calculated strain values using software's

CHAPTER 7

CONCLUSION

In this study, the effect of various factors affecting the performance geocell reinforcement of unbound subbase layer were studied using the LWD device. This paper has presented some results from field and laboratory tests on the performance of pavements with different types of geocell thicknesses. It is seen that both the strength and stiffness of the pavement system can be improved by the use of geocells. The performance under loads is also better with geocell reinforcement layers distributing the applied loads over a much wider area of the subgrade thus reducing the stresses at the subgrade level. In addition, the effect of modulus parameters on the results were studied in the Finite Element Modelling. Based on the results of 98 LWD tests conducted in this study, the following conclusions can be drawn:

- The modulus improvement factors obtained from both laboratory and field tests are close to each other. The modulus improvement factor is seen to be higher for RGC125 section as compared to other sections. The equivalent modulus improvement factor observed is 1.46 times of the unreinforced pavement section which indicates that the reinforced pavement section is stiffer than the unreinforced one and that too with the reduced thickness.

- With increase in the density of the fill aggregates there is an overall improvement in the load carrying capacity of the geocell-soil system. Therefore, the aggregate material in the geocells should be compacted to higher density.

- The structural design for thickness of flexible pavement for unreinforced section with high volume traffic is 640 mm. The design thickness of geocell reinforced flexible pavement with respect to design traffic of 50 msa is 540 mm. For design traffic 5 msa thickness are 440 mm for unreinforced section and 395 for geocell reinforced section.

- The results concluded that the pavement thickness is reduced by 15% by using geocell in granular subbase in the unreinforced section in flexible pavement.

- After comparing the cost analysis discussed in previous chapter, it clearly shows that reinforced pavement is 10% cheaper than the unreinforced pavement in high volume roads and 12% in low volume roads for every km 7m width road construction. The inclusion of geocell in subbase layer results in reducing the subbase thickness to 37.5% to that of the unreinforced one, which ultimately reduces the usage of the virgin material which is very scarce in nature.

- Influence of Subbase Modulus in FEM: The geocell reinforced layer reduced the strains up to 35% .The strains on the loaded geocell increased with a lower subbase modulus.

- Influence of Geocell-Reinforced Layer Thickness in FEM: The 100 mm geocell reinforced layer reduced the strains up to 20-25% compared with no geocell layer. The 125 mm geocell reinforced layer reduced the strains up to 30-45% from the center of the loading compared with no geocell layer. The 200 mm geocell reinforced layer reduced the strains 10-30% away from the center of the loading. Comparing the three geocell, the geocell 100mm performance is inferior to other geocell heights as it only reduced stresses up to 25% whereas geocell 125 mm and 200 mm reduced the stresses around 45%.

- Influence of Geocell-reinforced layer in Flexible Pavement Model: The 125 mm geocell reinforced layer reduced the strains up to 26% compared with no geocell layer.

- The FEM and laboratory test results showed similar trends with the IITPave software. A maximum difference of 10% (vertical stress on top of the subgrade) was observed between them, indicating that FEM analysis can be performed for any new material selected for analysis. These results will be of use in providing guide-lines for design and construction of geocell-reinforced sections, conducting large-scale model tests, and developing numerical models.

REFRENCES

Abu-Taleb, M.G. and Egeli, I. (1981): "Some Geotechnical Problems in the Eastern Province of Saudi Arabia." Proc., Symp. Geotechnical Problems in Saudi Arabia, King Saudi Arabia, Vol. I, 799-811.

Acharya, B. S. (2011) “Experimental study on geocell-reinforced flexible pavements with recycled asphalt pavement (RAP) bases under cyclic loading." PhD diss., University of Kansas.

Aiban, A. S. (1994): "A Study of Sand Stabilization in Eastern Saudi" Department of Civil Engineering, (King Fahd University of Petroleum and Minerals, Dhahran 31261), Saudi Arabia Received 24 March 1993; revised version accepted 5 July 1994.

Aiban, S., Al-Amoudi, O., Asi, I.M. and Zahrani, A. (1996):"Chemical Stabilization of Ras AL-Ghar Sabkha Soil", Twelfth Southeast Asian Geotechnical Conference, Kuala.

Al-Amoudi, O.S. and Abduljauwad, S.N (1991): " Geotechnical Considerations on Field and Laboratory Testing of Sabkha." Proc., Symp Recet Advances in Geotechnical Engineering III, Singapore, Vol. 1, 1-6.

Al-Qadi and Wang H:" Pavement Damage Due to Different Tire and Loading Configurations on Secondary Roads" USDOT.(2009).

Asha, M. N., and G. Madhavi Latha (2014) "Model studies on geocell reinforced granular subbases."In *Ground Improvement and Geosynthetics*, pp. 322-332.

ASTM D854-00: "Standard Test Method for Specific Gravity of Soil Solids by PycnometerLumpur, Malaysia, Vol. May, pp. 265-270.

Bush, D. I., C. G. Jenner, and R. H. Bassett. (1990) "The design and construction of geocell foundation mattresses supporting embankments over soft grounds." *Geotextiles and Geomembranes* 9, no. 1: 83-98.

Bathurst, Richard J., and Rajagopal Karpurapu. (1993) "Large-scale triaxial compression testing of geocell-reinforced granular soils." *Geotechnical testing journal* 16, no. 3 296-303.

Cowland, J.W. and Wong, S.C.K (1993). Performance of a road embankment on soft clay supported on a geocell mattress foundation. *Geotextiles and Geomembranes*, *12*(8), pp.687-705.

Emersleben, A., and N. Meyer (2008) "Bearing Capacity Improvement of Asphalt Paved Road Constructions Due to the Use of Geocells—Falling Weight Deflectometer and Vertical Stress

Measurements." In *Geosynthetics in Civil and Environmental Engineering*, pp. 747-753. Springer, Berlin, Heidelberg.

Fookes, P. C. and Higginbottom, I. E. (1975): "The Classification and Description of Nearshore Carbonate Sediments for Engineering Purposes. " Geotechnique, 2, 406-414

Han, Jie, Xiaoming Yang, Dov Leshchinsky, and Robert L. Parsons (2008) "Behavior of geocellreinforced sand under a vertical load." *Transportation Research Record* 2045, no. 1: 95 101.

Han, J., Pokharel, S.K., Parsons, R.L., Leshchinsky, D. and Halahmi, I., (2010), May. Effect of infill material on the performance of geocell-reinforced bases. In *Proc., 9th Int. Conf. on Geosynthetics* (pp. 1503-1506). São Paulo, Brazil: International Geosynthetics Society.

Hegde, Amarnath M., and T. G. Sitharam (2015) "Effect of infill materials on the performance of geocell reinforced soft clay beds." *Geomechanics and Geoengineering* 10, no. 3: 163-173.

Inti, Sundeep, and Vivek Tandon. (2015) "Design of geocell reinforced roads through fragility modeling." *Geotextiles and Geomembranes* .

Khedkar, M. S., and J. N. Mandal (2009) "Behaviour of cellular reinforced sand under triaxial loading conditions." *Geotechnical and Geological Engineering* 27, no. 5: 645-658.

Krishnaswamy, N. R., K. Rajagopal, and G. Madhavi Latha (2000) "Model studies on geocell supported embankments constructed over a soft clay foundation." *Geotechnical testing journal* 23, no. 1: 45-54.

Kouchaksaraei, Mohsen Kabiri, and Ahad Bagherzadeh Khalkhali (2020) "The effect of geocell dimensions and layout on the strength properties of reinforced soil." *SN Applied Sciences* 2, no. 10: 1-13.

Latha, G. Madhavi, and Vidya S. Murthy (2007) "Effects of reinforcement form on the behavior of geosynthetic reinforced sand." *Geotextiles and Geomembranes* 25, no. 1: 23-32.

Li, Xiaowei, Yunsheng Zhu, Tiansheng Su, Xianrong Wang, and Xiedong Zhang (2021): "Study on performance improvement of new geocell reinforced asphalt mixture." *Construction and Building Materials* 273 121693.

Madhavi Latha, G., K. Rajagopal, and N. R. Krishnaswamy (2006) "Experimental and theoretical investigations on geocell-supported embankments." *International Journal of Geomechanics* 6, no. 1: 30-35.

Mandal, J. N., and P. Gupta. (1994) "Stability of geocell-reinforced soil." *Construction and building materials* 8, no. 1: 55-62.

Medved, Samo Peter, Bojan Žlender, Stanislav Lenart, and Primož Jelušič (2016) "Modeling of a geocell-reinforced pavement: an experimental validation." *Acta Geotechnica Slovenica* 13, no. 2: 3-14.

Masood , G.G. "Experimental and Numerical Investigation of stabilized unbound Granular Pavement Materials" AL-Mustansiriya University College of Engineering Highway and Transportation Engineering Department Ms. Thesis(2013).

Pokharel, Sanat Kumar, Jie Han, Dov Leshchinsky, Robert L. Parsons, and Izhar Halahmi (2009) "Behavior of geocell-reinforced granular bases under static and repeated loads." In *Contemporary topics in Ground Modification, Problem Soils, and Geo-Support*, pp. 409-416.

Pokharel, S. K., I. Martin, M. Norouzi, and M. Breault (2015) "Validation of geocell design for unpaved roads." In *Proceedings of Geosynthetics*, pp. 15-18.

Rajagopal, K., A. Veeragavan, and S. Chandramouli. (2012) "Studies on geocell reinforced road pavement structures." *Geosynthetics Asia*.

Rajagopal, K., N. R. Krishnaswamy, and G. Madhavi Latha (1999) "Behaviour of sand confined with single and multiple geocells." *Geotextiles and Geomembranes* 17, no. 3: 171-184.

Salem L. A. (2011): " An Approach in Evaluating The Behavior of Dune sand Under Shallow Footing" Ms Thesis University of Baghdad, College of Engineering

Song, Gaofeng, Shiqin He, Xiaoruan Song, Zhongjian Duan, Yatao Zhang, Dezhong Kong, and Miansong Huang (2021) "The use of geocell as soil stabilization and soil erosion countermeasures." *Geomatics, Natural Hazards and Risk* 12, no. 1: 2155-2169.

STM D698-00a: "Standard Test Methods for Laboratory Compaction Characteristics of Using Standard Effort (600 kN-m/m).

Shastri Avinash, Rajesh Misra (2019) “Experiment on Soil Properties Made with Geocell- Shredded Tyres Reinforced Sand.” International Journal of Advance Research, Ideas and Innovations in Technology.

Tanyu, B. F., A. H. Aydilek, A. W. Lau, T. B. Edil, and C. H. Benson (2013) "Laboratory evaluation of geocell-reinforced gravel subbase over poor subgrades." *Geosynthetics International* 20, no. 2: 47-61.

Tafreshi, SN Moghaddas, and Andrew R. Dawson (2010)"Laboratory model tests for a strip footing supported on geocell reinforced sand bed." In *Ground Improvement and Geosynthetics*, pp. 353-360.

Wang, Yi-min, Ye-kai Chen, and Wei Liu (2008) "Large-scale direct shear testing of geocell reinforced soil." *Journal of Central South University of Technology* 15, no. 6: 895-900.

Wesseloo, Johan, A. T. Visser, and E. Rust (2009) "The stress–strain behaviour of multiple cell geocell packs." *Geotextiles and Geomembranes* 27, no. 1: 31-38.

Zhang, Ling, Minghua Zhao, Caijun Shi, and Heng Zhao (2010) "Bearing capacity of geocell reinforcement in embankment engineering." *Geotextiles and Geomembranes* 28, no. 5: 475-482.

ANNEXURE 1

LIGHT WEIGHT DEFLECTOMETER EQUIPMENT

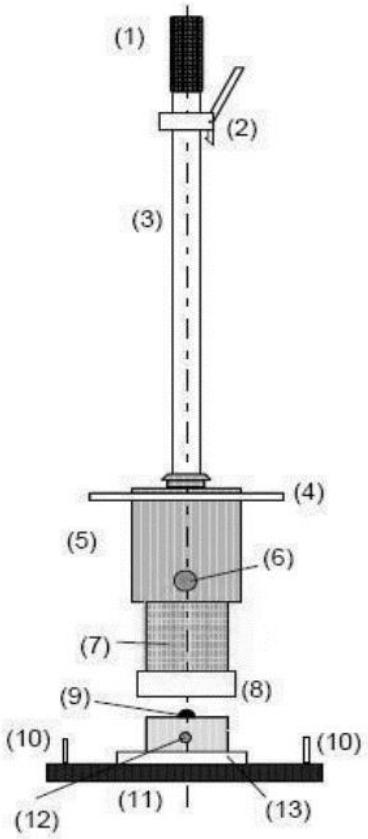

(1) grip
(2) top fix and release mechanism
(3) guide rod
(4) round grip
(5) 10 kg - falling weight
(6) lock pin
(7) set of steel springs
(8) anti tipping fixture
(9) load centre ball
(10) carry grip
(11) loading plate diameter (300 mm)
(12) socket for the connection to the electronic device
(13) adapter plate

ANNEXURE 2

IITPave Screenshots of different sections

High Volume Roads

SECTION 1:

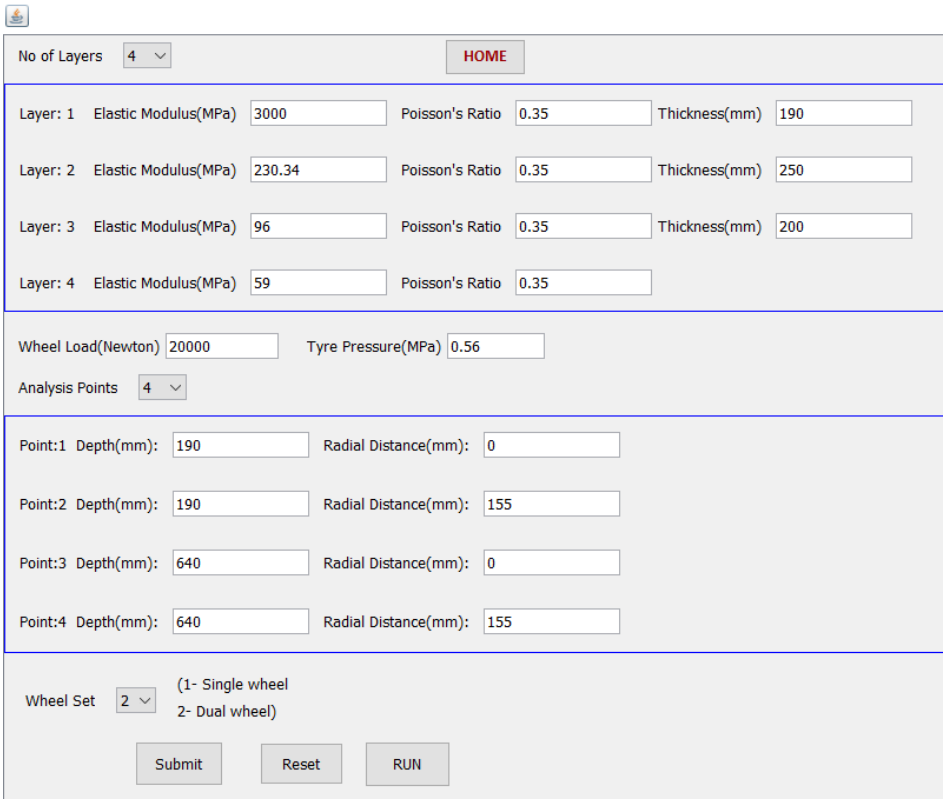

Figure A2 (a): Screen shot of input page of IIT Pave for URSB200 section

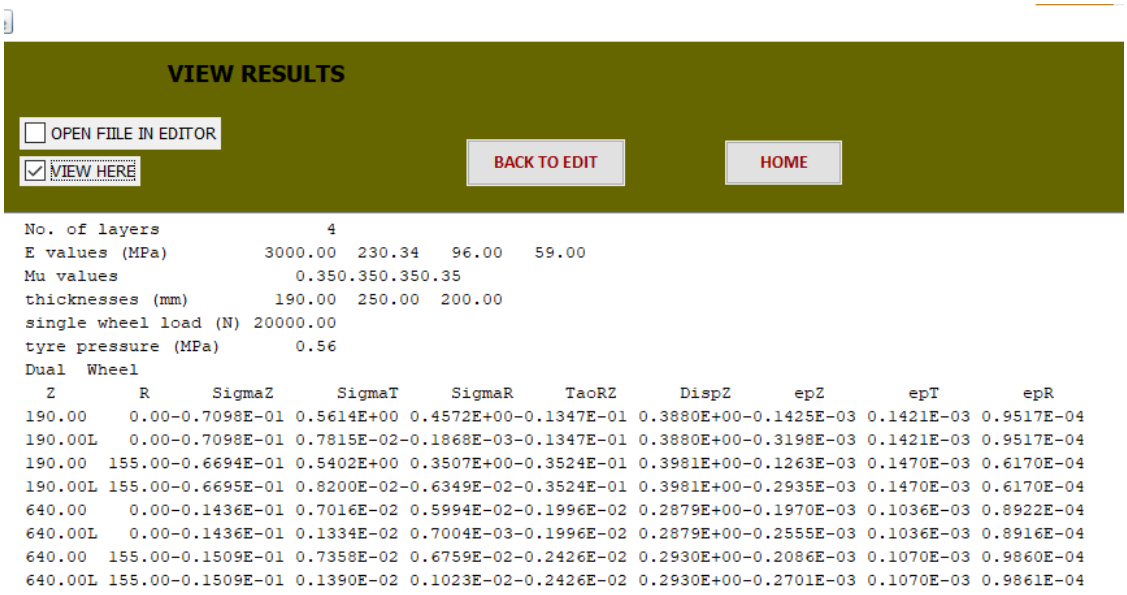

No. of layers 4
E values (MPa) 3000.00 230.34 96.00 59.00
Mu values 0.350.350.350.35
thicknesses (mm) 190.00 250.00 200.00
single wheel load (N) 20000.00
tyre pressure (MPa) 0.56
Dual Wheel

Z	R	SigmaZ	SigmaT	SigmaR	TaoRZ	DispZ	epZ	epT	epR
190.00	0.00	-0.7098E-01	0.5614E+00	0.4572E+00	-0.1347E-01	0.3880E+00	-0.1425E-03	0.1421E-03	0.9517E-04
190.00L	0.00	-0.7098E-01	0.7815E-02	-0.1868E-03	-0.1347E-01	0.3880E+00	-0.3198E-03	0.1421E-03	0.9517E-04
190.00	155.00	-0.6694E-01	0.5402E+00	0.3507E+00	-0.3524E-01	0.3981E+00	-0.1263E-03	0.1470E-03	0.6170E-04
190.00L	155.00	-0.6695E-01	0.8200E-02	-0.6349E-02	-0.3524E-01	0.3981E+00	-0.2935E-03	0.1470E-03	0.6170E-04
640.00	0.00	-0.1436E-01	0.7016E-02	0.5994E-02	-0.1996E-02	0.2879E+00	-0.1970E-03	0.1036E-03	0.8922E-04
640.00L	0.00	-0.1436E-01	0.1334E-02	0.7004E-03	-0.1996E-02	0.2879E+00	-0.2555E-03	0.1036E-03	0.8916E-04
640.00	155.00	-0.1509E-01	0.7358E-02	0.6759E-02	-0.2426E-02	0.2930E+00	-0.2086E-03	0.1070E-03	0.9860E-04
640.00L	155.00	-0.1509E-01	0.1390E-02	0.1023E-02	-0.2426E-02	0.2930E+00	-0.2701E-03	0.1070E-03	0.9861E-04

Figure A2 (b): Screen shot of output page of IIT Pave for URSB200 section

SECTION 2:

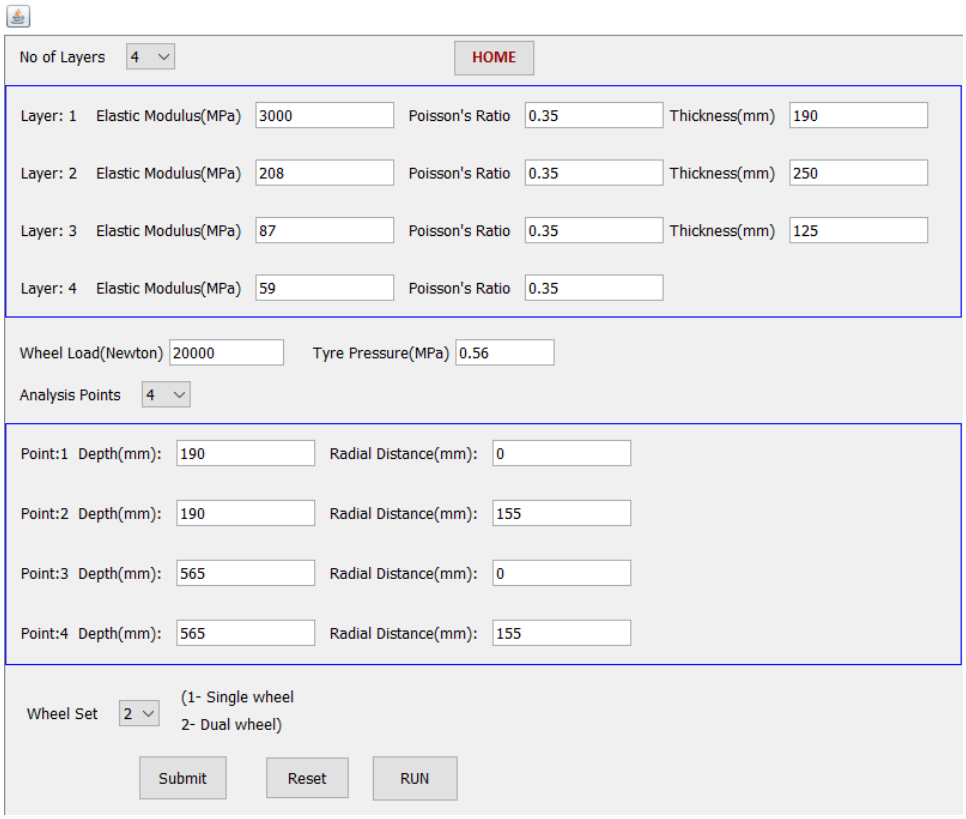

Figure A2 (c): Screen shot of input page of IIT Pave for URSB125 section

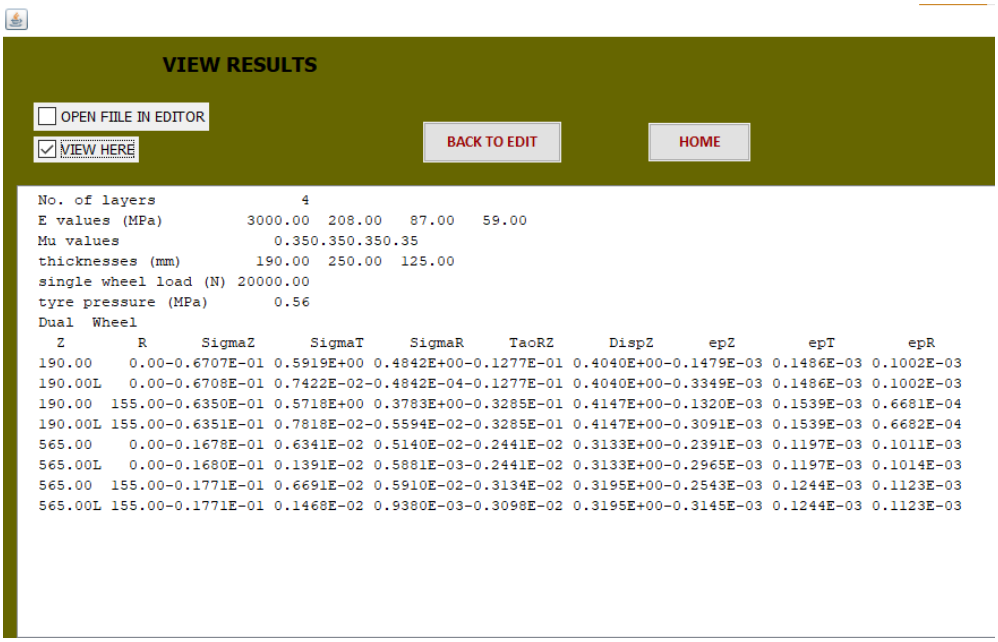

Figure A2 (d): Screen shot of output page of IIT Pave for URSB125 section

SECTION 3:

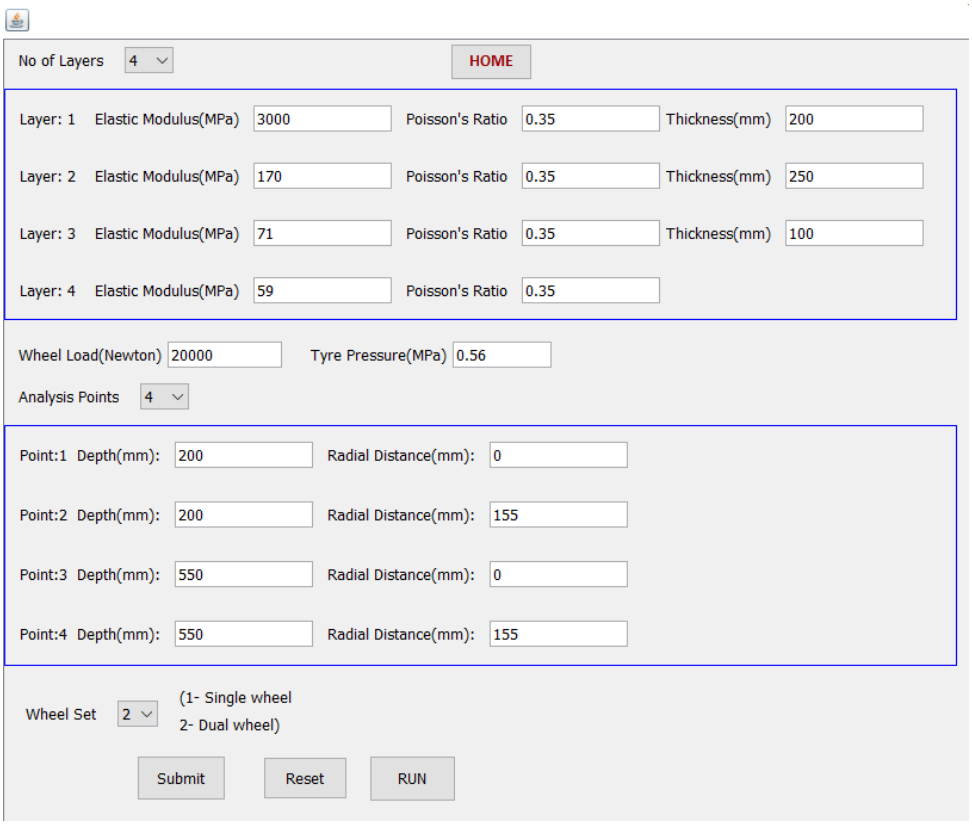

Figure A2 (e): Screen shot of input page of IIT Pave for URSB100 section

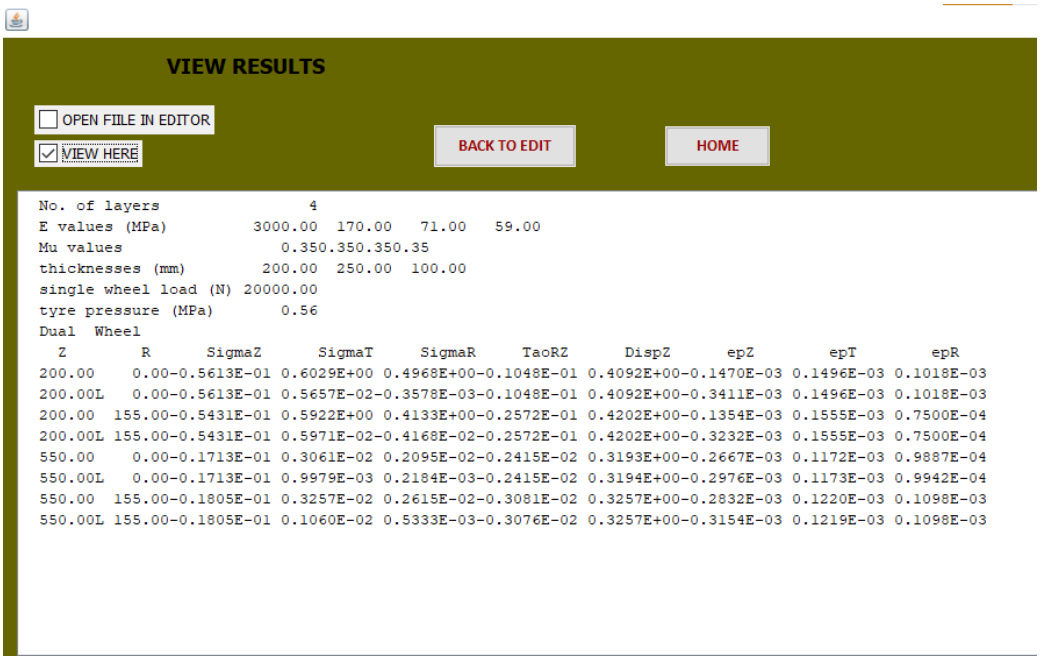

Figure A2 (f): Screen shot of output page of IIT Pave for URSB100 section

SECTION 4:

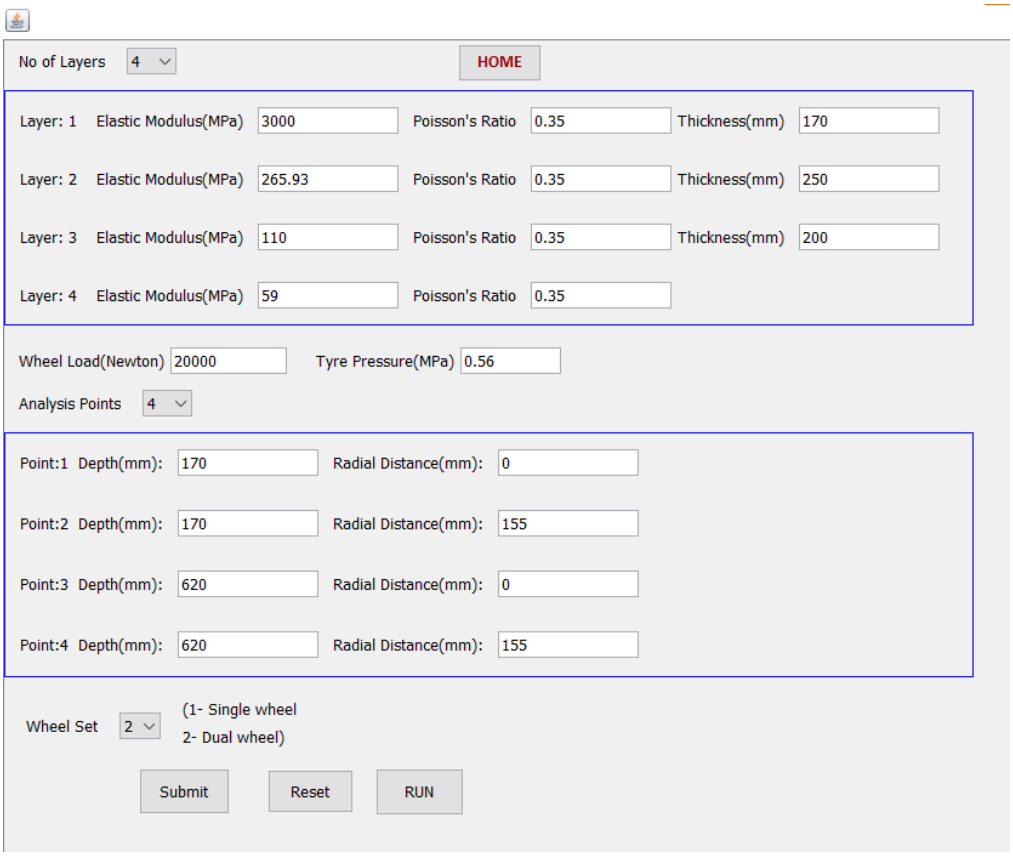

Figure A2 (g): Screen shot of input page of IIT Pave for RGC200 section

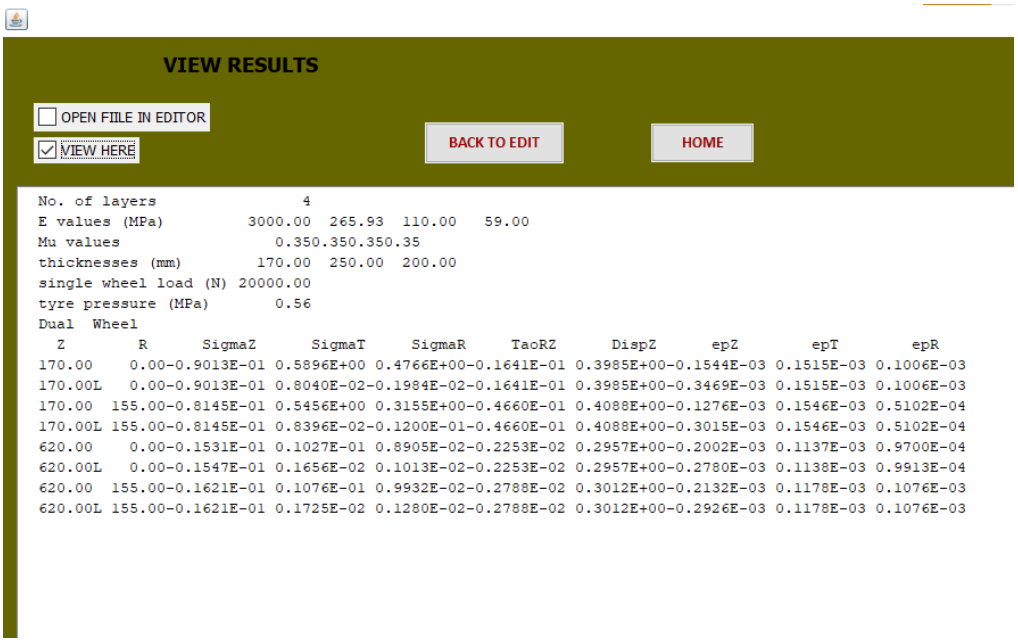

Figure A2 (h): Screen shot of output page of IIT Pave for RGC200 section

SECTION 5:

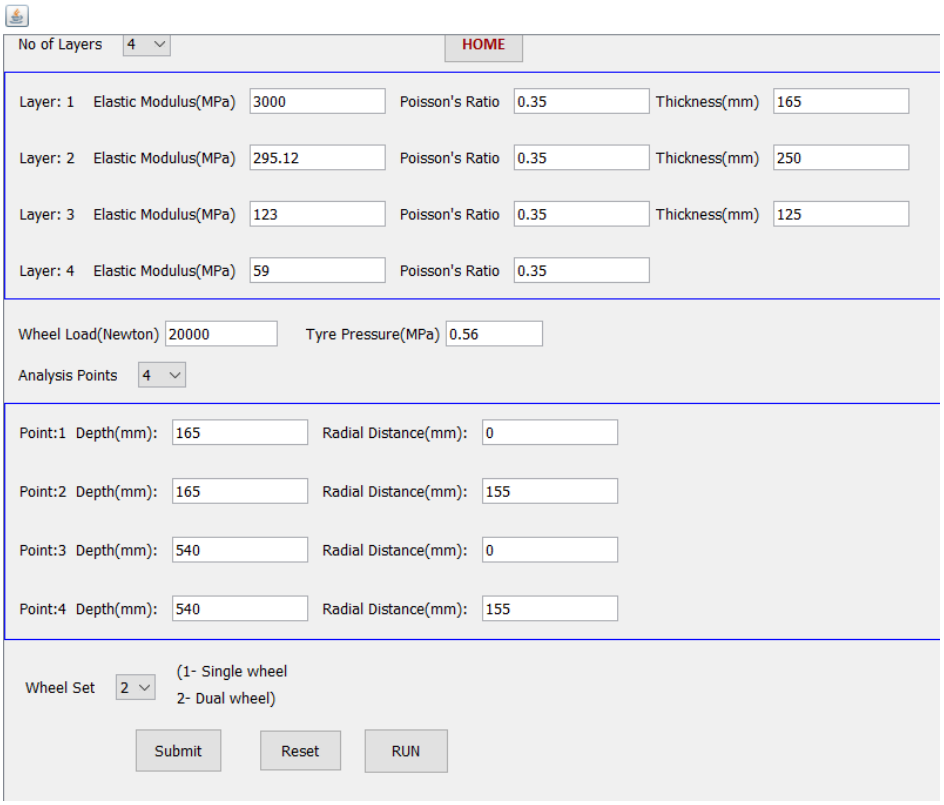

Figure A2 (i): Screen shot of input page of IIT Pave for RGC125 section

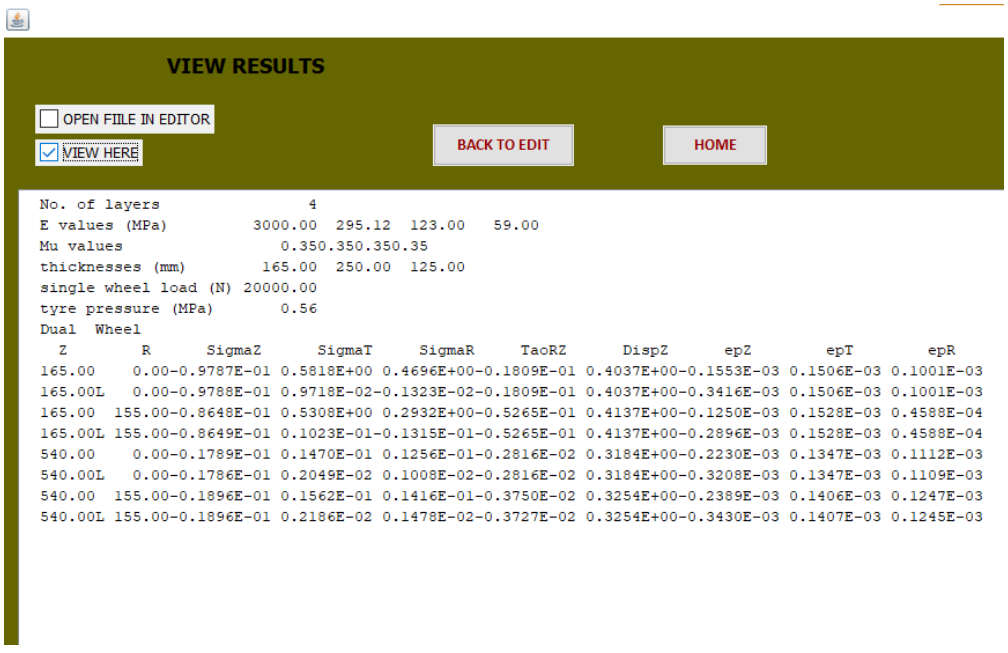

Figure A2 (j): Screen shot of output page of IIT Pave for RGC125 section

SECTION 6:

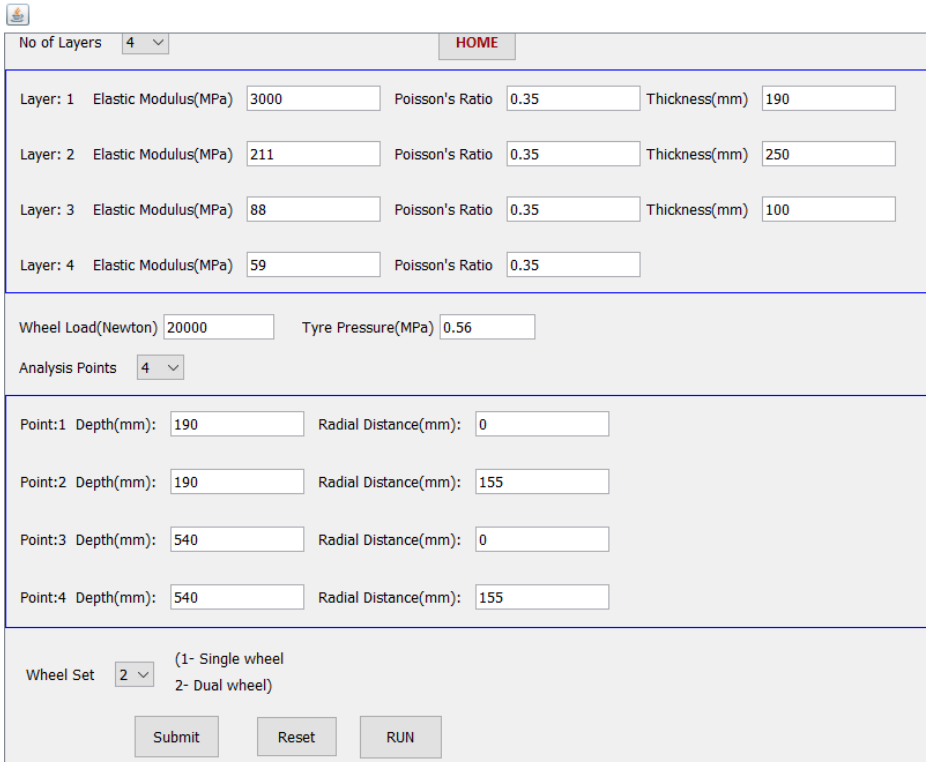

Figure A2 (k): Screen shot of input page of IIT Pave for RGC100 section

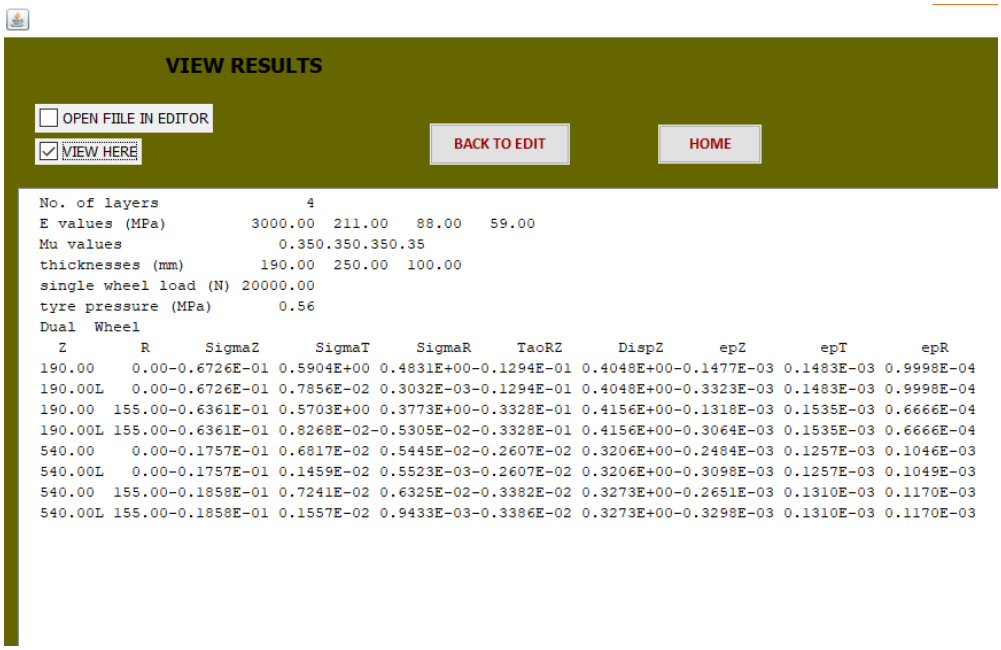

Figure A2 (l): Screen shot of output page of IIT Pave for RGC100 section

SECTION 7:

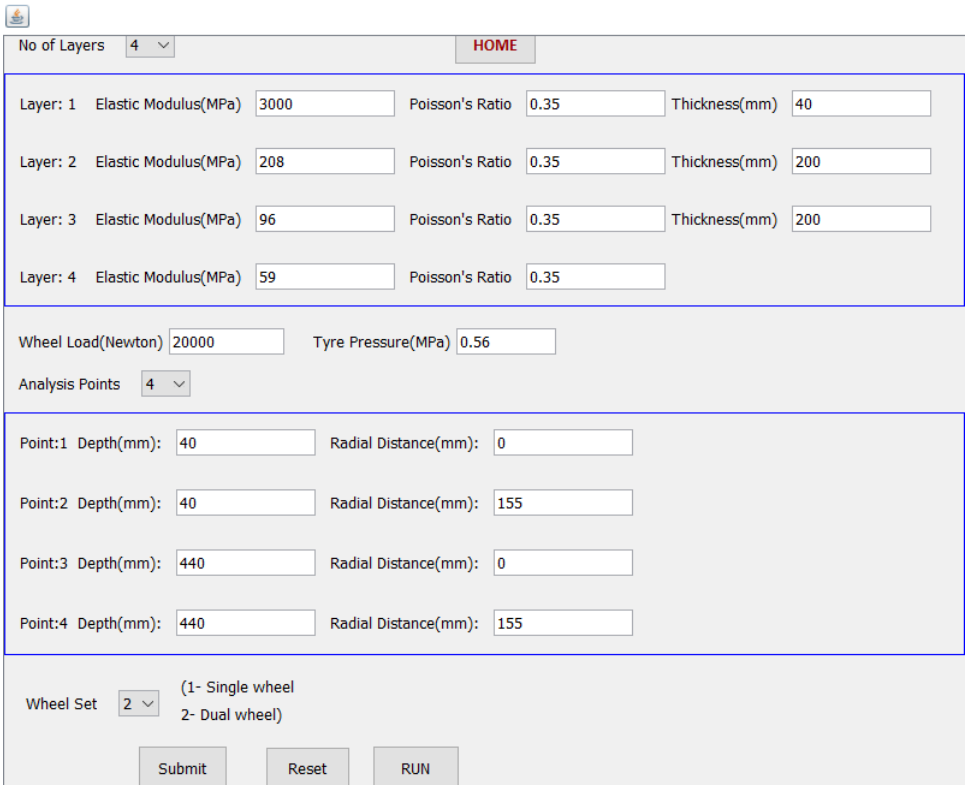

Figure A2 (m): Screen shot of input page of IIT Pave for URSB200 section

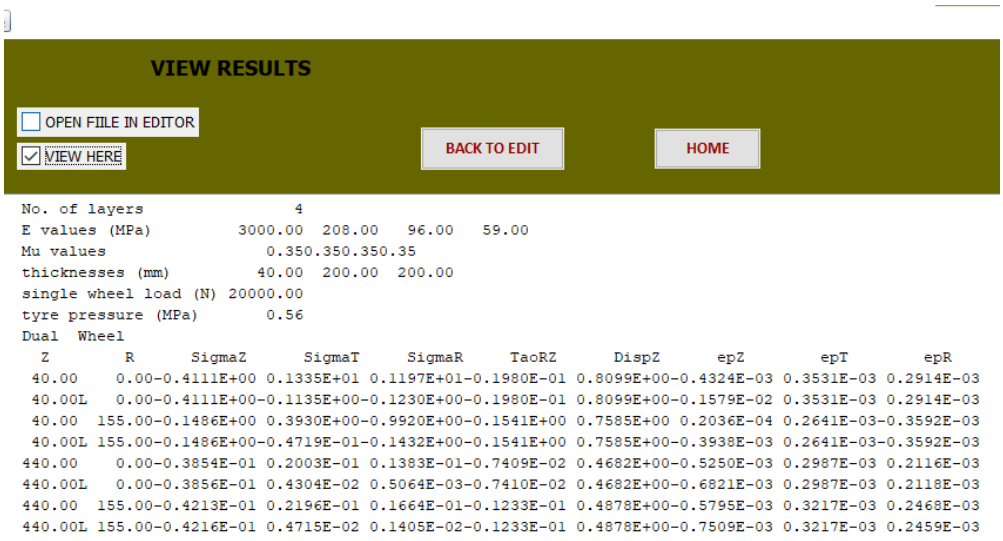

Figure A2 (n): Screen shot of output page of IIT Pave for URSB200 section

SECTION 8:

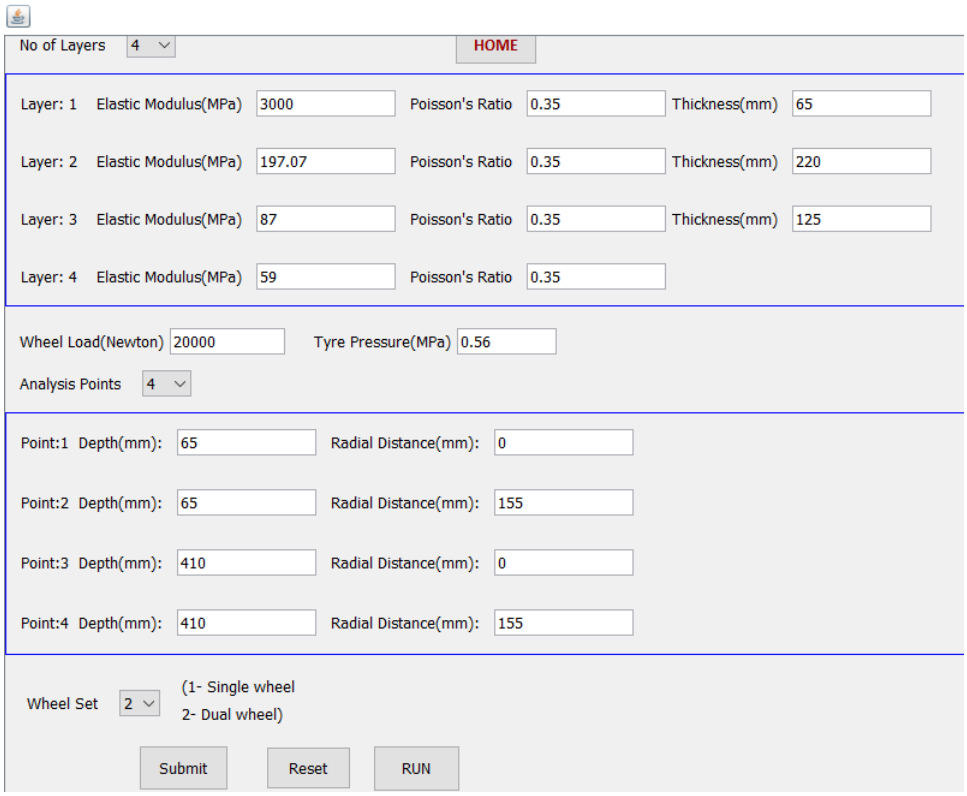

Figure A2 (o): Screen shot of input page of IIT Pave for URSB125 section

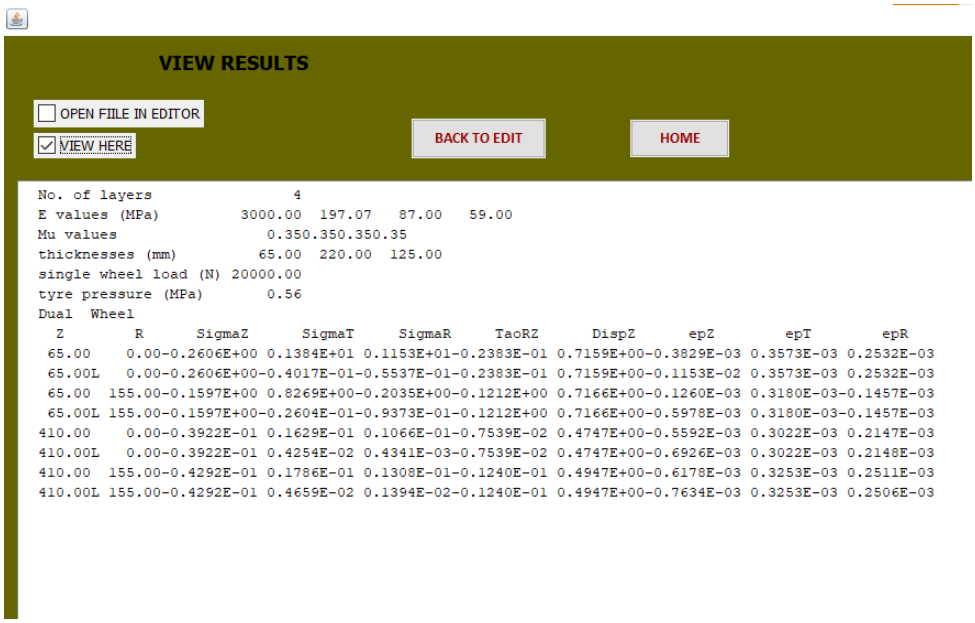

Figure A2 (p): Screen shot of output page of IIT Pave for URSB125 section

SECTION 9:

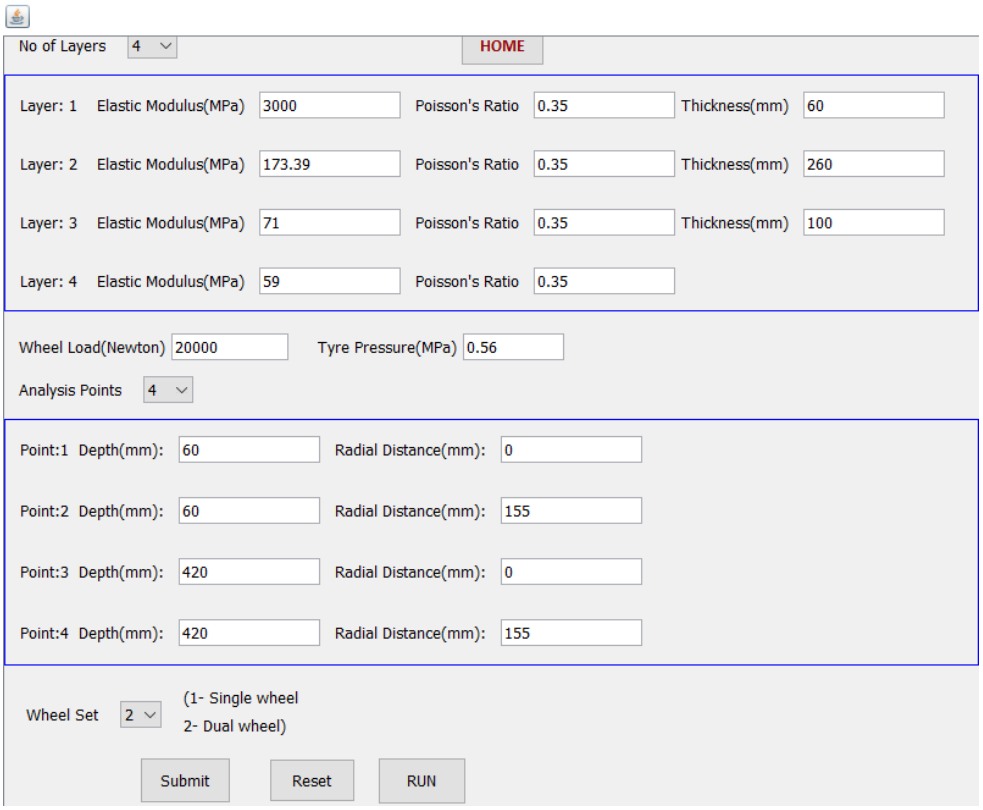

Figure A2 (q): Screen shot of input page of IIT Pave for URSB100 section

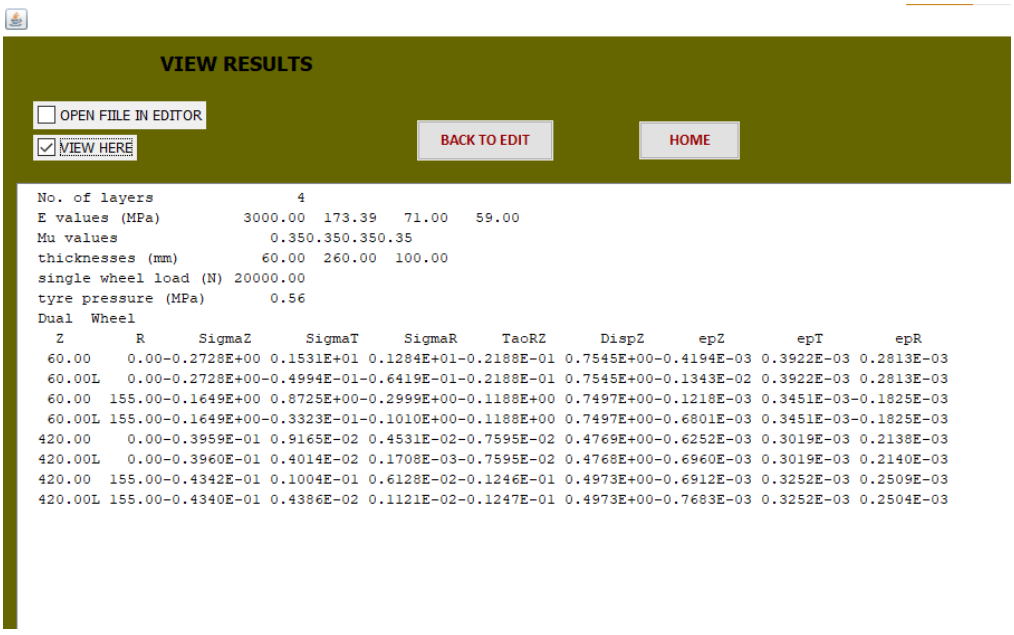

Figure A2 (r): Screen shot of output page of IIT Pave for URSB100 section

SECTION 10:

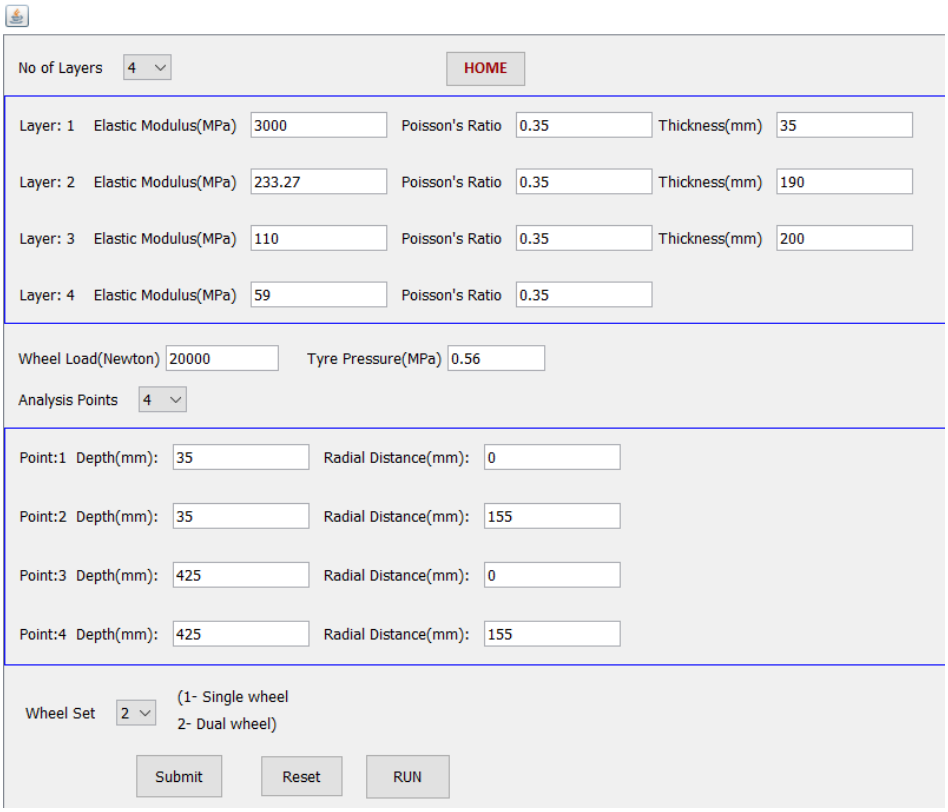

Figure A2 (s): Screen shot of input page of IIT Pave for RGC200 section

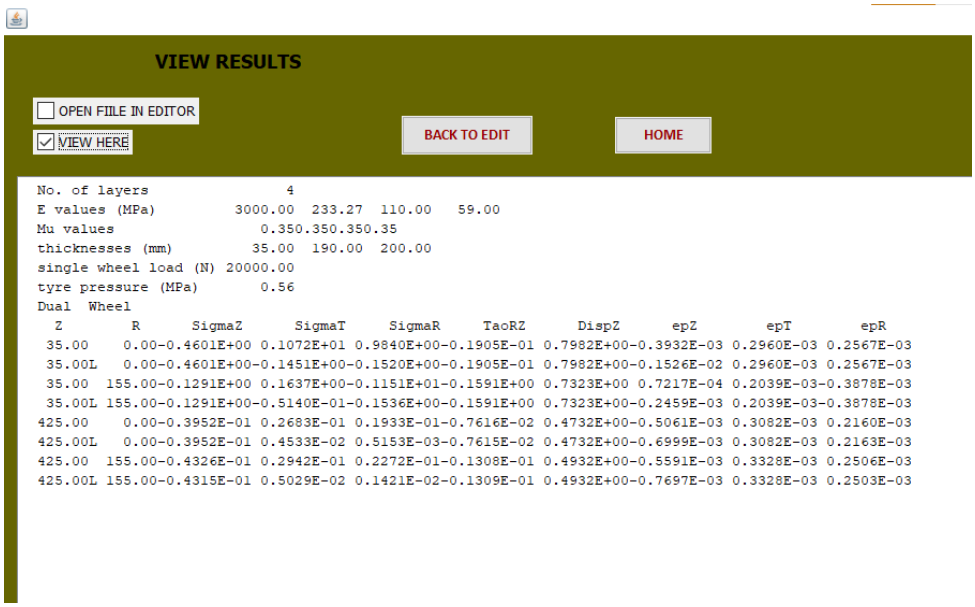

Figure A2 (t): Screen shot of output page of IIT Pave for RGC200 section

SECTION 11:

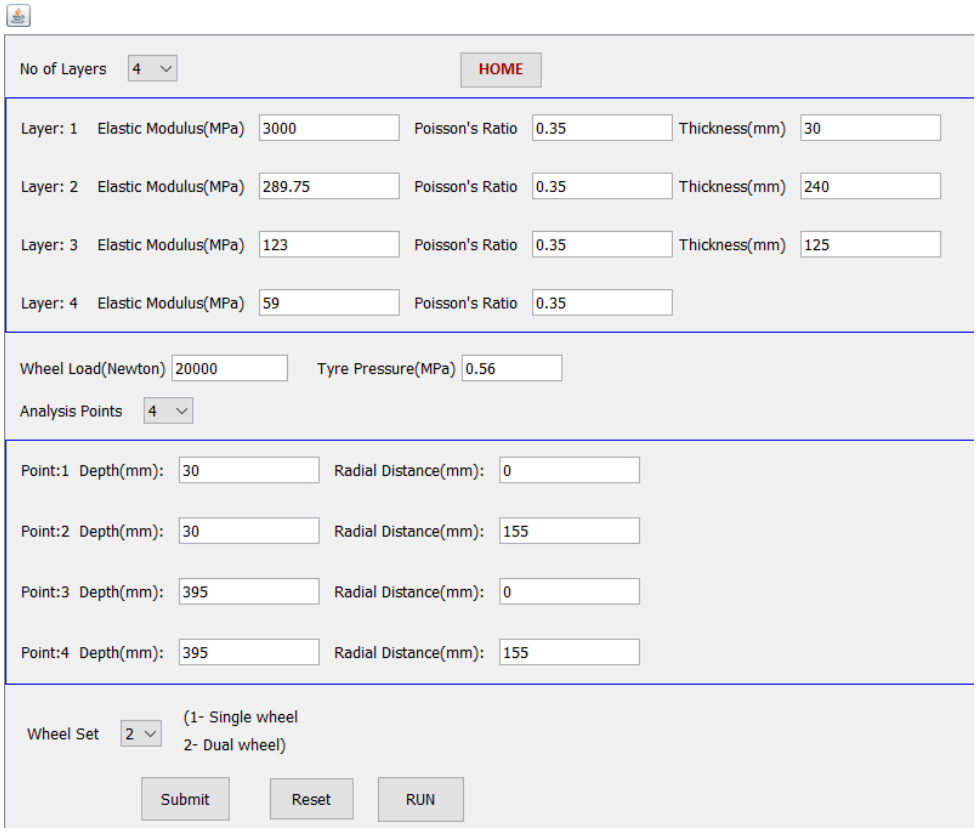

Figure A2 (u): Screen shot of input page of IIT Pave for RGC125 section

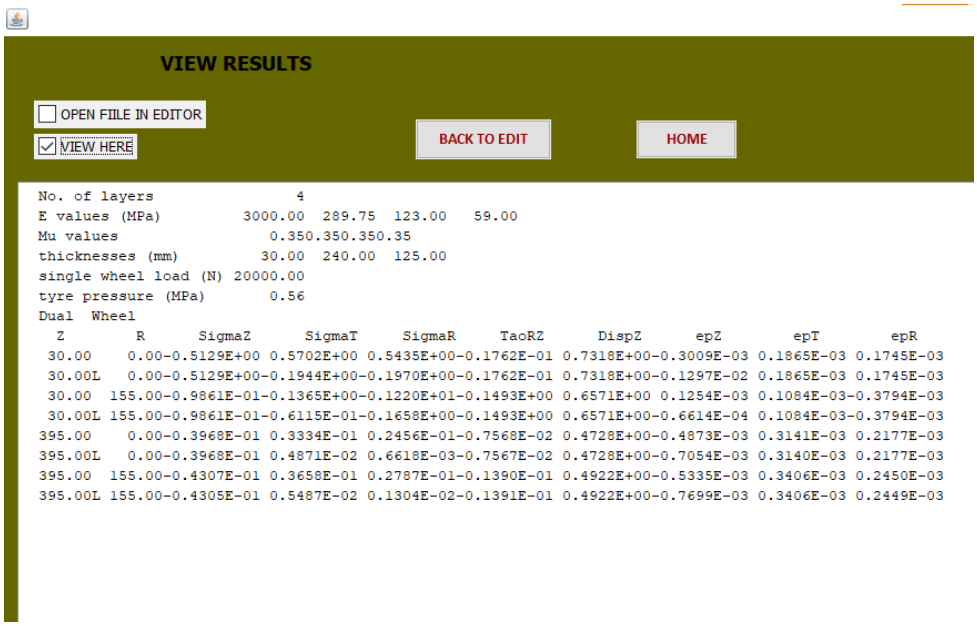

Figure A2 (v): Screen shot of output page of IIT Pave for RGC125 section

SECTION 12:

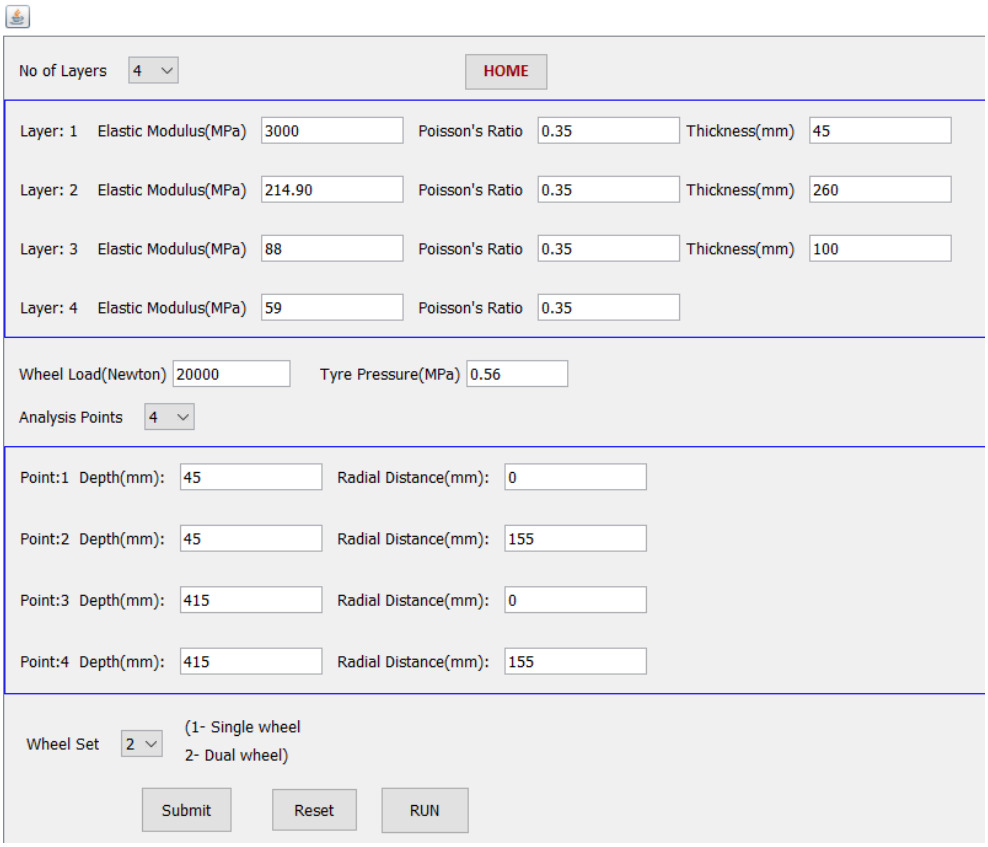

Figure A2 (w): Screen shot of input page of IIT Pave for RGC100 section

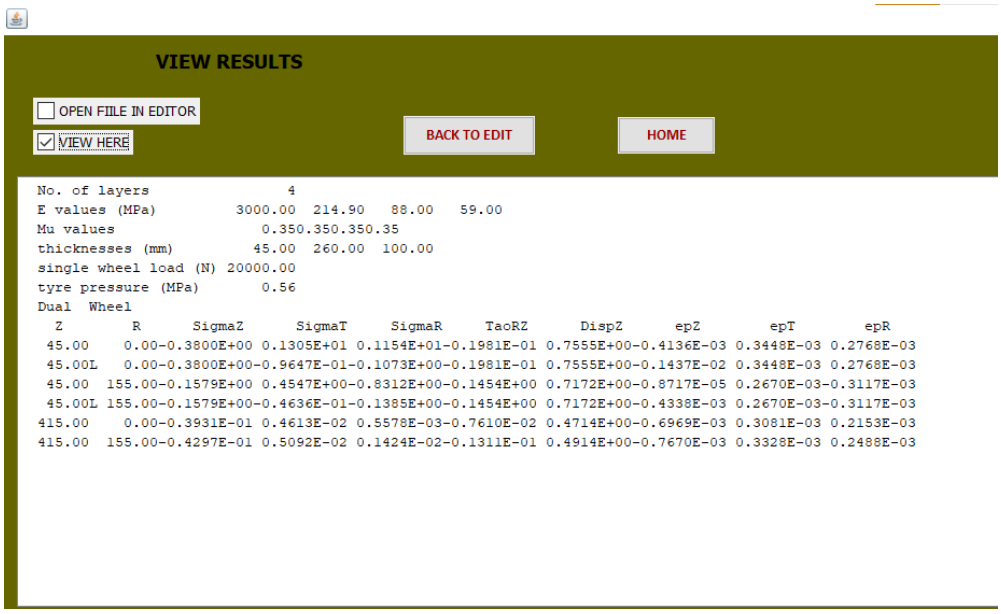

Figure A2 (x): Screen shot of output page of IIT Pave for RGC100 section

ANNEXURE 3

IITPave Screenshots of different sections used in Abaqus Software

IITPave Strain values calculated

Field value Analysis

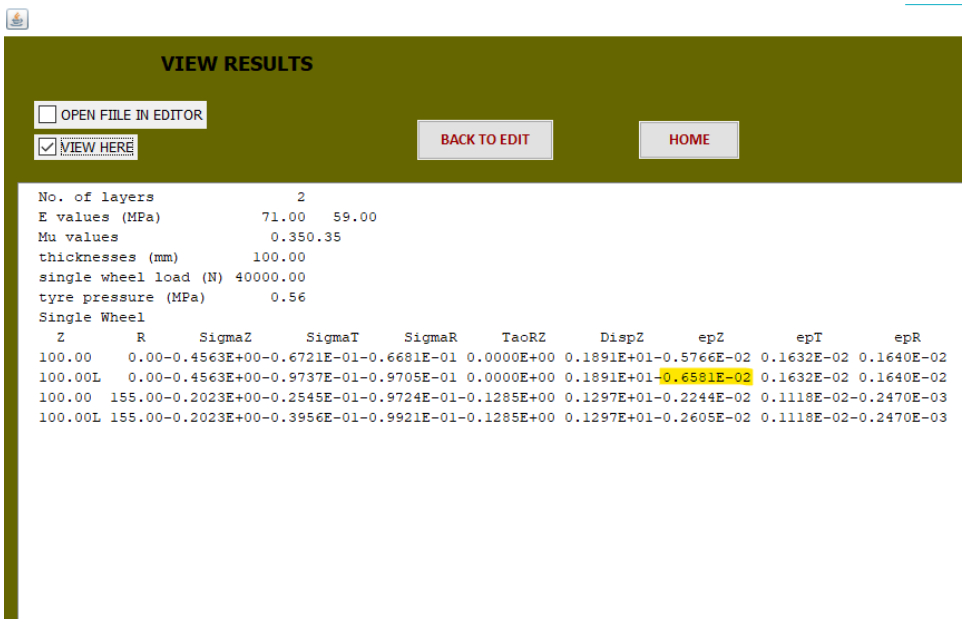

Figure A3 (a): Screen shot of output page of IIT Pave for URSB100 section

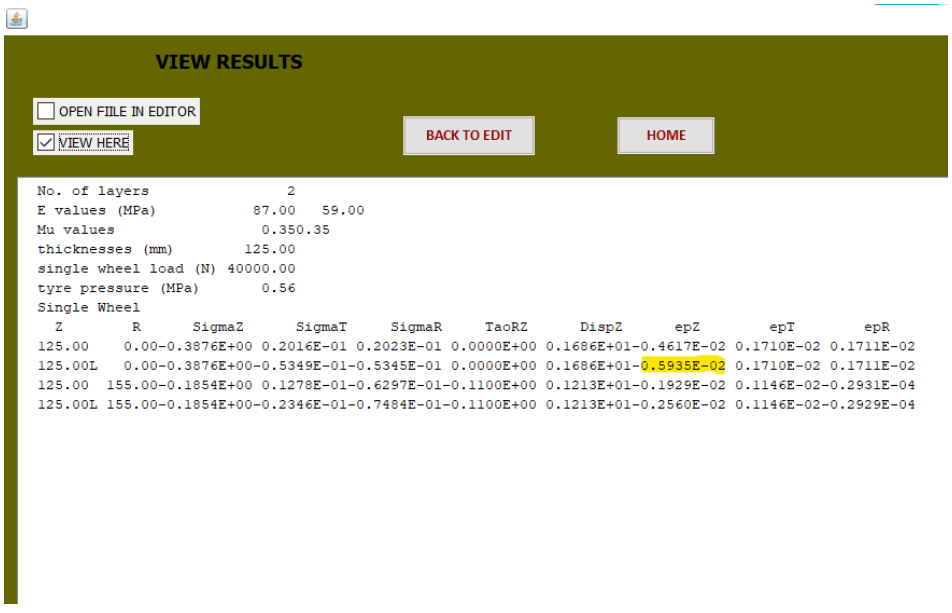

Figure A3 (b): Screen shot of output page of IIT Pave for URSB125 section

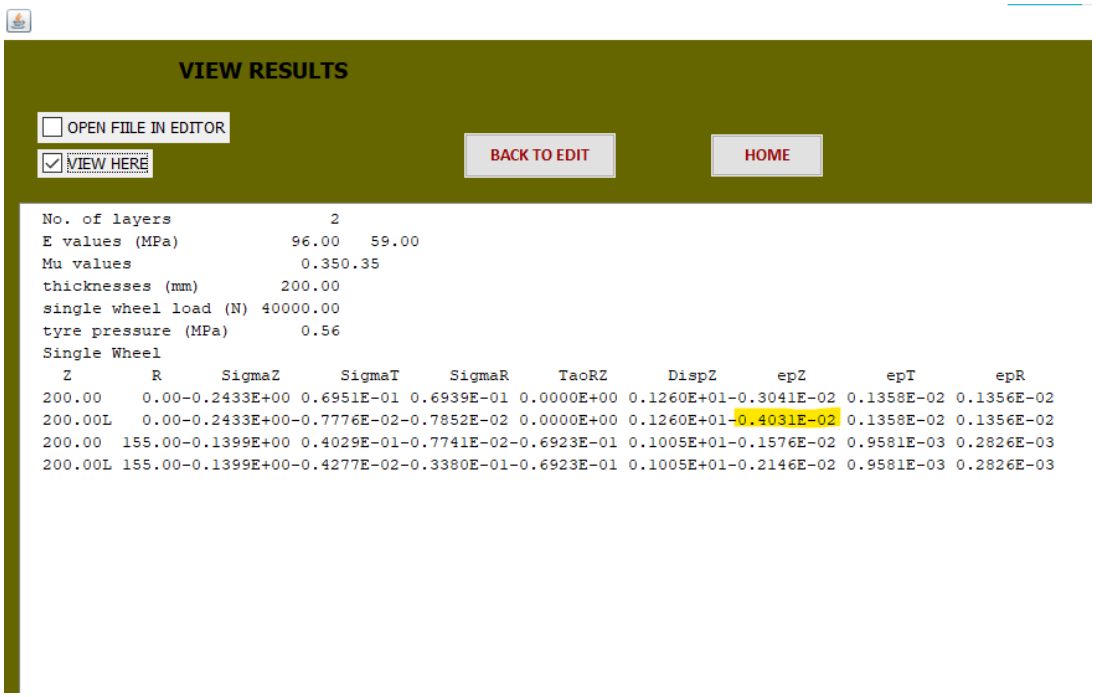

Figure A3 (c): Screen shot of output page of IIT Pave for URSB200 section

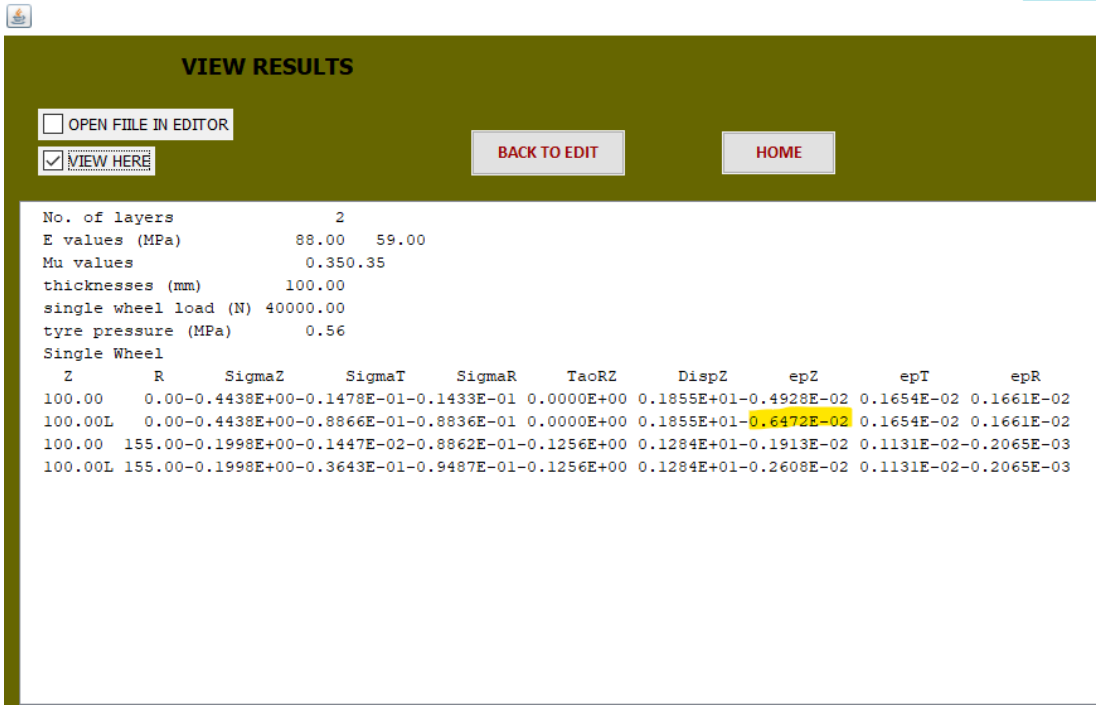

Figure A3 (d): Screen shot of output page of IIT Pave for RGC100 section

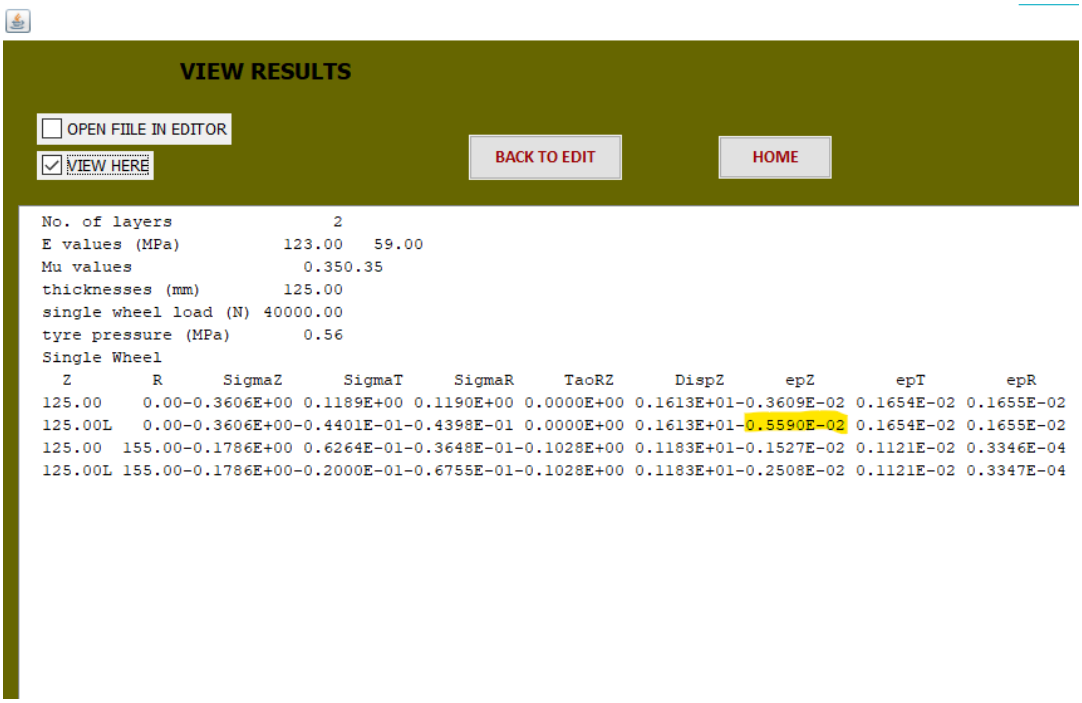

Figure A3 (e): Screen shot of output page of IIT Pave for RGC125 section

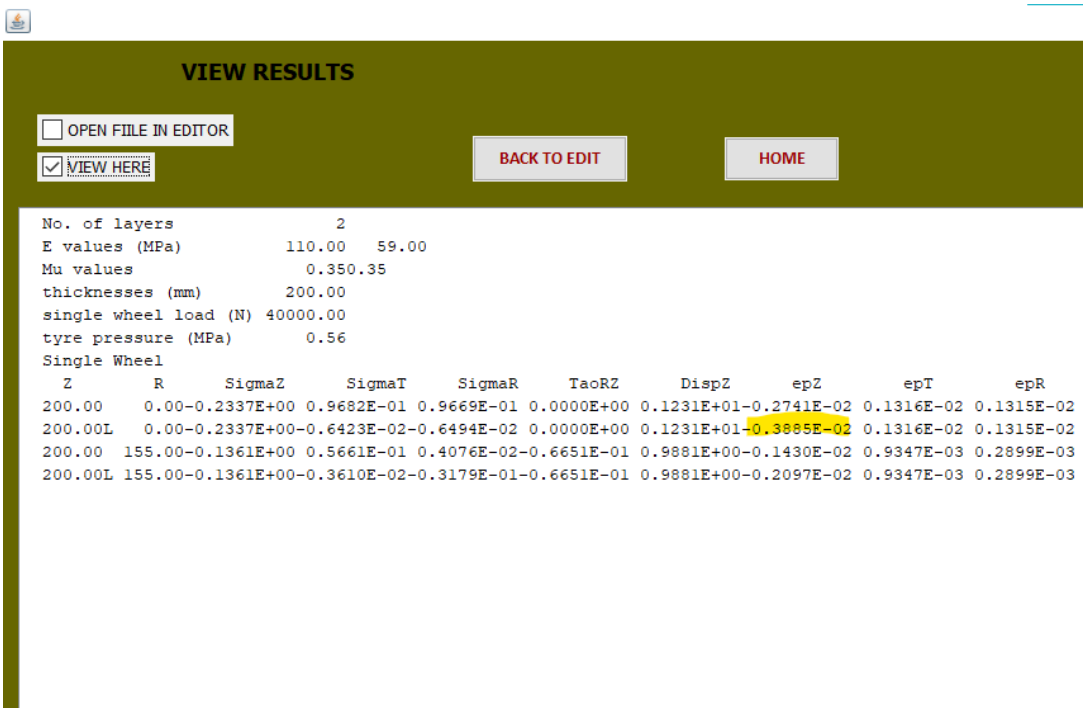

Figure A3 (f): Screen shot of output page of IIT Pave for RGC200 section

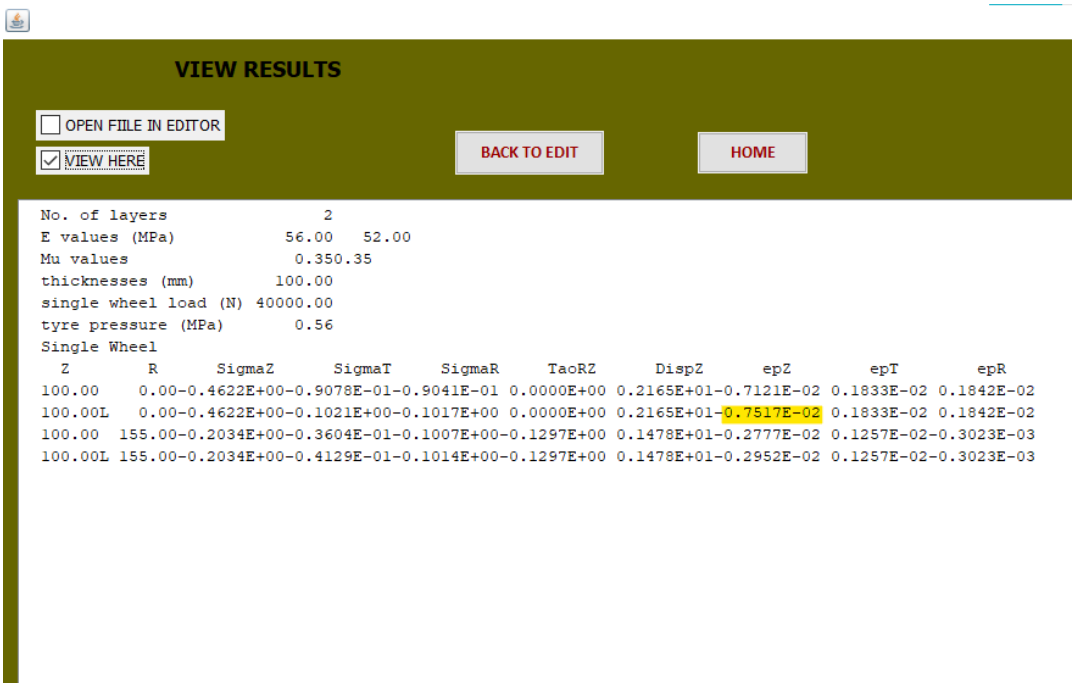

Figure A3 (g): Screen shot of output page of IIT Pave for URSB100 section

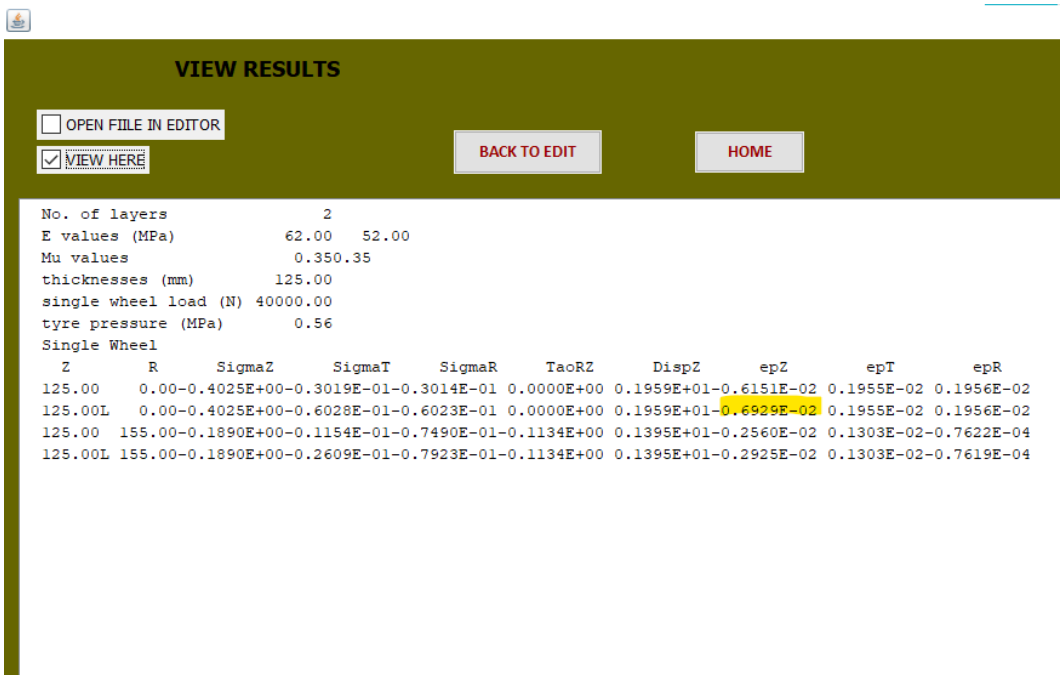

Figure A3 (h): Screen shot of output page of IIT Pave for URSB125 section

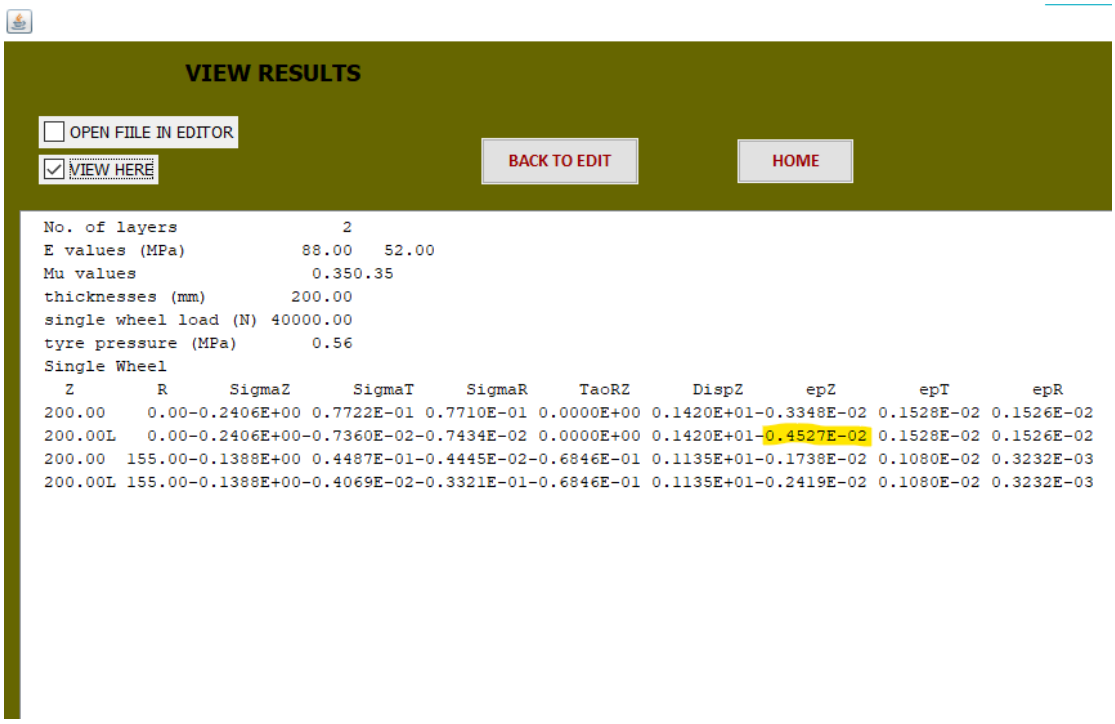

Figure A3 (i): Screen shot of output page of IIT Pave for URSB200 section

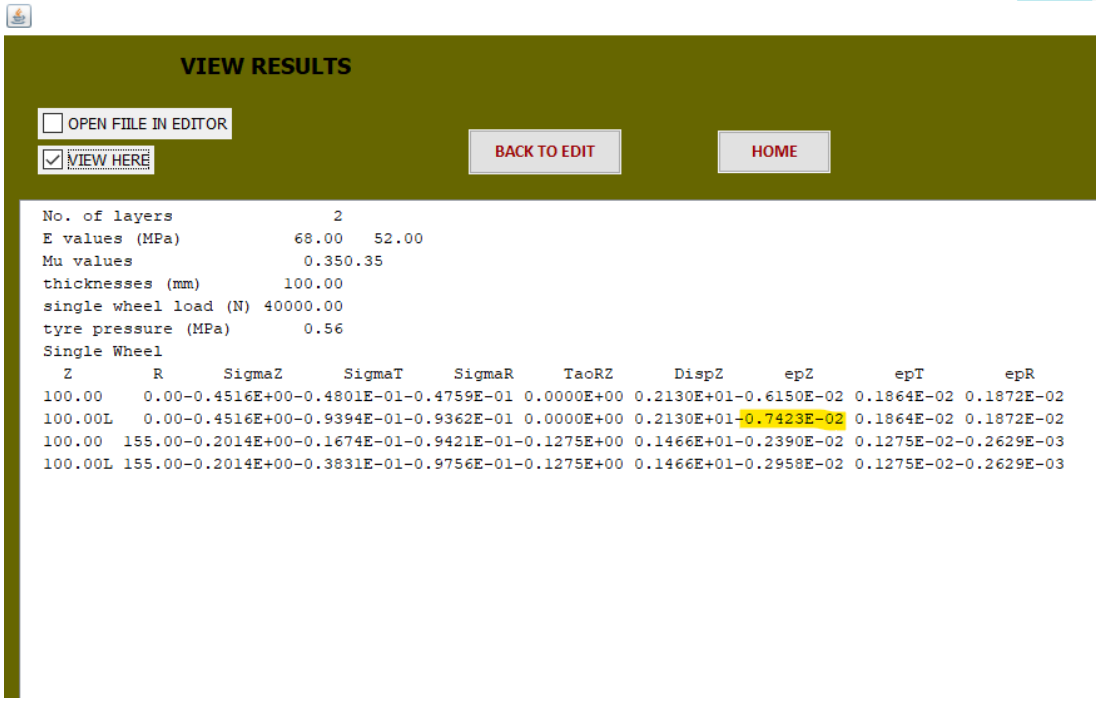

Figure A3 (j): Screen shot of output page of IIT Pave for RGC100 section

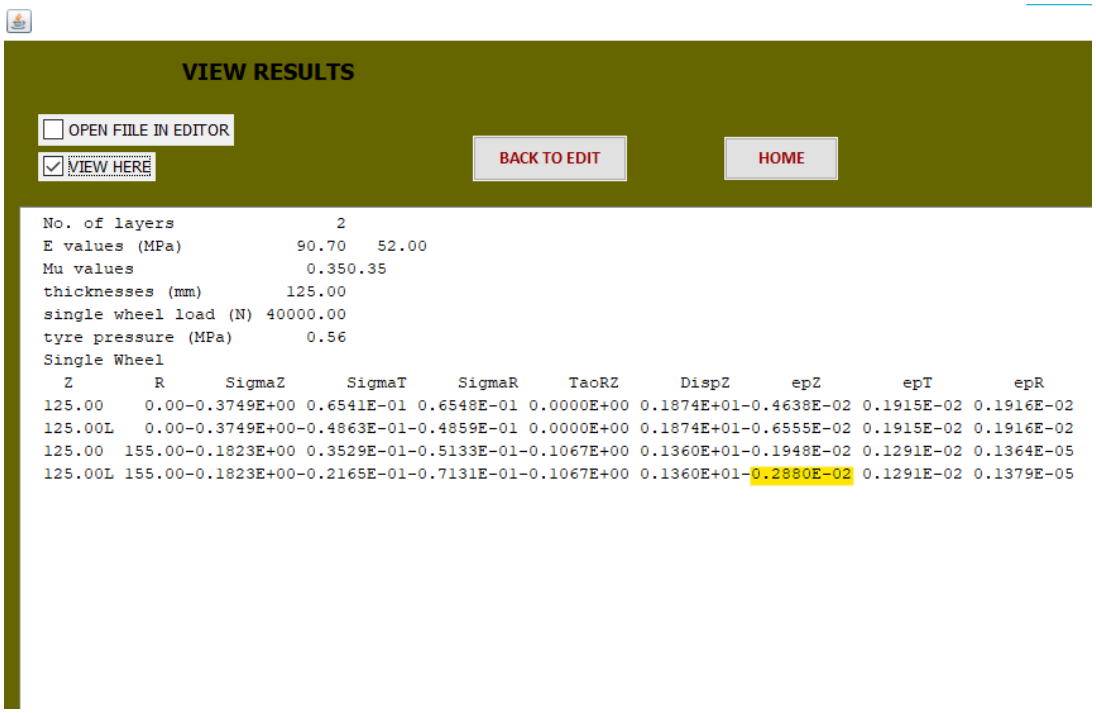

Figure A3 (k): Screen shot of output page of IIT Pave for RGC125 section

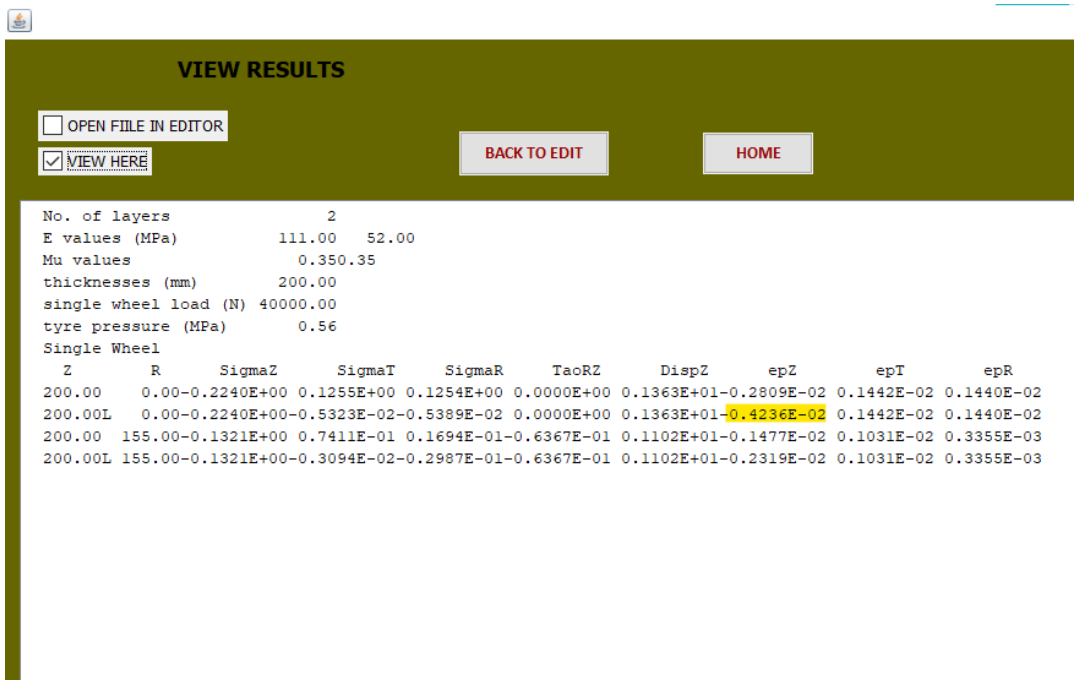

Figure A3 (l): Screen shot of output page of IIT Pave for RGC200 section

Ouriginal by Turnitin

Document Information

Analyzed document	22-6-22-report 1.pdf (D142532933)
Submitted	7/30/2022 6:56:00 AM
Submitted by	Vivek Gupta
Submitter email	vivek.gupta1@thapar.edu
Similarity	12%
Analysis address	vivek.gupta1.thapar@analysis.urkund.com

Sources included in the report

W	URL: https://rosap.ntl.bts.gov/view/dot/60786/dot_60786_DS1.pdf Fetched: 6/11/2022 4:58:44 PM	1
W	URL: https://archive.org/stream/gov.in.irc.sp.059.2018/irc.gov.in.sp.059.2018_djvu.txt Fetched: 3/28/2022 9:34:01 PM	7
W	URL: https://hammer.purdue.edu/articles/thesis/Use_of_geosynthetics_on_subgrade_and_on_low_and_variable_fill_foundation/17152706/1/files/31720796.pdf Fetched: 3/22/2022 6:06:35 AM	3
W	URL: https://library.ctr.utexas.edu/hostedpdfs/utep/0-6833-1.pdf Fetched: 6/25/2022 11:33:48 AM	59
SA	**Central University of Jharkhand / Chandrbhushan Kumar _ M Tech Thesis.pdf** Document Chandrbhushan Kumar _ M Tech Thesis.pdf (D109411279) Submitted by: information.scientist@cuj.ac.in Receiver: information.scientist.cuj@analysis.urkund.com	11
W	URL: https://core.ac.uk/download/pdf/213392091.pdf Fetched: 7/31/2020 3:46:46 PM	4
W	URL: https://trid.trb.org/view/408594 Fetched: 3/9/2020 12:59:14 PM	4
W	URL: https://core.ac.uk/download/pdf/213401792.pdf Fetched: 2/22/2021 2:03:05 PM	2
W	URL: https://core.ac.uk/download/pdf/213396123.pdf Fetched: 6/27/2021 8:34:03 AM	6
SA	**Anna University, Chennai / 11Anna univerisity rajakumar April.pdf** Document 11Anna univerisity rajakumar April.pdf (D27157868) Submitted by: tmeenambal_gct@yahoo.co.in Receiver: tmeenambal_gct.annauniv@analysis.urkund.com	1
SA	**Thapar Institute Of Engineering And Technology / Thesis combined.pdf** Document Thesis combined.pdf (D141784664) Submitted by: harsingh@thapar.edu Receiver: harsingh.thapar@analysis.urkund.com	29
SA	**Sardar Vallabhbhai National Institute Of Tech / P19TP009_SAURABH GARG_DISSERTATION_13072021.pdf** Document P19TP009_SAURABH GARG_DISSERTATION_13072021.pdf (D110444319) Submitted by: ajs@ced.svnit.ac.in Receiver: ajs.svnit@analysis.urkund.com	2
SA	**RIMT University / Bhawna Sharma.docx** Document Bhawna Sharma.docx (D95367505) Submitted by: sandeep.singla@rimt.ac.in Receiver: sandeep.singla.rimt@analysis.urkund.com	1
SA	**RIMT University / Bhawana Sharma Revised 2.docx** Document Bhawana Sharma Revised 2.docx (D107143228) Submitted by: sandeep.singla@rimt.ac.in Receiver: sandeep.singla.rimt@analysis.urkund.com	2
W	URL: https://rc.library.uta.edu/uta-ir/bitstream/handle/10106/27757/GEORGE-DISSERTATION-2018.pdf?sequence=1&isAllowed=y Fetched: 9/26/2019 9:31:40 AM	7
W	URL: https://www.researchgate.net/publication/242312160_Design_of_Geocell_Reinforcement_for_Supporting_Embankments_on_Soft_Ground Fetched: 3/9/2020 1:00:08 PM	1

Entire Document